EES Catalysis

REVIEW ARTICLE

Published on 08 July 2026

Cite this: *EES Catal.*, 2026, 4, 1036

Molecular copper systems for hydrogen production: from pre-catalyst activation to catalytic function

Abdullah M. Abudayyeh, *[a] Ludovic Troian-Gautier [bc] and Antoni Llobet [d]

Received 10th May 2026,
Accepted 4th July 2026

DOI: 10.1039/d6ey00102e

rsc.li/eescatalysis

The transition toward a carbon-neutral energy future places green hydrogen (H_2) at the forefront of sustainable fuel strategies. However, the large-scale deployment of hydrogen remains constrained by high production costs, underscoring the urgent need for the development of efficient and robust catalysts for the hydrogen evolution reaction (HER). Copper has played a role in hydrogen evolution research since the 1950s, when metallic copper electrodes were employed to probe the kinetics and mechanisms of hydrogen evolution in aqueous electrolytes. Despite this early involvement, systematic development of copper-based HER catalysts has emerged only in the past decade, driven largely by advances in CuO and Cu_2O nanomaterials for photo- and electrocatalytic hydrogen production. More recently, molecular copper complexes have gained attention as catalysts or pre-catalysts for hydrogen evolution, revitalizing interest in copper-centered HER chemistry. This review surveys recent progress in molecular copper catalysts and pre-catalysts operating under photo- and electrocatalytic conditions. We first outline the key metrics used to benchmark HER performance. We then summarize the principal methods used to probe catalyst homogeneity and critically assess the evidences commonly employed to distinguish molecular from heterogeneous active species. Finally, we discuss current challenges and future prospects for molecular HER catalysts in general, and copper-based systems in particular.

Broader context

The development of sustainable hydrogen production technologies is central to the global transition toward carbon-neutral energy systems. Molecular electrocatalysts offer unique opportunities for understanding and improving hydrogen evolution reaction (HER) mechanisms through precise control of catalyst structure, electronic properties, and reaction environments. While cobalt, nickel, and iron molecular catalysts have been extensively explored, molecular copper systems remain comparatively underdeveloped despite copper being earth-abundant, inexpensive, and capable of rich redox and coordination chemistry. Recent years have witnessed growing interest in copper-based molecular catalysts for both electro- and photocatalytic hydrogen production, driven by advances in ligand design, mechanistic understanding, and catalyst integration strategies. At the same time, distinguishing true molecular catalysis from catalytically active heterogeneous species formed *in situ* has emerged as a critical challenge across the field. This review provides a comprehensive overview of molecular copper systems for HER, emphasizing the relationship between catalyst structure, catalytic performance, and catalyst integrity. By critically discussing benchmarking metrics, mechanistic pathways, and homogeneity assessment methods alongside recent catalytic examples, this work aims to support the rational development of next-generation copper-based HER catalysts and contribute to the broader advancement of sustainable hydrogen production technologies.

1 Introduction

The development of carbon-neutral energy carriers, particularly green hydrogen (H_2) produced using renewable resources, has become an urgent global priority.[1] In line with this goal, the 2015 United Nations Climate Change Conference (COP21) held in Paris emphasized the necessity of limiting the global temperature rise to 1.5 °C above pre-industrial levels, a commitment endorsed by more than 195 countries.[2] Following this, COP28,[3] held in Dubai in December 2023, marked the first

[a] *Basic Science Department, Faculty of Science, Applied Science Private University, Amman, Jordan. E-mail: a_abudayyeh@asu.edu.jo*
[b] *Institut de la Matière Condensée et des Nanosciences (IMCN), Molecular Chemistry, Materials and Catalysis (MOST), Université catholique de Louvain (UCLouvain), Place Louis Pasteur 1, Box L4.01.02, B-1348 Louvain-la-Neuve, Belgium*
[c] *Wel Research Institute, Avenue Pasteur 6, 1300 Wavre, Belgium*
[d] *Institute of Chemical Research of Catalonia (ICIQ), Av. Països Catalans 16, Tarragona 43007, Spain*

global agreement committing to a transition away from fossil fuels as part of efforts to achieve net-zero emissions by 2050. In response, Europe has outlined a strategic roadmap for hydrogen deployment, including the establishment of hydrogen refueling infrastructure, reflecting the view that hydrogen will play a central role in the continent's energy transition toward a fully decarbonized system in compliance with the Paris and Dubai Agreements.[4]

Unlike fossil fuels, hydrogen is particularly attractive as an energy carrier because it can be produced in a carbon-free fashion *via* sustainable pathways. Upon combustion, hydrogen releases energy with water as only reaction by-product (eqn (1)). Moreover, hydrogen exhibits a higher gravimetric energy density than conventional fossil fuels[5] and than many electrochemical energy storage technologies such as batteries.[6] Hydrogen can be exploited either through direct combustion or electrochemical conversion in fuel cells, with both approaches yielding energy and water vapor as the sole products (eqn (1)).

$$2H_{2(g)} + O_{2(g)} \rightarrow 2H_2O_{(g)} + 486.6\ \text{kJ} \quad (1)$$

Hydrogen has been used in fuel cells for several decades, and hydrogen-powered vehicles are now available, albeit in small numbers to date.[7–9] Hence, hydrogen is currently receiving considerable attention as a fuel. Hydrogen is also a long-standing and key chemical that is used in numerous industrial processes but several fundamental challenges hinder its large-scale deployment.[10,11] These challenges include energy-intensive and costly production routes, low volumetric energy density requiring compression or liquefaction, storage and transportation safety concerns, and the lack of mature infrastructure for distribution and end use. In addition, the environmental benefit of hydrogen strongly depends on its production pathway. Accordingly, hydrogen is commonly classified by "color" based on its source and carbon footprint (Fig. 1): grey hydrogen is produced from fossil fuels *via* steam methane reforming with significant CO_2 emissions; blue hydrogen couples fossil-based production with carbon capture and storage, reducing but not eliminating emissions; green hydrogen is generated *via* water electrolysis powered by renewable electricity and represents the most sustainable route[12,13] while additional categories such as turquoise and pink hydrogen have recently emerged, relying on methane pyrolysis and nuclear-powered electrolysis, respectively.[6,14,15] Overcoming the economic, technical, and sustainability challenges associated with hydrogen production and utilization remains critical for its role in a future low-carbon energy system.[16] Addressing these challenges ultimately hinges on the development of efficient, durable, and earth-abundant electrocatalysts that can lower the energy input and cost of green hydrogen production *via* the hydrogen evolution reaction.

Over the past several decades, substantial efforts have been devoted to the development of efficient catalysts for the hydrogen evolution reaction (HER). In addition to heterogeneous systems including transition-metal carbides and nitrides,[17–20] alloys,[21,22] nanostructured metal phosphides,[23–25] transition-metal sulfides,[26–29] metal–organic frameworks (MOFs),[30–33] silver-based catalysts,[34,35] single-atom catalysts (SACs),[36–41] and metal clusters,[42–46] significant progress has also been achieved in the design of homogeneous molecular catalysts. Molecular catalysts benefit from well-defined coordination environments and operate in homogeneous solution, enabling detailed mechanistic investigation through *in situ* spectroscopic techniques. Their discrete nature allows systematic tuning of electronic properties *via* metal selection and rational ligand modification, often leading to high selectivity, robustness, and the possibility of immobilization on electrodes or solid supports.[47,48] These features make molecular systems particularly valuable for elucidating catalytic principles relevant to both natural hydrogenases[49–51] and synthetic analogues.

Molecular HER catalysts based on earth-abundant 3d metals, most notably cobalt,[52–62] nickel,[63–75] and iron[76–79] are especially well represented in the literature. In contrast, despite copper complexes exhibiting rich coordination chemistry, accessible redox states, and favorable photophysical properties, and despite their established utility in various types of transformations,[80–89] also including CO_2 reduction and water oxidation,[84–92] their application to HER has only gained significant momentum over the past decade (Fig. 2).[93–112] It is noteworthy, however, copper participation in HER research

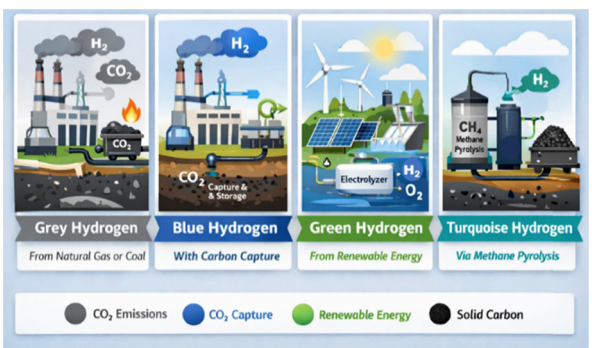

Fig. 1 Schematic showing types of hydrogen.

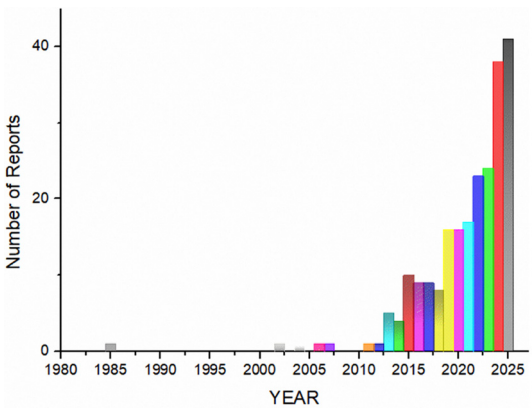

Fig. 2 Histogram depicting the upward trend in the number of publications per year identified through a Scopus search for molecular copper-based hydrogen evolution catalysts. Search query: TITLE-ABS-KEY ("copper complex" AND "hydrogen evolution catalyst"). Data retrieved on 12 February 2026.

dates back to Pentland's work in 1950s, when metallic copper electrodes, rather than discrete molecular copper complexes, were employed to investigate the kinetics of hydrogen evolution in aqueous media.[113,114] In contrast, the rational development of molecular copper HER catalysts has only attracted considerable attention during the past decade.

However, progress toward industrial use of molecular catalysts is constrained by short-lived activity and degradation pathways that compromise their molecular integrity. In fact, molecular catalysts generally have a strong propensity, under reducing conditions in the presence of acidic medium, to break down and form heterogeneous reduction products,[115–120] such as metallic nanoparticles or deposits either during photo- or electrocatalytic reaction, which can be active HER electrocatalysts in their own right.[49,101,102,105,108,121–125] While this challenge is common to molecular HER catalysts based on cobalt, nickel, iron, and copper, copper systems present additional complications owing to the inherent instability of Cu(I) intermediates, which may undergo disproportionation, ligand dissociation, or transformation into Cu(0) and CuO_x containing species. Therefore, the subtle distinctions between homogeneous and heterogeneous behavior should be carefully examined, and robust techniques for accurately identifying the true active catalytic species should be rigorously applied.

While copper-based nanomaterials, including oxides such as Cu_2O and CuO, as well as nanoclusters have demonstrated significant catalytic activity and played a pivotal role in advancing photo- and electrocatalytic hydrogen evolution,[98,126–128] molecular copper catalysts offer several distinct advantages that can enable greater control over catalytic performance. A primary advantage is the well-defined structure of molecular systems, which allows fine tuning of the coordination environment including both the first and second coordination sphere that influence the electronic properties such as redox potentials and kinetics through rational ligand design. This synthetic versatility and level of coordination control is not readily achievable in nanoparticle-based systems, where surface heterogeneity and ill-defined active sites often complicate mechanistic interpretation.

In addition, nanoparticle systems typically operate through complex surface processes whereas molecular catalysts provide direct insight into reaction mechanisms, enabling the identification of catalytic intermediates through detailed spectroscopic and electrochemical studies. Such mechanistic information is critical for guiding rational improvements. Furthermore, molecular platforms allow the incorporation of second-sphere functionalities, such as pendant proton relays and hydrogen-bonding networks, which can significantly enhance catalytic rates and lower overpotentials, features that are difficult to systematically engineer in metal oxide nanomaterials.

Another key advantage lies in the tunability and modularity of molecular catalysts. Ligand frameworks are not only used to optimize the activity, selectivity, and stability, but also to introduce anchoring groups for immobilization onto conductive supports, thereby bridging homogeneous and heterogeneous catalysis. Finally, molecular systems offer the possibility of integration into photocatalytic assemblies with tailored photosensitizers to produce dyads and triads.[129–131]

Despite these advantages, molecular copper catalysts still face challenges in stability and durability under operating conditions, which remain areas where metal oxide nanoparticles often outperform them. Nevertheless, the ability to achieve structure–function correlations and rational design positions molecular systems as a powerful platform for next-generation HER catalyst development, complementing, and in some aspects, offering advantages over traditional CuO/Cu_2O nanomaterials. This review therefore showcases recent examples of copper-based catalysts utilized for the hydrogen evolution reaction. Given that hydrogen production can be accomplished under both photocatalytic and electrocatalytic conditions, we begin with an explanation of key metrics and fundamental concepts, followed by a section outlining the methods and techniques used to probe the homogeneity of molecular catalysts. Subsequently, we analyze examples of copper-based catalysts, focusing on their structural features, synthetic strategies and catalytic performance, while precisely extracting catalytic metrics from each case, with particular attention to the true characteristics of the catalytically active species. We then conclude with an overview of the current challenges and future perspectives in this field.

2. Key metrics for evaluating catalytic performance

To evaluate the catalytic performance of a catalyst, certain figures of merit are generally used. The main figures of merit used to evaluate either photocatalytic or electrocatalytic activity are turnover number (TON) and turnover frequency (TOF). While other terms are used only for photocatalytic activity, such as quantum efficiency (Φ), others are highly specific to electrocatalytic performance, such as overpotential (η), Faradaic efficiency (FE), onset potential (E_{ons}) or the potential at half of the catalytic current ($E_{cat/2}$).

It should be noted that direct comparison between different catalytic systems is challenging because catalytic conditions under which the HER is performed generally vary between laboratories, such as proton source, electrolyte, solvent, working electrode and applied potential in the case of electrocatalytic activity, photosensitizer, sacrificial electron donor (SED) as well as irradiation time and source in the case of photocatalytic activity. Concise definitions of the principle figures of merit are provided below.

2.1. Turnover number (TON)

This defines the total number of catalytic cycles a catalyst can perform before it becomes inactive under given reaction conditions. As a result, TON serves as a direct measure of catalyst durability and operational lifetime, rather than intrinsic activity. A high TON indicates that the catalyst can sustain repeated turnover events without significant degradation, which is particularly important for practical and large-scale hydrogen

production. In molecular HER catalysis, TON is especially valuable for distinguishing between short-lived, highly active systems and those that combine activity with long-term stability. For example, a catalyst exhibiting high current but low TON may undergo rapid decomposition, often through ligand dissociation or conversion to heterogeneous species such as metal nanoparticles. Conversely, a high TON suggests that the molecular structure remains intact over extended operation, supporting true homogeneous catalysis. However, TON should always be interpreted alongside complementary metrics (see below) such as turnover frequency (TOF) and Faradaic efficiency (FE), as it does not provide information on catalytic rate or selectivity.

Importantly, a more rigorous definition is that the TON "specifies the maximum use that can be made of a catalyst for a special reaction under defined reaction conditions by the number of molecular reactions or reaction cycles occurring at the reactive centre up to the decay of activity."[132,133] As in eqn (2), the TON achieved by the catalyst reflects the number of hydrogen molecules (n_{H_2}) produced per active species of the catalyst (n_{Cat}).

$$\mathrm{TON} = \frac{\text{moles of } H_2 \text{ molecules}}{\text{moles of catalyst}} = \frac{n_{H_2}}{n_{cat}} \qquad (2)$$

It is worth mentioning, as implied in the definition above, that TON should be interpreted with caution, as not all catalyst molecules are activated under the catalytic process, and a fraction of the active species may undergo deactivation during catalysis (Fig. 3). Thus, the TON is essentially based on the actual fraction of catalyst species that are activated and truly undergo catalytic cycles, meaning that some catalyst molecules may be activated during the reaction and others may not. For example, during electrocatalysis, molecules that are in close proximity to the electrode surface, *i.e.* within the double layer, are expected to successfully undergo charge transfer reaction and eventually get activated. Therefore, these molecules will probably be involved in the catalytic cycle, while other molecules may never be activated due to mass transport or other reasons like degradation or substrate depletion. Finally, the activated molecules may remain in the catalytic cycle and be regenerated again to undergo another catalytic cycle or be deactivated. This can be illustrated in Fig. 3.

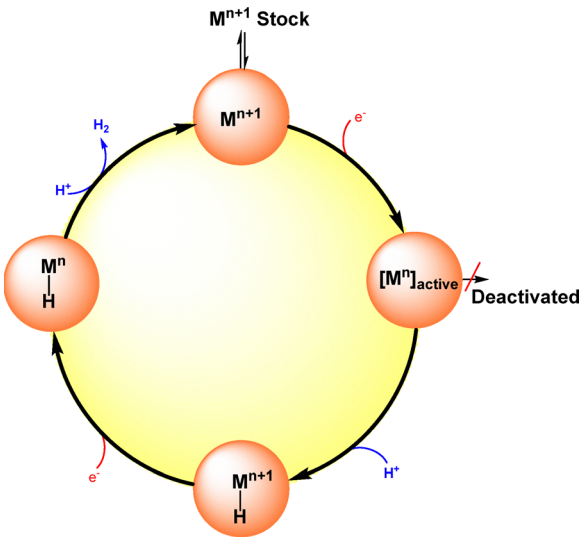

Fig. 3 Schematic diagram illustrates a general catalytic cycle in which a metal complex M^{n+1} functions as the active site for the hydrogen evolution reaction (HER). For simplicity, the electron-proton sequence mechanism (ECEC) has been selected; however, the other possible HER catalytic mechanism (EECC) remains applicable.

2.2. Turnover frequency (TOF)

It reflects the intrinsic catalytic rate, describing how rapidly a catalyst can convert substrate to product per active site per unit time. In contrast to TON, which measures durability, TOF provides direct insight into the kinetic efficiency of the catalytic process. A high TOF indicates fast and efficient catalytic turnover, making it a key parameter for comparing the activity of different catalysts under similar conditions. However, TOF must be interpreted with care, as it is often derived under specific assumptions regarding the number of active sites and the reaction mechanism. Overestimation can occur if not all catalyst molecules are catalytically competent or if heterogeneous species contribute to the observed activity. Therefore, TOF is most meaningful when considered alongside TON, overpotential, and mechanistic evidence to provide a balanced assessment of catalytic performance.

The most rigorous definition of TOF is that "It measures the instantaneous efficiency of the catalyst, it can be derived from the number of the turnovers of the catalytic cycle with respect of the time per active site".[132] Eqn (3) is commonly used to estimate the TOF of molecular catalysts.[133]

$$\mathrm{TOF} = \frac{\text{moles of } H_2 \text{ molecules}}{\text{moles of catalyst} \times \text{time}} = \frac{\mathrm{TON}}{\text{time}} \qquad (3)$$

It is important to note that this turnover frequency is typically obtained from the controlled potential electrolysis (CPE) experiment. In the case of photo or electrocatalytic HE experiments, it can be derived from the overall turnover number (TON) per unit time of the experiment. Additionally, the maximum TOF (TOF_{max}) is a distinctive characteristic of the catalyst and will be discussed later in this section.

2.3. Quantum yield (Φ)

It is a key parameter in photocatalytic systems, representing the efficiency with which incident photons (monochromatic) are converted into chemical products. A high quantum yield indicates minimal energy loss through recombination or non-productive pathways, and is therefore essential for evaluating and comparing photocatalysts. However, it should be interpreted carefully, as it depends on experimental conditions such as light intensity, wavelength, and reactor geometry.

Quantum yield therefore measures the ratio between the number of photons used to convert protons into H_2 and the number of incident photons (I_0), eqn (4). The quantum yield

reflects the efficiency of the photocatalytic system in converting light to hydrogen.

$$\Phi_{H_2} = \frac{\text{moles of } H_2 \text{ molecules}}{\text{moles of incident photons}} \times 100\% = \frac{n_{H_2}}{I_0} \times 100\% \quad (4)$$

The number of incident photons (I_0); can be calculated as follows:[134]

$$I_0 = PSt\frac{\lambda}{hc} \quad (5)$$

where P is the total power of the light in Joules per second, S is the incident irradiation area in m^2, t is the irradiation time in s, λ is the incident wavelength in m, h is the Planck's constant (6.626×10^{-34} J s) and c is speed of light (3×10^8 m s^{-1}).

2.4. Diffusion coefficient (D)

The diffusion coefficient reflects the rate at which a catalyst or reactant is transported through solution to the electrode surface, and thus plays a critical role in determining mass transport during electrocatalysis. A higher diffusion coefficient enables faster replenishment of active species at the electrode interface, supporting sustained catalytic currents and minimizing diffusion limitations. In molecular HER systems, D is particularly important for interpreting electrochemical data, as it helps distinguish between kinetic and mass transport effects. Consequently, accurate evaluation of D is essential for reliable analysis of catalytic performance and for comparing systems under different experimental conditions. Since the peak current (i_p) in cyclic voltammetry depends on the catalyst concentration, its intrinsic electrochemical properties, and the scan rate, the diffusion coefficient (D) of the catalyst can therefore be determined from the slope of the linear plots of peak current (i_p) and the square root of the scan rate ($\upsilon^{1/2}$) using the Randles–Ševčík equation (eqn (6)).[135–137]

$$i_p = 0.4463nFAC^0\left(\frac{nF\upsilon D}{RT}\right)^{\frac{1}{2}} \quad (6)$$

In this equation, n is the number of electrons transferred (n = 1 for one electron process), F is the Faraday's constant (96 485 C mol^{-1}), A is the electrode surface area (0.071 cm^2 for common 3 mm-diameter glassy carbon electrode), C^0 is the catalyst's concentration (mol cm^{-3}), R is the gas constant (8.314 J mol^{-1} K^{-1}), υ is the scan rate (V s^{-1}), D is the diffusion coefficient (cm^2 s^{-1}), and T is the temperature in Kelvin.

2.5. Electrocatalytic rate constant

The observed catalytic rate constant (k_{obs}) is a widely used kinetic parameter for benchmarking molecular hydrogen evolution catalysts, as it provides a quantitative measure of the intrinsic rate of H_2 formation under defined conditions. In electrochemical studies, k_{obs} is most commonly known as TOF_{max} and extracted from cyclic voltammetry (CV) data using the plateau catalytic current (i_{cat}) observed in the presence of a proton source. Under conditions where catalysis is diffusion-controlled and substrate is in excess, k_{obs} can be estimated using the relationship developed by Savéant and co-workers,[133,138,139] where the ratio of catalytic to non-catalytic current (i_{cat}/i_p) is plotted *versus* the inverse of the square root of the scan rate (ν = scan rate) as shown in eqn (7) below. This approach allows k_{obs} to be determined without bulk electrolysis and enables rapid comparison of catalyst kinetics across different systems.

$$\frac{i_{cat}}{i_p} = \frac{n_{cat}}{0.446}\sqrt{\frac{RTk_{obs}}{F\nu}} \quad (7)$$

where n_{cat} is the number of electrons involved in the catalytic process, R is the universal gas constant (8.314 J mol^{-1} K^{-1}), T is the temperature in K, and F is the Faraday's constant (96 485 C mol^{-1}) and ν is the scan rate (V s^{-1}).

It should be pointed out that eqn (7) is based on an approximate kinetic treatment assuming a first-order or pseudo-first-order EC mechanism involving freely diffusing molecular species. In certain studies, this equation was used to estimate catalytic rates even for systems governed by more complicated or not fully elucidated catalytic mechanisms.[86,140,141] It is important to consider that CVs of the molecular catalytic system provide insight into the nature of the electrocatalytic process. The peaked wave shapes observed usually during addition of proton source indicate that, under these conditions, the electrocatalytic response is influenced by both substrate diffusion and the kinetics of the catalytic reaction. In contrast, under "pure kinetic" control, where the current is limited solely by the homogeneous catalytic steps in solution and substrate depletion effects are negligible, the CVs are expected to exhibit *S*-shaped profiles that reach a well-defined limiting catalytic current (i_{cat}).[86,142] A final remark concerning eqn (7) is that, under "pure kinetic" catalytic conditions, the catalytic current (i_{cat}) is not expected to depend on the scan rate. Achieving this regime often requires the use of very high scan rates (typically >1–20 V s^{-1}), where mass-transport limitations are minimized. In this kinetic regime, i_{cat}/i_p remains approximately constant, whereas the peak current of the noncatalytic redox couple (i_p) retains its characteristic dependence on the square root of the scan rate. Consequently, the i_{cat}/i_p ratio is expected to decrease with increasing scan rate, and therefore, a plot of i_{cat}/i_p *versus* the inverse square root of the scan rate should yield a linear relationship, from its slope TOF_{max} (k_{obs}) can be extracted.

2.6. Faradaic efficiency (FE)

It is important in electrocatalysis and is analogous to quantum yield (Φ) in a photocatalytic system, as it relates to the efficiency of electron utilization in electrochemistry compared to the efficiency of photon utilization in photochemistry.

Faradaic efficiency reflects the selectivity of an electrocatalytic process, indicating the fraction of the total charge that is effectively converted into the desired product, such as H_2 in HER. A high FE signifies that parasitic side reactions are minimized and that the measured current predominantly arises from the targeted catalytic transformation. This parameter is therefore essential for evaluating catalyst performance beyond activity alone, particularly in distinguishing efficient

catalysts from those that generate significant byproducts or undergo competing processes. Reliable determination of FE is critical for assessing the practical applicability and energy efficiency of electrocatalytic systems.

Faradaic efficiency measures the fraction of the total electrical input (charge) used to convert proton to hydrogen. Faradaic efficiency (FE) can therefore be calculated on the basis of the total charge (Q) consumed and the amount of H_2 evolved, using eqn (8).

$$\mathrm{FE}\% = \frac{2Fn}{Q} \times 100 \tag{8}$$

where F is Faraday's constant = 96 485 C mol^{-1}, n = number of moles of H_2 and Q is the charge consumed.

2.7. Overpotential (η)

It is the difference between the applied potential (E_{appl}) required to drive the HER at specific rate and the known (formal) thermodynamic potential of the HER (E°) in the absence of the catalyst.[142] The overpotential can therefore be formulated as follows:

$$\eta = |E_{\mathrm{appl}} - E^{\circ}| \tag{9}$$

The overpotential (η) is a useful parameter in electrocatalysis. It is proportional to the catalytic current density (j) in the Tafel plot.[143] Within the kinetically controlled regime, increasing overpotential (η) increases the current density (j), which gives rise to the linear Tafel region, the latter can be utilised to extract valuable mechanistic data and electrocatalytic performance.[144]

Determination of the overpotential (η) sometimes vary in literature and care should be taken when comparing overpotential of different catalysts for the HER.[145] In some cases, overpotential is determined using the onset potential, which is the potential at the base of the catalytic wave at which the current begins to deviate from the background current obtained in the absence of catalyst. Appel and Helm, in 2014, recommended using $E_{\mathrm{cat/2}}$ (see Fig. 4),[143] the potential at which the current is half that of the catalytic wave current (i_{cat}), to be chosen to determine the overpotential. Applying this method would enable more consistency in the literature with regard to determining and reporting both $E_{\mathrm{cat/2}}$ and overpotential (η) used for various catalysts.

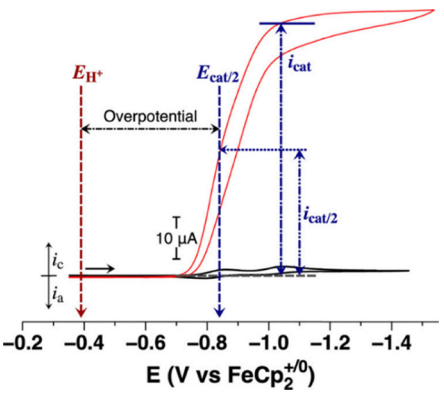

Fig. 4 Cyclic voltammogram used to illustrate $E_{\mathrm{cat/2}}$ and the definition of overpotential (η) proposed by Appel and Helm.[143] Reproduced from ref. 143 with permission from American Chemical Society,[143] copyright 2015.

The half-wave potential ($E_{\mathrm{cat/2}}$) is the potential at which the catalytic wave reaches half of its plateau current (i_{cat}) (Fig. 4).[143] At this point it is important to note that the thermodynamic potential for proton reduction $\left(E^{\circ}_{\mathrm{H^+/H_2}}\right)$ is not a fixed value but depends strongly on both the proton source (Brønsted acid) and the solvent. Variations in acid strength across different media lead to changes in pK_a values, which in turn directly influence the thermodynamic driving force for hydrogen evolution. For weak proton donors, the formal thermodynamic potential for H_2 generation $\left(E^{\circ}_{\mathrm{H^+/H_2}}\right)$ is directly related to the pK_a of the acid and can be estimated using established thermodynamic relationships (eqn (10) and (11)) that incorporate pK_a values in the relevant organic solvent.[50,149] Extensive compilations of pK_a values for a wide range of acids in nonaqueous media are available in the literature.[146,150] Fig. 5 summarizes the thermodynamic potentials of common Brønsted acids referenced to the ($Fc^{+/0}$) couple in acetonitrile, along with their corresponding pK_a values, as adapted from McCarthy *et al.*[146] and other studies.[147,148]

$$E^{\circ}_{\mathrm{HA/A^-,H_2}} = E^{\circ}_{\mathrm{H^+/H_2}} - \left(2.303\frac{RT}{F}\right) \times \mathrm{p}K_a \tag{10}$$

Substituting R, F and T values as defined previously into eqn (10) yields eqn (11).

$$E^{\circ}_{\mathrm{HA/A^-,H_2}} = E^{\circ}_{\mathrm{H^+/H_2}} - 0.059 \times \mathrm{p}K_a \tag{11}$$

Fig. 5 presents the pK_a scale of Brønsted acids in acetonitrile together with their corresponding thermodynamic proton reduction potentials $\left(E^{\circ}_{\mathrm{H^+/H_2}}\right)$ referenced to the $Fc^{+/0}$ couple.

Finally, a variety of reference electrodes are employed in electrochemical studies, and redox potentials are typically reported with respect to the reference electrode used in the experiment. However, it is good practice to recognize that the International Union of Pure and Applied Chemistry (IUPAC) recommends the ferrocene/ferrocenium (Fc^+/Fc) redox couple as a convenient internal reference for reporting and comparing electrochemical data.[151,152] Expressing potentials relative to Fc^+/Fc ($Fc^{+/0}$) facilitates meaningful comparison across different HER studies and experimental setups. Accordingly, conversion equations are often required to translate potentials measured *versus* commonly used reference electrodes, such as $Ag^+/AgNO_3$, Ag/AgCl, saturated calomel electrode (SCE), normal hydrogen electrode (NHE), relative hydrogen electrode (RHE) to the Fc^+/Fc scale. The following eqn (12)–(15) provide practical relationships for these conversions.[153,154] Unless otherwise stated, all the potentials discussed herein are referenced to $Fc^{+/0}$

$$E(\mathrm{V}\ \textit{vs.}\ \mathrm{Fc^{+/0}}) = E(\mathrm{V}\ \textit{vs.}\ \mathrm{NHE}) - 0.63 \tag{12}$$

$$E(\mathrm{V}\ \textit{vs.}\ \mathrm{Fc^{+/0}}) = E(\mathrm{V}\ \textit{vs.}\ \mathrm{SCE}) - 0.38 \tag{13}$$

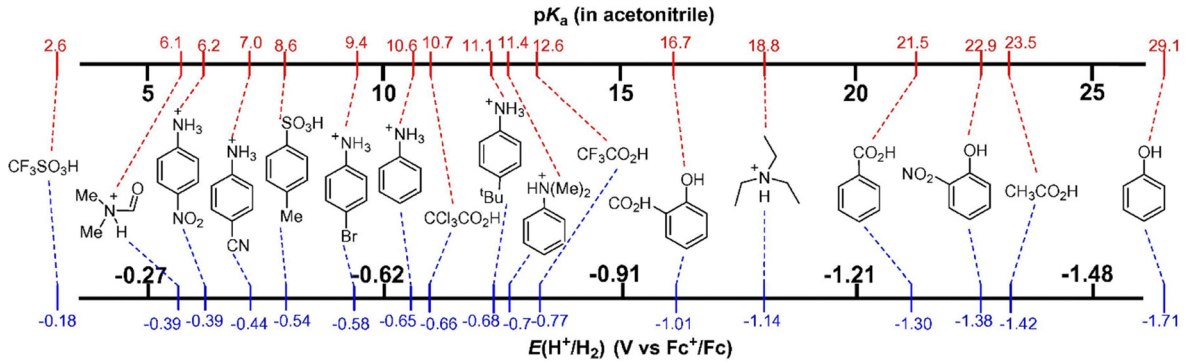

Fig. 5 The thermodynamic potential $\left(E^{\circ}_{H^+/H_2}\ vs.\ Fc^+/Fc\right)$ of common Brønsted acids and their corresponding pK_a values in MeCN adopted from McCarthy *et al.*[146] and other corresponding ref. 147 and 148. Reproduced from ref. 148 with permission from Elsevier,[148] copyright 2020.

Table 1 Summary of the figures of merit used in electro- and photo-catalytic HER

Metric	Meaning	Main use	Limitation
TON	Total turnovers	Durability	Active fraction uncertainty
TOF	Rate	Kinetic	Active site counting
FE	Selectivity	Electrolysis efficiency	Gas quantification/cell-design dependant
η	Energy efficiency	Benchmarking	Reference dependence
k_{obs}	Kinetic	Kinetic data from CV	Kinetic control
Φ	Photon efficiency	Photocatalysis	Reactor dependence

$$E(\text{V } vs.\ \text{Fc}^{+/0}) = E(\text{V } vs.\ \text{Ag/AgCl}) - 0.41 \quad (14)$$

$$E(\text{V } vs.\ \text{RHE}) = E(\text{V } vs.\ \text{Ag/AgCl}) + 0.059\ \text{V} \times \text{pH} + 0.197\ \text{V} \quad (15)$$

Table 1 summarizes the figures of merit discussed above, highlighting the utility and limitations of each metric. It is important to note as well that it is often difficult to obtain a complete and consistent set of parameters for every catalyst reported in the literature. This underscores the need for greater standardization in the measurement and reporting of catalytic metrics in future studies.

3. Evaluating catalyst homogeneity in molecular systems

As discussed in Section 1, establishing whether a molecular catalyst operates through a truly homogeneous pathway remains a central challenge in molecular catalysis. Under catalytic conditions, many transition metal complexes can transform into heterogeneous species, necessitating careful and systematic evaluation of catalyst integrity. This section outlines the key tools and techniques commonly employed and recommended for identifying the nature of the active species during molecular catalysis. For further detailed discussion, the reader is referred to several comprehensive reviews in the field, including the tutorial review by Dempsey and co-workers,[155] the seminal work by Finke and Widegren,[156] and contributions by Artero and Fontecave,[118] among others.[119,157,158]

3.1. Stripping analysis

Stripping peaks refer to anodic (and occasionally cathodic) signals observed upon the re-oxidation of species that have been deposited on the electrode surface during a preceding electrochemical step.[159] In molecular electrocatalysis, particularly for copper and other transition metal complexes, these signals provide critical insight into the nature of the active species, enabling differentiation between homogeneous molecular catalysis and heterogeneous processes involving electrodeposited metals.

In copper-based systems, reduction of a Cu(II) complex typically generates Cu(I), which is often thermodynamically unstable and prone to disproportionation into Cu(II) and Cu(0) (eqn (16)). Under sufficiently negative potentials, further reduction can lead directly to the formation of metallic Cu(0), which readily deposits onto the electrode surface. Upon reversing the scan toward more positive potentials, the deposited Cu(0) is re-oxidized to soluble Cu(I) or Cu(II), producing a characteristic anodic stripping peak.

$$2Cu^+ \rightarrow Cu + Cu^{2+} \quad (16)$$

The position of the stripping peak is often diagnostic of the deposited metal, while its intensity is proportional to the amount of deposited material, providing a semi-quantitative measure of metal accumulation. The observation of such features during catalytic experiments frequently indicates that at least part of the observed activity may arise from *in situ* generated heterogeneous species rather than the intact molecular catalyst.

Fig. 6 illustrates the cyclic voltammetry of N_4-macrocyclic copper(II) complex (**Cu_{26}**, for the structure of this complex see

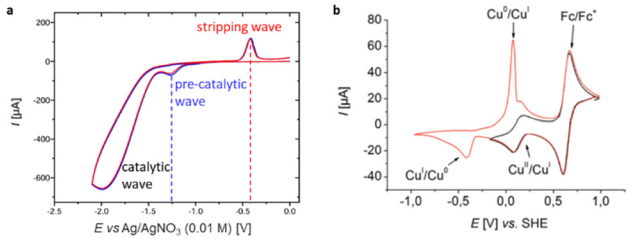

Fig. 6 Cyclic voltammetry of a 1 mM MeCN solution of (a) **Cu_{26}**, in presence of 80 mM of acetic acid, (blue) in the absence of mercury and (red) in the presence of 0.5 mL of mercury. Conditions: 0.1 M $(NBu_4)PF_6$, glassy carbon working electrode (d = 3 mm, A = 0.071 cm^2), 293 K, scan rate 100 mV s^{-1} (reproduced from ref. 100 with permission from Royal Society of Chemistry,[100] copyright 2021), (b) N_5-copper complex reported as a HER pre-catalyst by Siewert's group showing the stripping wave of Cu^0 with reference to Fc. Reproduced from ref. 101 with permission from Royal Society of Chemistry,[101] copyright 2016.

Fig. 22), which exhibits excellent catalytic activity at a relatively low overpotential of ~0.21 V in acetonitrile in the presence of 80 mM acetic acid. Notably, a distinct stripping wave is observed in the reverse anodic scan at approximately −0.45 V *vs.* Fc^+/Fc (Fig. 6a), indicating the formation of electrodeposited copper species under catalytic conditions. These observations are consistent with earlier studies on copper-based HER systems reported independently by Siewert[101] and Chen[160] in 2016. The Siewert group investigated a series of N_5-donor copper complexes and demonstrated high catalytic activity at pH 2.5 in phosphate buffer, while providing compelling evidence that the true active species arise from a combination of Cu(0) and Cu_2O deposited on the electrode surface. Importantly, their cyclic voltammetry data revealed a similar anodic stripping feature at nearly identical potentials (Fig. 6b), closely mirroring that reported later in Brooker's work (2021).[100] Similarly, Chen and co-workers[160] described a Cu(II) oxime-based system that generates Cu(0) nanoparticle films during CPE experiment, as confirmed by SEM and EDX analyses. These *in situ* formed deposits were shown to be responsible for the observed high and sustained HER activity in neutral aqueous media.

Noteworthy, similar phenomena are observed for other first-row transition metals,[118,124,155,161,162] including cobalt, nickel, and iron, where electrodeposition under catalytic conditions can complicate mechanistic interpretation. Consequently, stripping analysis has become increasingly employed as diagnostic observation/tool for assessing catalyst integrity and for distinguishing true homogeneous catalysis from surface-mediated processes.

3.2. Rinse test

The rinse test is a simple and widely employed diagnostic method for assessing the homogeneity of molecular electrocatalysts.[118,156,162] In this procedure, the working electrode used typically during controlled-potential electrolysis (CPE), and in some cases after CV, is gently rinsed with the reaction solvent or electrolyte, and then transferred to a fresh electrolyte solution containing no dissolved catalyst. Electrolysis (and CV) is subsequently performed under identical conditions to evaluate whether catalytic activity persists. The observation of sustained activity in the absence of the molecular catalyst is typically taken as evidence for the formation of catalytically active, electrodeposited species, indicating a heterogeneous contribution.

While straightforward and convenient, the rinse test should be interpreted with caution. False positives and negatives are possible, and the method alone cannot unambiguously establish the nature of the active species. For instance, loosely bound deposits may be partially removed during rinsing, leading to underestimation of heterogeneous contributions, whereas strongly adsorbed molecular species may still exhibit activity and be misinterpreted as deposited materials. Therefore, rinse tests are most informative when combined with complementary techniques such as cyclic voltammetry (*e.g.*, stripping analysis), surface characterization (SEM, EDX, XPS), and spectroscopic monitoring.

Further details regarding this diagnostic can be found in the literature.[155,156] A representative example in the context of copper-based HER catalysis is provided by Brooker and co-workers, who subsequently investigated **Cu_{26}** in neutral phosphate buffer.[102] The rinse test revealed significant residual activity, with catalytic performance comparable to that observed in the homogeneous solution (Fig. 7a). Subsequent surface characterization confirmed the presence of deposited species on the glassy carbon electrode, predominantly composed of copper and cuprous oxide (Fig. 7b). All together, these results indicate that the observed HER activity is at least partially attributable to *in situ* generated heterogeneous species rather than exclusively to the molecular catalyst. Most importantly, these results would not be possible without the initial signs from Rinse test data.

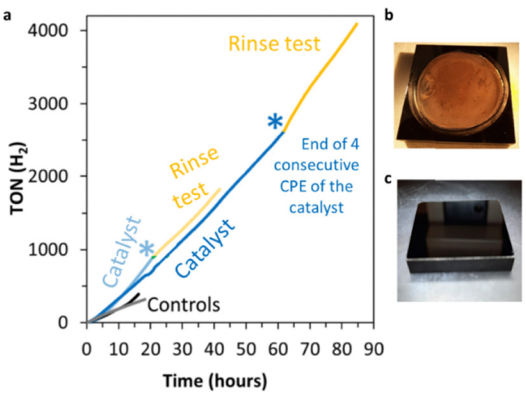

Fig. 7 (a) Hydrogen production over time by **Cu_{26}** (0.3 mM) in 1 M pH 7 aqueous phosphate buffer solution, with a large plate glassy working electrode (working A = 2.7 c m^2), held at $E_{applied}$ = −1.1 V *vs.* Ag|AgCl. A star indicates when the electrolyte has been changed. Dark and light blue: initial CPE runs (dark blue = four consecutive experiments with no changes; light blue = single short CPE run); gold: 'rinse and repeat test' results *i.e.* after rinsing the glassy working electrode after the initial CPE run, the cell was rinsed and refilled with fresh electrolyte (containing no additional **Cu_{26}**); grey: control, $Cu(OAc)_2{\cdot}H_2O$; black: control, $Cu(BF_4)_2{\cdot}6H_2O$. (b and c) glassy carbon working electrode after and before CPE experiment. Adapted from ref. 102 with permission from Royal Society of Chemistry,[102] copyright 2024.

3.3. Mercury test

Mercury is well known for its ability to amalgamate with metallic particles and to adsorb onto metal surfaces, thereby effectively poisoning heterogeneous metal catalysts. As a result, mercury poisoning has long been employed as a classical diagnostic test to distinguish between homogeneous and heterogeneous catalysis.[156,158,163,164] In practice, the experiment is performed under standard catalytic conditions in the presence of a drop of elemental mercury. A significant suppression of catalytic activity upon addition of mercury is generally taken as evidence for heterogeneous, metal-based catalysis. In contrast, if the catalytic activity is retained, the test is considered negative, supporting a homogeneous catalytic pathway. Despite its simplicity and ease of implementation, the mercury poisoning test has notable limitations. It is not universally applicable, as mercury may participate in side reactions or interact directly with molecular catalysts,[163] potentially leading to misleading conclusions. Therefore, it is essential to verify that mercury does not react with the pre-catalyst or active species, for example by conducting appropriate control experiments. A useful approach to validate the reliability of this test is to perform a control experiment using a known heterogeneous catalyst under identical conditions in the presence of mercury, thereby confirming that the metal surface is indeed susceptible to poisoning. Failure to conduct such controls can lead to erroneous interpretations. For instance, in some past report on a supposed homogeneous ruthenium catalyst, the absence of proper validation of the Hg(0) test led to an incorrect assignment of the catalytic species; subsequent reinvestigation revealed that the observed activity originated from metal nanoclusters rather than a molecular catalyst.[157] Due to its high toxicity and disposal concerns, tests based on mercury as are increasingly substituted by alternative other strategies and analyses.

3.4. Electrode surface assessment

The possible presence of heterogeneous species on the electrode surface can be probed using microscopic techniques such as scanning electron microscopy (SEM) and transmission electron microscopy (TEM).[165] These methods provide valuable information on deposited films or particles, including their size, morphology, surface topology, and film thickness. Complementary spectroscopic techniques, such as energy-dispersive X-ray spectroscopy (EDX) and X-ray photoelectron spectroscopy (XPS), enable elemental analysis and can provide insight into the oxidation state and composition of the deposited material.[166] More advanced approaches, including atomic force microscopy (AFM), can further track the growth and evolution of nanostructures during catalysis, offering mechanistic insight into catalyst transformation pathways.[167] Noteworthy, scanning electrochemical microscopy (SECM)[168] is now a well-established technique that has found widespread application in electrocatalysis.

TEM, in particular, is highly sensitive for detecting nanoclusters formed under catalytic conditions, even at low concentrations. However, such sensitivity can also be misleading, as the mere presence of nanoparticles does not necessarily confirm their catalytic relevance. Moreover, imaging very small clusters (<1 nm), especially for first-row transition metals, remains challenging due to low contrast. Consequently, the absence of observable deposits in SEM or TEM analyses cannot definitively rule out the formation of catalytically active nanoclusters. These limitations highlight the importance of combining microscopy with other diagnostic techniques to reliably assess catalyst homogeneity.

A notable example in the context of HER catalysis is the cobalt clathrochelate complex $[Co(dpg)_3(BF)_2]^+$ (dpg = diphenylglyoxime), first reported in 2008.[169] Despite the saturated coordination environment of the cobalt center, which initially obscured the catalytic mechanism, subsequent studies revealed that the observed activity originated from heterogeneous species.[19] Evidence included a positive rinse test following electrolysis, bleaching of UV-vis absorption features, and SEM images showing cobalt-containing nanoparticle deposits on the electrode surface after catalysis. This seminal case underscores the necessity of employing a combination of complementary techniques to distinguish between true homogeneous catalysis and catalysis arising from *in situ* generated heterogeneous materials.

3.5. *In situ* spectroscopy

Spectroelectrochemistry (SEC) and UV-visible spectroscopy enable *in situ* monitoring of the spectral properties of catalytic systems under electro- and photocatalytic conditions, respectively.[170] These techniques provide valuable insight into structural changes, intermediate transformation, and the evolution of catalytically active species during catalysis. In contrast to conventional approaches, where aliquots are withdrawn during or after the reaction for *ex situ* analysis, SEC and UV-visible spectroscopy allow continuous monitoring with minimal sample volumes while the system is actively undergoing electron transfer or light-driven processes.

In many HER systems, UV-visible spectroscopy can offer compelling evidence of catalyst transformation, such as ligand dissociation or aggregation, often manifested by a loss of characteristic absorption bands or an increase in background scattering due to precipitate formation. Despite their diagnostic power, SEC and UV-visible spectroscopy remain underutilized in studies of hydrogen evolution and other small-molecule catalytic activation.[155,171] Their broader adoption is expected to significantly enhance mechanistic understanding and catalyst evaluation in the near future.

3.6. Dynamic light scattering (DLS)

Importantly, the diagnostic tests discussed above are primarily applied to electrocatalytic HER systems, whereas assessing catalyst homogeneity becomes more challenging under photocatalytic conditions.[172,173] In such cases, dynamic light scattering (DLS) offers a convenient and powerful complementary technique, as it enables the detection of colloidal particles in solution, typically within the $\sim$1 nm to 1 μm size range.[156] Because DLS measurements are performed directly in solution,

Table 2 Summary of recommended tests used to evaluate the homogeneity of photo- or electro-catalysts

Method	Detects	Strength	Limitation
Stripping CV	Deposited metal	Quick electrochemical evidence	Indirect
Rinse test	Persistent surface activity	Simple	False +/−
Hg test	Metal nanoparticles/surfaces	Classical poisoning test	Non-universal
SEM/TEM	Particles/films	Visual evidence	*Ex situ*
XPS/EDX	Composition	Elemental information	Surface only
UV-Vis/SEC	Transformation in solution	*In situ* characterization	Indirect
DLS	Colloids	Solution-based	Contamination sensitive

they are particularly useful for identifying nanostructured species formed *in situ* during photocatalysis, as well as particles that may detach from the electrode under electrocatalytic conditions. This can also be supported by spectroscopic data, as degradation of the electrocatalyst and/or photosensitizer can often be readily detected by absorption spectroscopy.

However, while DLS can confirm the presence of nanoscale aggregates or clusters, it does not provide direct evidence of their catalytic relevance. As such, the detection of particles alone cannot establish whether these species are responsible for the observed activity. Additionally, DLS measurements are highly sensitive to contaminants such as dust or impurities, which can generate misleading signals and artificially inflate particle sizes. Therefore, careful sample preparation and data interpretation are essential to avoid false positives. As a result of that, DLS measurements should be interpreted in conjunction with complementary techniques such as electrochemical analysis, microscopy, and spectroscopy, to obtain a more comprehensive understanding of the nature of the active catalyst. While Table 2 summarizes the tests discussed above, along with their respective strengths and limitations, no single diagnostic method can unambiguously establish catalyst homogeneity. Reliable assignment of the active species requires joining evidence from electrochemical, spectroscopic, and surface-sensitive techniques.

4. Copper-based HER catalytic systems

Reported molecular copper catalysts or pre-catalysts for the HER can be broadly grouped into two principal classes: polypyridine-based systems and copper macrocyclic complexes alongside a few additional systems. Section 4.1 discusses the parameters that control the molecular design of copper-based HER catalyst, Section 4.2 is dedicated to discussing pre-catalyst activation and catalyst reconstruction for copper-based HER systems, then Sections 4.3 and 4.4 explore the examples of each category in details, with a comparative summary of their catalytic performances is provided in Table 3.

4.1. Molecular design parameters governing copper-based HER catalysts

Like other transition metal systems, copper offers earth abundance, low cost, and rich coordination chemistry, yet its catalytic performance is highly dependent on ligand environment and electronic stabilization of reactive intermediates. Accordingly, ligand design plays a central role in determining activity, selectivity, and long-term stability. Fig. 8 summarizes the possible ligand platforms that have been employed to coordinate Cu(II) centers, together with additional ligand designs that remain unexplored for HER.

One of the most important parameters is the nature of the donor atoms coordinating the copper center. Nitrogen-based ligands such as polypyridines,[106,110,174–178] and macrocycles[100,179–187] often provide strong coordination, tunable electronics, and access to well-defined Cu(I)/Cu(II) redox couples. Sulfur or oxygen containing ligands (Fig. 8, middle),[176,188] can enhance electron donation and mimic biological copper sites, while mixed donor frameworks such as N,S-, P,N-, or P,S-chelates may combine electronic flexibility with structural rigidity, with further examples still to be introduced. Control over the donor strength can modulate reduction potentials, proton affinity, and metal hybricity, all of which are critical for HER turnover.

A second key factor is the coordination geometry and structural flexibility of the copper center. Depending on its oxidation state and ligand environment, copper can readily adopt tetrahedral (commonly Cu(I)), square-planar (sp), square pyramidal (spy), or other distorted geometries. Because catalytic HER frequently involves interconversion between Cu(II) and Cu(I) states, ligand frameworks that can accommodate geometric reorganization may lower the energetic differences associated with electron-transfer steps. However, excessive structural lability can promote catalyst decomposition or demetallation. Comparisons between macrocyclic multidentate *versus* noncyclic systems, such as those leading to square-pyramidal and trigonal bipyramidal structures (Fig. 8), provide valuable insight into structure–activity relationships and the stability of catalytic intermediates. Therefore, the most effective systems generally balance sufficient flexibility to enable catalysis with adequate rigidity to maintain molecular integrity under reducing conditions.

Another major design principle is the incorporation of proton relays and second-sphere functionality. In the case of copper-based HER catalysts, this area remains comparatively underdeveloped and offers substantial opportunities for future advancement, unlike cobalt- and nickel-based systems where such strategies are already well established in the literature.[64,189–192] Pendant amines, carboxylates, alcohols, or other proton-responsive groups positioned near the metal center can facilitate proton-coupled electron transfer, accelerate H–H bond formation, and

Table 3 Summary of performance metrics for copper-based catalysts/pre-catalysts employed in the HER

Catalyst	TON	k_{obs}/TOF_{max}/s^{-1}	Applied potential[a]/V *vs.* Fc	Photo-electrocatalytic conditions[b] (solvent/proton source)	FE/%	CPE duration/h	Diffusion coefficient/D/cm^2 s^{-1}	Ref.
Cu_1	—	1377	−1.9	CH_3CN/AcOH (100 mM)	99	1	2.9×10^{-6}	174
Cu_2	—	81.38	−1.65	H_2O/AcOH (60 mM)	91	3	5.7×10^{-4}	196
Cu_{3a}	10	—	−1.75	DMF/AcOH (0.625 mM)	—	1	—	175
	2980 ± 20	—	—	H_2O/pH 1	80	3	—	175
Cu_{3b}	14 000	1000	−1.53	H_2O/pH 2.5	96	2		110
Cu_4	73	241.75	−1.65	H_2O/AcOH (30 mM)	94	1.6	1.1×10^{-5}	176
Cu_5	1450	—	−2.0	H_2O/pH 5	>80	1–2	—	188
Cu_6	19.7± 3.9	—	−1.9	CH_3CN/AcOH (1 M)	—	4	—	199
Cu_7	15.3 ± 2.4	—	−1.9	CH_3CN/AcOH (1 M)	—	4	—	199
Cu_8	12.8 ± 2.9	—	−1.9	CH_3CN/AcOH (1 M)	—	4	—	199
Cu_9	0	—	−1.9	CH_3CN/AcOH (1 M)	—	4	—	199
Cu_{10}	—	1473	−1.9	DMF/H_2O (95 : 5 v/v) (30 mM AcOH)	—	0.5–1	7.24×10^{-6}	177
	—	—	−1.4	0.1 M KHP buffer/pH 1.6	93	0.5	—	177
Cu_{11}	—	700	−1.9	DMF/H_2O (95 : 5 v/v) (30 mM AcOH)	—	0.5–1	2.7×10^{-6}	177
	—	—	−1.4	0.1 M KHP buffer/pH 1.6	93–98	0.5	—	177
Cu_{12}	—	926	−1.9	DMF/H_2O (95 : 5 v/v) (34 mM AcOH)	—	0.5–1	3.8×10^{-6}	177
	—	—	−1.4	0.1 M KHP buffer/pH 1.6	98	0.5	—	177
Cu_{13}	—	1153	−1.9	DMF (34 mM AcOH)	90	1	1.2×10^{-6}	106
	—	—	−1.9	0.1 M KHP buffer/pH 7	—	—	—	106
Cu_{14}	—	1682	−1.9	DMF (30 mM AcOH)	95	1	2.6×10^{-6}	106
	—	—	−1.9	0.1 M KHP buffer/pH 7	—	—	—	106
Cu_{15}	—	—	—	DMF/TFA	—	—	—	200
Cu_{16}	—	2×10^6	—	DCM/TFA	—	—	—	179
$Cu_{17a–d}$	—	—	−1.35	MeCN/TFA (70 mM)	>97	1	9.95×10^{-6} 1.55×10^{-5} 6.85×10^{-6} 7.12×10^{-6}	180
Cu_{17a}	—	4.3×10^4	−1.25	MeCN/TFA (60 mM)	>96	1	9.95×10^{-6}	181
Cu_{18}	—	6.8×10^4	−1.25	MeCN/TFA (60 mM)	>95	1	1.51×10^{-5}	181
Cu_{19}	—	—	−1.20	MeCN/TFA (100 mM)	>95	∼2	—	182
Cu_{20}	—	—	−1.40	MeCN/TFA (100 mM)	>95	∼2	—	182
$Cu_{21a–d}$	—	—	−1.35–−1.70	MeCN/TFA (60 mM)	>90	1	—	183
Cu_{22}	102	0.5×10^7	−1.05	DMF/TFA (100 mM)	97	0.5	—	184
Cu_{23}	18	—	−1.05	DMF/TFA (100 mM)	71	0.5	—	184
Cu_{24c}	—	—	—	H_2O/0.1 M KOH	—	2	—	185
Cu_{25}	23	—	−1.50	MeCN/TFA (150 mM)	99	2	—	186
Cu_{26}	12.5	—	−1.70	MeCN/AcOH (80 mM)	—	6	7.7×10^{-6}	100
	2628	—	−1.60	H_2O/buffer pH 7	93	62		102
Cu_{27}	2.5	—	−1.70	MeCN/AcOH (80 mM)	—	6	3.4×10^{-6}	100
Cu_{28}	<1	—	−1.70	MeCN/AcOH (80 mM)	—	6	5.4×10^{-6}	100
Cu_{29}[c]	6820	13.5	—	DMF : H_2O (4 : 1) /BIH	—	530	—	224
Cu_{30}[c]	3738	11.7	—	DMF : H_2O (4 : 1) /BIH	—	530	—	224
Cu_{31}[c]	2240	13.3	—	DMF : H_2O (4 : 1) /BIH	—	530	—	224

[a] Potentials referenced to SCE were converted to the Fc^+/Fc by subtracting 0.38 V.[153] [b] Solvents contain 0.1 M $TBAPF_6$ as the supporting electrolyte. [c] catalysts studied for HER under photocatalytic conditions.

lower the overpotential. These secondary-sphere interactions mimic enzymatic active sites, where proton delivery pathways are precisely regulated. Further discussion of this concept is provided in Section 5.1.

The first highly efficient molecular copper catalyst reported for the hydrogen evolution reaction appeared in 2014 (**Cu_{3b}**, Fig. 9). This complex features diamine–tripyridine ligand, exhibited remarkable activity in buffered aqueous solution at pH 2.5, with an estimated turnover frequency of 10 000 s^{-1}.[110] It should pointed out that this polypyridine system was well established for the cobalt(III)-based HER systems.[57,193] The discovery of this system represented an important milestone for molecular copper HER catalysis, as copper complexes had previously been explored more extensively for CO_2 reduction than for hydrogen evolution. Notably, the catalyst delivered TOF values comparable to those reported for benchmark systems based on other metals, such as nickel-diphosphines and cobalt-dioixmes.[66,141,194,195] A key structural feature of **Cu_{3b}** is its distorted trigonal bipyramidal geometry, which may facilitate the Cu(II)/Cu(I) transformation by lowering the associated activation barrier. The pentadentate ligand strongly chelates the copper center, thereby enhancing catalyst stability and suppressing decomposition. In addition, the three pyridine donors may help stabilize the reactive Cu(I) intermediate through electronic interactions, while the pendant amine groups can serve as proton relays during catalysis.

Generally, high-performance molecular copper HER catalysts are expected to combine (i) tunable donor environments, (ii) accessible Cu(I)/Cu(II) redox chemistry, (iii) efficient proton relays, (iv) resistance to decomposition, and (v) compatibility with device integration. Future progress will likely arise from

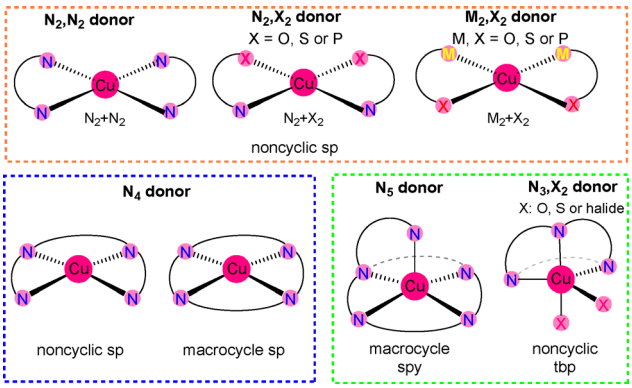

Fig. 8 Representative ligand scaffolds governing the coordination environment of Cu(II) centers employed in copper-based HER catalysts, spy: square pyramidal, tbp: trigonal bipyramidal, sp: square planar.

coupling ligand-centered design with operando mechanistic studies and computational screening, enabling more predictive development of sustainable copper-based hydrogen evolution catalysts.

These design features are also reflected in other classes of molecular copper catalysts, particularly copper macrocycles. One notable example is copper corrole, which was reported at approximately the same time as the polypyridine-based **Cu_{3b}** system.[186] This class of complexes (**Cu_{25a}**) was shown to be active toward HER, although its catalytic performance is strongly influenced by the electronic environment at the periphery of the macrocyclic framework. Similar behavior has also been observed in related systems such as copper porphyrins and other macrocyclic architectures, as discussed in the corresponding sections below. Finally, it is evident that copper-based systems represent a promising platform for HER; however, the rational design principles and lessons derived from the earliest active copper complexes (**Cu_{3b}** and **Cu_{25a}**) were not fully recognized at the initial stages of the field. As a result, many catalysts reported over the past 10 years displayed modest activity and, in several cases, underwent decomposition to form copper oxides or other heterogeneous species. This motivated us to highlight these lessons and convey their broader implications through the present review, with particular emphasis on the significant efforts devoted to identifying the true catalytically active species

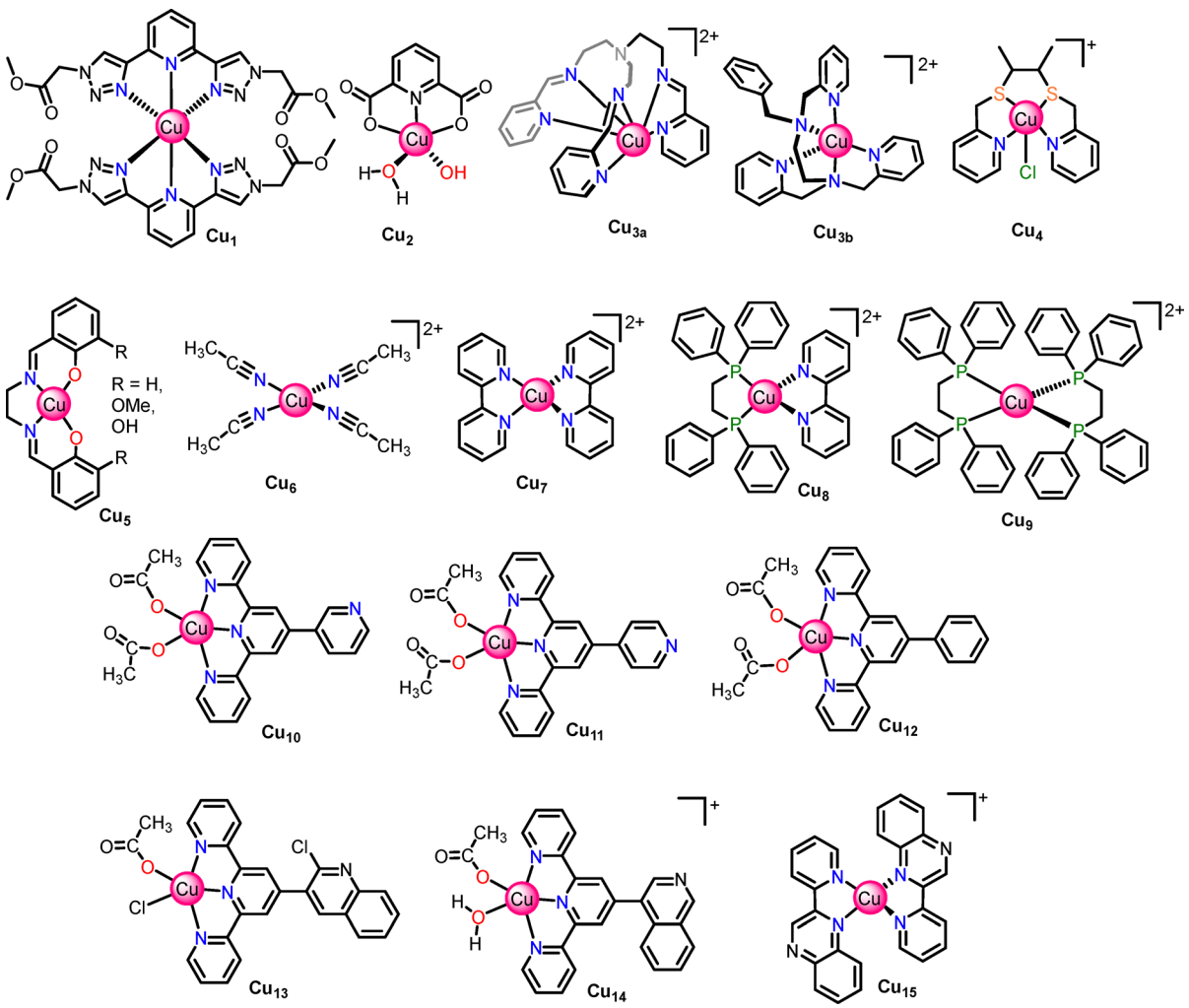

Fig. 9 Chemical structures of polypyridine-copper complexes used for HER.

in highly active copper-based HER systems. In the following sections, a more detailed analysis of these catalysts, their mechanistic activation behavior as well as lessons learned from their designs are presented.

4.2. Pre-catalyst activation and catalyst reconstruction

Unlike many idealized catalytic cycles, the initially synthesized molecular complex is often not the true catalytically active species under operating conditions. This phenomenon is not unique to copper and has been widely observed in molecular HER catalysts based on earth-abundant metals such as cobalt, nickel, and iron,[119,155–158] where reduction-induced structural rearrangements, ligand dissociation, and catalyst transformation frequently precede productive hydrogen evolution. Molecular copper systems, however, present additional complexity owing to the inherent instability of Cu(I) intermediates, which can undergo disproportionation, ligand reorganization, or transformation into heterogeneous copper-containing species. Consequently, the initially synthesized copper complex often functions as a pre-catalyst rather than the actual catalytic species. Understanding these activation pathways is therefore essential for correctly interpreting catalytic performance, establishing meaningful structure–activity relationships, and distinguishing genuine molecular catalysis from activity arising from transformed heterogeneous species. Following reduction-induced activation, molecular copper pre-catalysts generate Cu(I) intermediates that represent a key branching point in catalyst evolution (Fig. 10). Depending on catalyst structure and operating conditions, these intermediates may either remain molecular and participate in homogeneous HER or undergo disproportionation and catalyst transformation, leading to Cu(0), CuO_x, or surface-bound species that contribute to heterogeneous HER activity. The relative importance of these pathways is governed by ligand properties and reaction conditions.

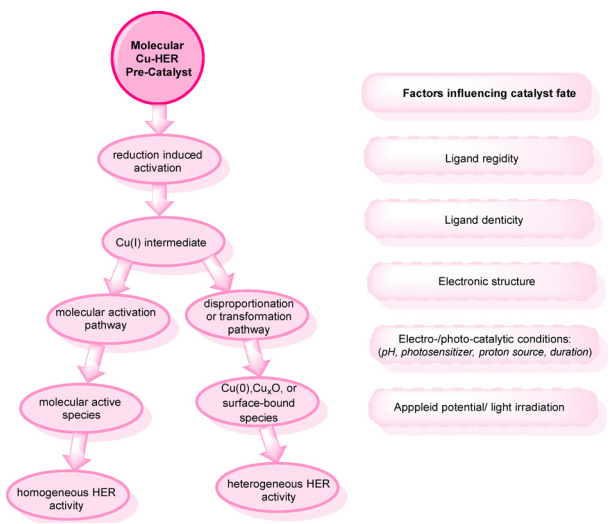

Fig. 10 Generalized activation pathways and catalyst fate in molecular copper HER systems.

Evidence for the activation pathways illustrated in Fig. 10 has been reported for numerous molecular copper HER systems discussed throughout this review. In many cases, electrochemical reduction of Cu(II) precursors generates Cu(I) intermediates that are proposed to participate directly in proton reduction.[100–102,160] However, several studies discussed in Section 3 of this review have also reported catalyst transformation through Cu(I) disproportionation, ligand dissociation, or the formation of Cu(0)- and Cu_xO-containing deposits, as evidenced by stripping experiments, rinse tests, mercury poisoning studies, and post-catalytic surface characterization using SEM, EDX, and XPS (see Sections 3, 4.3–4.5). These observations highlight that catalyst activation, catalyst integrity, and catalytic function are often closely interconnected. Consequently, evaluating the nature and stability of the active species should be regarded as an essential component of catalyst development rather than merely a mechanistic consideration.

4.3. Copper-polypyridine systems

Chen *et al.* reported in 2025 a pyridine-bistriazole octahedral diacetate copper complex (**Cu_1**, Fig. 9)[174] and investigated its efficiency as an electrocatalyst for hydrogen evolution in acetonitrile, using acetic acid (AcA), trifluoroacetic acid (TFA), or *p*-toluenesulfonic acid (TsOH) as proton sources. The **Cu_1** complex was prepared by first synthesizing the ligand, followed by coordination with copper(II) perchlorate in a 1:2 ligand-to-metal ratio. The ligand was obtained *via* a click reaction between 2,6-bis(ethynyl)pyridine and methyl 2-azidoacetate. The complex in acetonitrile displayed two irreversible reduction events; at −0.280 V assigned to $Cu^{II/I}$ and −0.866 V assigned to $Cu^{I/0}$, with a sharp 'stripping' peak at −0.50 V observed in the reverse scan of the CV, consistent with Cu^{I} disproportionation (see Section 3 for more information about stripping signals). The findings indicate that **Cu_1** exhibits a catalytic performance with an overpotentials ranging from 520 to 550 mV, faradaic efficiency of 99% and a maximum TOF of 1377 s^{-1} in acetic acid, and 535 s^{-1} and 519 s^{-1} in TFA and TsOH, respectively.

In this study, the controlled potential electrolysis (CPE) experiment was carried out at −1.9 V *vs.* Fc for one hour. Subsequent rinse tests indicated some activity of the electrode, suggesting that a small amount of catalytically active species was deposited, although this was less than the activity observed for the catalyst solution. SEM and EDX analyses of an electrode that had been immersed in the catalyst solution after 20 cyclic voltammetry (CV) scans or following CPE experiments revealed no significant deposition of the catalyst, with only trace amounts of nitrogen (N) and copper (Cu) detected (<10%). High-resolution XPS analysis was consistent with the presence of species containing Cu(0), oxide, hydroxide, and nitrogen. Overall, the study demonstrates the effect of the proton source on catalytic activity by altering the mechanism pathway, utilizing a comprehensive application of characterization techniques to identify the true active species. Additionally, the study observes the minor deposition of copper-based species on the electrode, which may serve as a high-efficiency electrocatalyst.

As the group did not conduct prolonged electrolysis, significant deposition of the active species cannot be ruled out.

In 2024, Chettri *et al*. reported the development of a soluble copper pincer catalyst (**Cu_2**, Fig. 9).[196] This complex was synthesized by reacting hydrated copper(II) nitrate with the pyridine-2,6-dicarboxylate ligand (pdc) in a 1 : 1 ratio in an ethanol–water mixture following previous literature protocol. The electrocatalytic performance of **Cu_2** for hydrogen generation was investigated in acidic aqueous environments, using KCl as the electrolyte and acetic acid (AcOH) (60 mM) as a proton source.[196] The catalyst adopted a distorted square pyramidal geometry (Fig. 9), with a water molecule occupying the axial position. It demonstrated a stability in water for of 72 hours, as well as under electrocatalytic conditions. The catalyst exhibits two distinct reduction events: one occurring at −0.99 V, attributed to the $Cu^{II/I}$ redox couple, and the other one at −1.80 V, likely associated with ligand-based reduction. The diffusion coefficient of **Cu_2** was determined in a 0.1 M KCl solution as 5.7×10^{-4} cm^2 s^{-1}. The control experiment conducted on hydrated Cu(II) nitrate in the presence of 4 mM acetic acid did not exhibit a significant increase in catalytic current readings when compared to the catalyst. The rate constant, which corresponds to the turnover frequency, was determined using the i_{cat}/i_p ratio (eqn (7), Section 2) as 81.38 s^{-1}. Nonetheless, this rate constant was established at a scan rate of 100 mV s^{-1}, and there is currently no data indicating the conditions under which catalytic current becomes independent of the scan rate, thereby enabling the appropriate application of the equation. CPE experiment conducted at E_{appl} of −1.65 V *versus* Fc, using 1 mM of the catalyst and 60 mM acetic acid (AcOH) in 0.1 M KCl aqueous electrolyte for three hours, resulted in a charge accumulation of 10.55 C. Gas chromatography (GC) analysis of the headspace confirmed the production of hydrogen gas, yielding a Faradaic efficiency of 91%. The integrity of the molecular catalyst was further demonstrated by monitoring the ultraviolet (UV) absorption at pre-and post-CPE experiment, revealing a negligible difference.

The post-CPE rinse test demonstrated no significant catalytic activity. Additionally, a soak test was performed, in which the glassy carbon electrode (GCE) was immersed overnight in an aqueous solution of 0.1 M KCl containing 1 mM of the catalyst and 60 equivalents of AcOH. Following this, the GCE was thoroughly rinsed with deionized water and subsequently placed in a fresh 0.1 M aqueous KCl solution in absence of dissolved catalyst or acid. CV analysis of the treated GCE did not reveal any redox waves, indicating the absence of detectable adsorption of any species. However, this does not definitively prove that deposition did not occur during the prolonged electrolysis in the presence of acid and catalyst. Energy-dispersive X-ray (EDX) measurements of the electrode post-CPE indicated the presence of carbon only, with no evidence of metallic copper or its oxides. Finally, the group conducted a 10-hour CPE electrocatalytic experiment similar to the previous one, it was observed that approximately 13% of the copper catalyst, as determined by UV analysis of the solution at pre-and postCPE, was converted into a deposit on the electrode, with EDX analysis revealing the presence of metallic copper along with oxygen and nitrogen elements.

Shah *et al.* synthesized in 2025 a hexa-coordinated copper catalyst ligand (**Cu_{3a}**, Fig. 9), which incorporates the tris(2-aminoethyl)amine (TREN) Schiff base ligand featuring seven nitrogen donors.[175] This configuration includes a tertiary amine in the outer coordination sphere, facilitating flexibility within the ligand framework and providing an additional site for protonation. The multidentate N-donor ligand, tris-[4-(2-pyridyl)-3-azabut-3-enyl]amine widely known as TPA, was synthesized following classical protocol, typically by reacting tris(2-aminoethyl)amine with three equivalents of pyridine-2-carbaldehyde in dry methanol. Subsequent addition of one equivalent of $Cu(ClO_4)_2 \cdot 6H_2O$ salt to a dry methanolic solution of TPA in anaerobic conditions afforded a green solution which on exposure to air for one hour afforded a green solution of **Cu_{3a}**.

The protonation of the tertiary amine significantly influences the catalytic process by promoting energetically favourable pathways for electron and proton transfer, thereby enhancing catalytic efficiency under acidic conditions. **Cu_{3a}** demonstrated two redox events in dimethylformamide (DMF) at approximately −0.60 V and −1.80 V, with the first reduction attributed to the Cu^{II}/Cu^{I} couple and the second centered on the ligand. At an applied potential of −1.75 V in DMF, in the presence of 0.625 mM acetic acid, a turnover number (TON) of 10 was achieved during a one-hour CPE experiment. Furthermore, the catalyst proved effective for hydrogen production from water across a pH range of 1.0 to 7.0, with a series of CPE experiments conducted at each pH value, resulting in relatively large overpotentials ranging from 0.686 to 0.914 V. Notably, at pH 1.0, the catalyst exhibited enhanced activity, achieving a TON of 2980 ± 20 over three hours and a faradaic efficiency exceeding 80%. In contrast, a control experiment utilizing $Cu^{II}(ClO_4)_2$ demonstrated minimal activity under similar conditions. A combination of rinse tests and SEM with energy-dispersive spectroscopy (SEM–EDS) analyses confirmed that no significant deposition of any copper-based material was observed on the electrode after the bulk electrolysis, supporting the molecular integrity of the catalyst throughout the electrolysis process, thereby substantiating its homogeneous nature.

Notably, this TREN-based copper catalyst bears close structural resemblance to one of the earliest reported molecular copper HER catalysts, (**Cu_{3b}**, Fig. 9) synthesized by Wang *et al.* in 2014.[110] Interestingly, synthesis of this complex was achieved conveniently by reaction of $Cu(BF_4)_2 \cdot 6H_2O$ with the tripodal bztpen ((bztpen = *N*-benzyl-*N*,*N*′,*N*′-tris(pyridin-2-ylmethyl)ethylenediamine) ligand in water.

Both systems incorporate polypyridine frameworks; however, **Cu_{3b}** demonstrated markedly superior activity in aqueous media. Electrochemical studies revealed two one-electron reduction events at −0.53 V (Fig. 11a), assigned to the $Cu^{II/I}$ couple, and a quasi-reversible process at −1.22 V, attributed to $Cu^{(I/0)}$. Remarkably, **Cu_{3b}** exhibited a k_{obs} of 1000 s^{-1} (Fig. 11b), obtained using eqn (7) (Section 2), among the highest reported for a copper-based molecular HER catalyst. Under

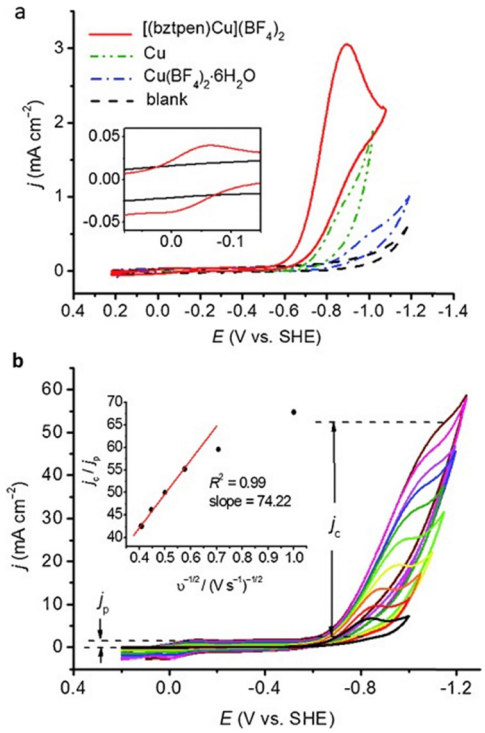

Fig. 11 (a) Cyclic voltammograms of **Cu_{3b}** ([(bztpen)Cu]$(BF_4)_2$) (0.5 mm; red) and Cu$(BF_4)_2$ $6H_2O$ (0.5 mm; blue); the blank CVs of a copper plate electrode (green) and a glassy carbon electrode (black) in 0.1 M phosphate buffer at pH 2.5 under N_2 atmosphere at a scan rate of 50 mV s^{-1} are also shown. Inset: Enlarged view of the reversible reduction wave at −0.03 V. (b) CV of **Cu_{3b}** (0.5 mm) at various scan rates from 0.05 to 6.00 V s^{-1}. Inset: Plot of j_c/j_p *versus* the reciprocal of the square root of scan rate. Adapted from ref. 110 with permission from Wiley-VCH,[110] copyright 2015.

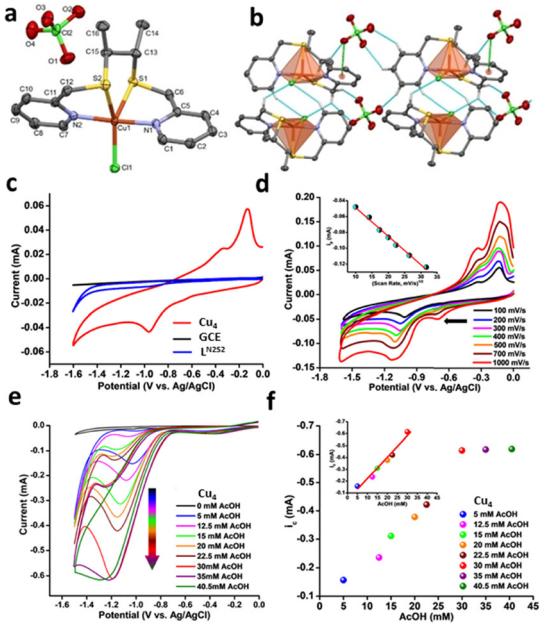

Fig. 12 (a) ORTEP drawing of [**Cu_4**]ClO_4 with a 30% probability of thermal ellipsoids. Hydrogen atoms are omitted for clarity; (b) supramolecular framework of [**Cu_4**]ClO_4. (c) CVs of 1 mM **Cu_4**, the L^{N2S2} ligand and bare glassy carbon electrode (GCE) in 0.1 M aqueous KCl at 100 mV s^{-1}; (d) CVs of the complex at various scan rates. Inset represents the variation of peak current (i_p) *vs.* square root of the scan rate; (e) CVs of 1 mM **Cu_4** in 0.1 M aqueous KCl at 10 mV s^{-1} scan rate without acid addition (black) and upon the addition of different concentrations of AcOH; (f) i_c *vs.* [AcOH] fitted with a linear correlation exhibiting an R^2 value of 0.997. Adapted from ref. 176 with permission from Wiley-VCH,[176] copyright 2025.

controlled-potential electrolysis (CPE) in 0.1 M phosphate buffer (pH 2.5) at −1.53 V *vs.* $Fc^{+/0}$, **Cu_{3b}** achieved a turnover number (TON) of 1.4×10^4, corresponding to a TOF of 7000 h^{-1}, with a Faradaic efficiency of 96% over two hours. The molecular nature of the catalyst was carefully evaluated: Cu$(BF_4)_2$ salt was inactive under identical conditions (Fig. 11a), and rinse tests performed after CPE in fresh electrolyte showed negligible residual activity, largely excluding catalysis by deposited species. Although SEM and EDX analyses indicated minor copper deposition on the working electrode surface after bulk electrolysis, the authors concluded that hydrogen evolution was predominantly mediated by the molecular **Cu_{3b}** complex. Furthermore, the proposed Cu^I intermediate suggested to be the catalytically active species was independently prepared and isolated, providing additional mechanistic support for the catalytic pathway.

Within the same year (2025) of **Cu_{3a}** report, Diyali *et al.* presented a water-stable copper catalyst incorporating N_2 and S_2 donor ligands (**Cu_4**, Fig. 12).[176] The ligand was synthesized by coupling 2-picolyl chloride with 2,3-butanedithiol in the presence of sodium ethoxide (NaOEt) in ice-bath, followed by reflux. The corresponding **Cu_4** complex, was then obtained by reacting the N_2S_2 ligand with hydrated Cu$(ClO_4)_2$ in methanol. This complex exhibits a square pyramidal geometry, with a chlorido-ligand occupying the axial position (Fig. 12a). The catalyst demonstrated stability in water for 72 hours. Cyclic voltammetry conducted in an aqueous KCl aqueous solution reveals two primary irreversible reduction events at −1.11 V and −1.51 V (*vs.* Fc). The first reduction event is attributed to the $Cu^{II/I}$ couple, followed by the loss of chloride, while the second event is confirmed as a ligand-centered event by comparing it with the CV of the zinc complex under identical conditions. The diffusion coefficient of the complex is consistent with those of the copper complexes, 1.1×10^{-5} cm^{-1} s^{-1}. The i_{cat}/i_p value of 35.4 was achieved by this catalyst in the presence of 30 mM AcOH in an aqueous solution, which corresponds to a turnover frequency (TOF) of 241.75 s^{-1} as calculated using eqn (7) (Section 2). However, this measurement was not conducted under a CV scan rate-independent regime, which is essential for accurately deriving this value. It is important to exercise caution when applying this equation, particularly when side phenomena are potentially present, as indicated by the catalytic current readings not being proportional to the scan rate, suggesting an unlimited amount of substrate or other side phenomena. A CPE experiment in a 0.1 M KCl aqueous electrolyte was conducted at −1.65 V *vs.* Fc for 1.6 hours on a glassy carbon electrode, resulting in a turnover number (TON) of 73 and a faradaic efficiency of 94.2%. The research team assumed an overpotential of 660 mV. To investigate catalyst degradation, the team performed extensive cyclic voltammetry and detailed control experiments, although copper salt was not included.

Furthermore, the team assessed the possibility of catalyst deposition on the glassy carbon electrode after a 5-hour CPE experiment, which provided sufficient time to detect deposited species including copper(II) oxide, as revealed by XPS analysis. A key finding from this study indicates that CuO species are more prevalent during prolonged CPE experiments exceeding 1.6 hours; thus, shorter CPE experiments may minimize decomposition, favouring a homogeneous catalytic pathway.

Ghorai *et al*. synthesized in 2025 a series of water-soluble distorted square-planar copper complexes that incorporate a common N_2O_2 Schiff base (salen-type) ligand, with *ortho*-substituents (–H, –OH, and –OMe) in their secondary coordination spheres (**Cu$_5$**, Fig. 9), and examined their electrocatalytic performance for hydrogen generation in nearly neutral aqueous environments.[188] It is noteworthy that salen-type complexes are versatile in literature and serve as a diverse platform for pre-catalysts in various transformations.[197,198] These complexes can be conveniently prepared following established procedures. Typically, the salen ligand is formed *via* a Schiff base reaction between ethylenediamine and the corresponding aldehyde precursors, such as *o*-vanillin, 2,3-dihydroxybenzaldehyde, or related 2-hydroxyaldehydes. The resulting salen ligands are then refluxed with stoichiometric amounts of Cu(II) salts in methanol to afford the desired copper complexes.

Cyclic voltammograms of the complexes in DMF exhibited a reversible $Cu^{II/I}$ redox peak at approximately $E_{1/2}$ = −1.65 V, similar event was also observed in neutral aqueous solutions within the same potential range (−1.65 V to −1.63 V). In aqueous electrolyte additional irreversible peak was noted for the complexes at more negative potentials (−1.9 V to −2.1 V), attributed to the electrocatalytic hydrogen evolution process. Under more acidic conditions, a greater enhancement in current was achieved, accompanied by an anodic shift in the catalytic potential. However, a significant reduction in the catalytic rate was observed at pH as low as 4, with all three complexes exhibiting a marked decrease in activity, which was attributed to the potential hydrolysis of the imine functionality, resulting in deactivating of the catalysts. Among the complexes studied, the hydroxyl-substituted complex was identified as the most catalytically active, likely due to the stabilization of the catalytic intermediate through hydrogen bonding facilitated by the *ortho*-OH substitution. This complex achieved a turnover number (TON) of approximately 1450 on a plastic chip graphite electrode (1 cm × 2 cm) in aqueous buffer electrolyte at pH of 5.0, while the complex with the –OCH_3 substituent displayed a TON of only 520, compared to 1320 for the unsubstituted complex (H), under an applied potential of around −2 V *vs*. Fc, demonstrating a faradaic efficiency of 80% with an overpotential range of 700 mV to 900 mV across a pH range of 7 to 4. A series of analyses were conducted to confirm the homogeneous nature of the complexes, including cyclic voltammetry before and after the CPE experiment, albeit no control copper salt experiment was conducted in the study. A more reliable analysis utilizing SEM, EDX of a carbon paper electrode used as the working electrode for CPE experiment over 1–2 hours revealed no detectable copper deposition on the electrode surface.

Loke *et al*. reported in 2021 a systematic electrochemical evaluation of four tetrahedral Cu(I) complexes; $[Cu(MeCN)_4]PF_6$, $[Cu(dppe)_2]PF_6$, $[Cu(bpy)_2]PF_6$, and $[Cu(bpy)(dppe)]PF_6$ (**Cu$_6$-Cu$_9$**, Fig. 9) as molecular electrocatalysts for proton reduction to dihydrogen in acetonitrile using acetic acid as the proton source.[199] **Cu$_7$–Cu$_9$** were readily synthesized by direct coordination of the desired ligands to the Cu(I) center of **Cu$_6$**. In each case, two bidentate ligands displaced the weakly bound acetonitrile ligands, resulting in the formation of four-coordinate copper(I) complexes.

Cyclic voltammetry revealed that complexes bearing labile nitrogen donors, **Cu$_6$** and **Cu$_7$**, exhibit efficient catalytic activity with low overpotentials (determined using Appel and Helm method;[143] difference between $E_{cat/2}$ and the E° of acetic acid, see Section 2) of approximately 0.4 V and TON of 19.7 ± 3.9 and 15.3 ± 2.4, respectively, whereas the phosphine-rich complex $[Cu(dppe)_2]PF_6$ (**Cu$_9$**) was catalytically inactive and the mixed-ligand complex $[Cu(bpy)(dppe)]PF_6$ (**Cu$_8$**) required a higher overpotential (*ca.* 0.6 V) with TON = 12.8 ± 2.9. Electrochemical features, including ligand-dependent $Cu^{I/0}$ redox behaviour, acid-dependent catalytic currents, and scan-rate-dependent curve crossing, support an ECEC-type mechanism involving initial reduction of Cu(I), ligand dissociation, protonation of surface-associated Cu(0) species, and subsequent formation of transient Cu–hydride intermediates leading to H_2 release. Overall, the results demonstrated that ligand lability is a key determinant of catalytic efficiency in Cu(I)-mediated proton reduction. Overall, in addition to modest TON achieved by the active system, the study does not provide definitive proof that proton reduction proceeds *via* a purely homogeneous Cu(I) molecular catalyst. Several observations, particularly ligand dissociation upon reduction, emergence of stripping wave features in the electrocatalytic CVs consistent with Cu(0) formation suggest possible involvement of heterogeneous, surface-bound copper species.

Rai *et al*. reported in 2020 three Cu(II) terpyridine-based molecular electrocatalysts (**Cu$_{10}$-Cu$_{12}$**, Fig. 9).[177] All complexes feature square-pyramidal Cu(II) centers ligated by terpyridine frameworks, with acetate occupying equatorial/axial positions and labile aqua coordination under acidic conditions.

The terpyridine ligand was synthesized following a reported procedure. Typically, one equivalent of pyridine-4-carbaldehyde was reacted with two equivalents of 2-acetylpyridine in ethanol. This was followed by the addition of KOH and aqueous ammonia, and the reaction mixture was refluxed overnight, resulting in the formation of an off-white precipitate. The isolated ligand was subsequently treated with $Cu(OAc)_2{\cdot}H_2O$ to afford the corresponding copper complexes.

Electrochemical studies in DMF reveal quasi-reversible $Cu^{II/I}$ couples at *ca.* −0.27 to −0.33 V *vs.* SCE, followed by more cathodic (Cu(I)L) ligand-cantered reductions. Upon addition of acetic acid as a proton source to the DMF/H_2O solution, all complexes display significant catalytic currents with onset potentials appear at approximately −1.25 to −1.36 V *vs.* SCE and plateaued near −1.6 to −1.8 V *vs.* SCE. Kinetic analysis

shows first-order dependence on catalyst concentration and second-order dependence on acid concentration. The maximum TOF values (from CV analysis) reach 1473 s^{-1} for **Cu_{10}**, 700 s^{-1} for **Cu_{11}**, and 926 s^{-1} for **Cu_{12}**. CPE for proton reduction was performed at −1.5 V *vs.* SCE (−1.9 V *vs.* Fc) in DMF/H_2O with 34 equivalents of AcOH for 0.5–1 h. Faradaic efficiencies range of 81–95 ± 2% was obtained. TOFs derived from bulk electrolysis correspond to 86, 57, and 38 mol H_2 $h^{-1}mol^{-1}$ catalyst for **Cu_{10}**, **Cu_{11}**, and **Cu_{12}**, respectively; with no TON values reported. The catalysts were also active for electrocatalytic water reduction in 0.1 M phosphate buffer at pH 1.62, with catalytic onset at *ca.* −0.75 V *vs.* SCE. CPE conducted at −1.0 V *vs.* SCE for 0.5 h produced hydrogen with Faradaic efficiencies of 93–98%. Homogeneous catalysis is supported by diffusion-controlled voltammetry, first-order dependence on catalyst concentration, acid-order kinetics, and unchanged CVs before and after electrolysis; however, no rinse tests or direct electrode surface analyses were reported to clearly exclude Cu/Cu_xO particle deposition. While the study provides a comprehensive electrochemical and mechanistic analysis with high TOFs and excellent faradaic efficiencies, long-term durability metrics are not systematically reported, and benchmarking turnover against state-of-the-art molecular HER catalysts is limited.

Similarly, in the following year, the same group reported a series of mononuclear Cu(II) molecular complexes that are supported by terpyridine ligands. This time featuring a quinoline moiety (**Cu_{13}–Cu_{14}**, Fig. 9).[106] The resulting complexes, which adopt distorted square-pyramidal coordination geometries with labile axial solvent or aqua ligands, were synthesized following the same protocols used for the terpyridine ligand and the **Cu_{10}–Cu_{12}** complexes. Electrochemical studies reveal quasi-reversible $Cu^{II/I}$ redox couples in −0.65 to −0.69 V range ascribed to $Cu^{II/I}$ redox couple and several irreversible peaks after −1.72 V due to ligand reduction. Electrocatalytic proton reduction was examined in 95 : 5 DMF/H_2O (v/v) using acetic acid as the proton source as well as in aqueous phosphate buffer (pH ≈ 7). In DMF, catalysis occurs at applied potentials of approximately –1.9 V *vs.* Fc, whereas in neutral aqueous media the catalytic onset shifts positively to around −1.45 to −1.55 V *vs.* Fc. CPE experiment was conducted for 60 minutes, during which hydrogen evolution was confirmed by gas analysis, with faradaic efficiencies exceeding 90–95%. Turnover frequencies were estimated from electrochemical data (using eqn (7), Section 1) to be for 1682 s^{-1} **Cu_{13}** and 1153 s^{-1} for **Cu_{14}**. Catalytic currents scale linearly with catalyst and acid concentration, suggesting a homogeneous proton-coupled electron-transfer mechanism. Homogeneous behavior was further supported by diffusion-controlled voltammetry and unchanged cyclic voltammograms before and after electrolysis in addition to EDX and SEM analysis of the working electrode after bulk electrolysis for 30 minutes. However, no rinse tests or mercury poisoning experiments so copper deposition under prolonged operation of at least several hours, cannot be definitively precluded.

In 2020 Drosou *et al.* reported a molecular copper(I) pyridine-quinoxaline (**Cu_{15}**, Fig. 9).[200] The authors conveniently prepared this complex by reacting 2-pyridin-2-yl-quinoxaline (pq) with $[Cu(MeCN)_4]BF_4$ in a 2 : 1 ratio. The reaction mixture was stirred for 2 hours under anaerobic conditions, affording the desired complex in 63% yield. HER catalyst under photo- and electrocatalytic conditions using redox active ligand frameworks capable of stabilizing the low-valent copper center,[200] the non-innocent nature of the quinoxaline ligand anticipated to mediate electron storage and facilitates proton. The CV of **Cu_{15}** in DMF features a slightly negative event (−0.18 V *vs.* Fc) attributed likely to $Cu^{I/0}$ transformation and two more negative events (−1.70 and −1.97 *vs.* Fc) ascribed to ligand reduction. Electrochemical investigations carried out in DMF with trifluoroacetic acid (TFA) as a proton source demonstrated by authors suggested that catalytic hydrogen evolution occurred at moderate overpotentials, with catalytic currents increasing systematically upon acid addition. Cyclic voltammetry reveals that HER activity is closely associated with ligand-based reduction events rather than purely metal-centered redox processes, highlighting the importance of metal–ligand cooperativity in the catalytic mechanism. The authors didn't specify any CPE experiments with all electrocatalytic features were extracted from the CVs recorded for the complex in TFA/DMF medium. The electrocatalytic behaviour was also examined in aqueous solution with the presence of acetic acid as a proton source. However, no extended CPE experiment or any catalytic metrics were reported. The authors support molecular catalysis with ligand-centred redox processes rather than metallic copper. However, the unperformed prolong electrolysis experiment, post-electrolysis rinse test, mercury poisoning experiments and any electrode-deposition analysis limits the definitive activity of this complex. Mechanistic analysis indicates that HER proceeds *via* accumulation of reducing equivalents on the quinoxaline ligand followed by protonation steps leading to H–H bond formation, although no discrete hydride intermediates are directly observed. Overall, this work provides an important early demonstration that redox-active pyridine-quinoxaline ligand can enable copper-based molecular HER catalysis as supported by photocatalytic HER activity as well, offering a conceptual framework that has influenced subsequent catalyst designs. However, further advances in long-term stability, kinetic efficiency, and operation under application-relevant conditions (aqueous) are required to fully establish the practical potential of this catalyst class.

4.3.1. Design lessons from polypyridyl copper systems. Although direct comparison of molecular HER catalysts is inherently challenging because of differences in solvent, proton source, pH, electrode configuration, and applied potential, several consistent design rules from the studied polypyridyl copper architectures can be learnt.

First, ligand rigidity and high denticity generally enhance catalyst stability by suppressing coordination sphere rearrangement and minimizing ligand dissociation under reducing conditions. For example, copper complexes incorporating pentadentate polypyridyl ligands (**Cu_{3a}** and **Cu_{3b}**) consistently exhibit superior electrochemical durability and catalytic performance compared to systems based on more flexible tridentate

(**Cu$_1$**, **Cu$_2$**, **Cu$_{10}$–Cu$_{14}$**) or bidentate ligands (**Cu$_7$–Cu$_9$**, **Cu$_{15}$**). This trend is reflected in their ability to sustain prolonged electrolysis experiments (2–3 h), achieving TON values exceeding 3000–14 000, and operate under highly acidic conditions (pH 1–2.5), where many other molecular copper catalysts display rapid deactivation.

Second, incorporation of proton-responsive functionalities can substantially improve catalytic efficiency. Pendant amines and related proton relays facilitate proton-coupled electron transfer (PCET), lowering kinetic barriers associated with proton delivery and often reducing the overpotential required for HER. This effect is particularly evident in terpyridine-based systems such as **Cu$_{10}$** and **Cu$_{14}$**, where strategically positioned pyridyl or quinoline moieties enhance both proton transfer and electronic communication with the metal center, resulting in significantly improved catalytic rates (TOF = 1473–1682 s^{-1}) relative to analogous complexes lacking such features (**Cu$_{11}$–Cu$_{13}$**).

Third, ligand donor identity appears to play an important role in determining catalyst activity and durability. Overall, copper complexes supported by exclusively nitrogen-donor environments (*e.g.* **Cu$_1$**, **Cu$_{3a}$**, **Cu$_{3b}$**, and **Cu$_6$**) tend to outperform related mixed-donor systems containing N/O, N/S, or N/P donor sets. This trend is manifested in both improved operational stability and enhanced catalytic kinetics, suggesting that polypyridyl coordination environments are particularly effective in stabilizing catalytically relevant copper intermediates.

Importantly, catalytic activity and catalyst longevity do not necessarily correlate. Several complexes display exceptionally high TOF values (*e.g.*, **Cu$_1$** and **Cu$_{10}$–Cu$_{14}$**) but suffer from limited long-term stability, likely due to ligand degradation, catalyst reconstruction, or metal deposition. In contrast, more robust systems (**Cu$_6$–Cu$_8$**) often operate at lower rates while maintaining catalytic activity over extended periods.

Finally, despite significant advances in ligand design, stabilization of reduced copper intermediates remains a major challenge. Many Cu(II) complexes generate Cu(I) species during catalysis that can undergo disproportionation, further reduction, or conversion into electrode-bound Cu/Cu$_x$O deposits. These observations highlight the delicate balance between catalyst activation and catalyst degradation and underscore the importance of developing ligand architectures capable of stabilizing reactive copper intermediates while suppressing pathways leading to catalyst decomposition.

Additionally, from an activation perspective, this catalyst family largely follows the molecular activation pathway shown in Fig. 10, though evidence for catalyst transformation has not frequently been reported in several systems.

4.4. Copper macrocycles

The development of macrocyclic transition-metal complexes as catalysts is strongly inspired by naturally occurring tetrapyrrolic metalloproteins, which play essential roles in vital biological processes such as electron transfer, redox catalysis, and small-molecule activation.[201–207] These bioinspired systems have provided fundamental design principles that continue to influence the development of molecular catalysts for emerging applications in electrocatalysis and energy conversion technologies.

Porphyrinoids, a class of tetrapyrrolic macrocycles (Fig. 13), are well-established and robust N_4-donor ligands that efficiently stabilize monometallic centers, giving rise to a wide range of molecular complexes that exhibit high catalytic activity. Owing to their high denticity and pronounced macrocyclic effect, metal porphyrins have long been recognized for their exceptional stability and rich bioinspired reactivity, enabling diverse chemical transformations.[208,209]

Several well-established protocols exist for the synthesis of porphyrins, with origins tracing back to the pioneering work of Rothemund in the 1930s.[210] In this early method, pyrrole was condensed with aromatic aldehydes in sealed tubes at elevated temperatures. This approach was later refined by Adler–Longo reactions in the 1960s,[211] in which propionic acid served both as a high-boiling solvent and a catalyst, enabling the efficient large-scale synthesis of meso-aryl-substituted porphyrins. Further methodological advancements have since been reported, including [2+2] condensation strategies involving the reaction of 1,9-diformyldipyrromethane with 1,9-unsubstituted dipyrromethane (Fig. 14).[212] These later approaches offer improved regioselectivity and help to suppress pyrrole decomposition, a common limitation associated with earlier one-pot synthetic procedures.

The application of metal porphyrins as catalysts for the hydrogen evolution reaction dates back to the 1990s. At that time Savéant and co-workers demonstrated that Fe(0) porphyrins function as effective electrocatalysts for hydrogen production.[77] In contrast, the development of macrocyclic copper-based electrocatalysts for HER has emerged only within the past decade. This section surveys representative examples of copper macrocycles that have been reported as HER catalysts.

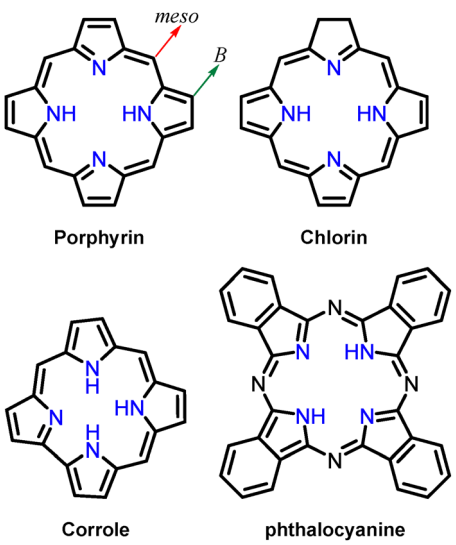

Fig. 13 Chemical structure of selected porphyrinoids, showing the two distinct positions (β and *meso*) of the porphyrin framework.

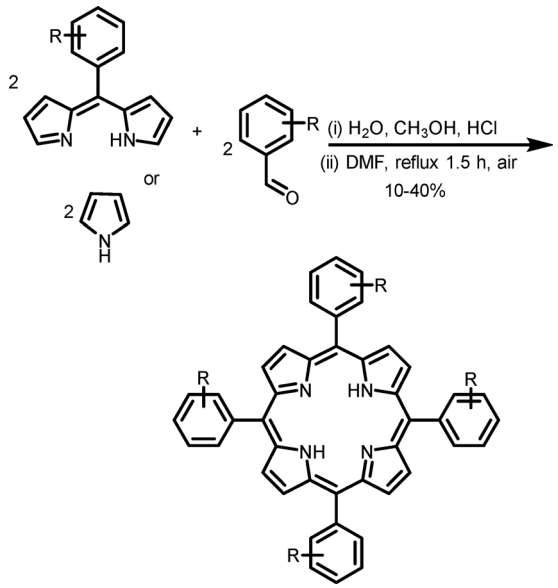

Fig. 14 Synthetic scheme for the preparation of *meso*-substituted porphyrins *via* condensation of aldehydes with either pyrrole to afford symmetric A_4 porphyrins, or with dipyrromethene to yield *trans*-A_2B_2 porphyrins.

Khusnutdinova *et al*. reported in 2018 a binuclear copper molecular catalyst designed to probe the influence of metal–metal cooperativity on electrocatalytic hydrogen evolution.[179] Structurally, the complex consists of two copper centers bridged by a fused porphyrins framework (**Cu_{16a}**, Fig. 15) that

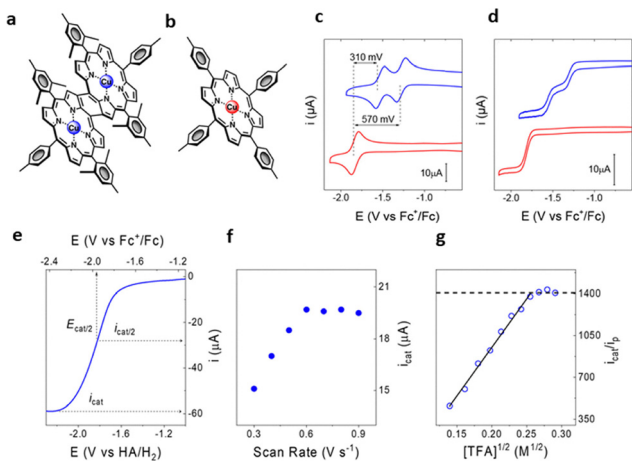

Fig. 15 Chemical structure of (a) binuclear **Cu_{16a}** and (b) mononuclear **Cu_{16b}** (c) CVs recorded in a 0.1 M $TBAPF_6$ dichloromethane solution using a 3 mm diameter glassy carbon electrode and a scan rate of 500 mV s^{-1} of binuclear **Cu_{16a}** (blue) and mononuclear **Cu_{16b}** (red) under (c) nonrotating conditions (0.34 mM) and (d) rotating conditions (1000 pm, 0.1), (e) CV of **Cu_{16b}** recorded in 0.1 M $TBAPF_6$ dichloromethane solution with 65 mM TFA at 600 mV s^{-1} with the potential recorded *versus* the equilibrium potential of TFA/H_2 in dichloromethane, calculated using the open circuit potential method. (f) Plot of i_{cat} *versus* the scan rate for 0.01 mM **Cu_{16a}** in a 0.1 M $TBAPF_6$ dichloromethane solution with 19.5 mM TFA. (g) Plot of i_{cat}/i_p *versus* the square root of the concentration of TFA for 0.1 mM **Cu_{16b}**. Adapted from ref. 179 with permission from American Chemical Society,[179] copyright 2018.

enforces close metal–metal proximity while maintaining distinct coordination environments. This architecture is intended to facilitate multi-electron/proton transfer processes and to stabilize key hydride or protonated intermediates during catalysis. The cyclic voltammograms of the fused binuclear copper porphyrin (**Cu_{16a}**) display two successive reduction processes that are attributed to sequential $Cu^{II/I}$ and $Cu^{I/0}$ redox couples, which occur at $E_{1/2}$ = −1.27 V and −1.53 V. Notably, the first of **Cu_{16a}** is shifted anodically by approximately 570 mV relative to the corresponding mononuclear copper porphyrin (**Cu_{16b}**, Fig. 15b), which is reduced at *ca.* −1.84 V (Fig. 15d). This substantial potential shift reflects strong electronic communication within the fused porphyrin framework and underpins the enhanced electrocatalytic hydrogen evolution activity observed for the binuclear system. Electrocatalytic hydrogen evolution by **Cu_{16a}** was evaluated in dichloromethane using trifluoroacetic acid (TFA) as the proton source. Under these conditions, the complex exhibited catalytic wave at potentials negative of the second reduction event. Kinetic data obtained using eqn (7) (Section 2) showed that the scan rate independent catalytic current can be observed beyond 600 mV s^{-1} (Fig. 15f), which in turn allowed the determination of a turnover frequency (TOF) of 2 x 10^6 s^{-1} for **Cu_{16a}**. Notably, while the electrochemical properties of mononuclear analogues are discussed elsewhere in the study, no direct controlled-potential electrolysis comparison between mono- and binuclear copper complexes is reported. With respect to catalyst integrity and homogeneity, the study primarily relies on carrying the electrolysis in mercury pool with no noticed change in current density. LSV of the rinsed electrode suggested the absence of active catalysts deposited on the electrode. However, prolonged bulk electrolysis experiments or glassy carbon electrode surface analysis can further preclude any possible formation of catalytically active copper deposits under strongly reducing conditions.

Peng *et al*. synthesized a series of Cu-porphyrin catalysts featuring single and double β-lactone groups through controlled β-oxidation of the porphyrin ring (**Cu–Cu_{17a-d}**, Fig. 16a).[180]

The double β-oxidation process resulted in β-lactone groups in both *cis* and *trans* configurations, designated as **Cu_{17c-d}**. The cyclic voltammograms of compounds **Cu–Cu_{17a-d}** exhibited two reversible reduction waves (Fig. 16b). In comparison, the reference compound **Cu_{17a}** demonstrated reductions at $E_{1/2}$ values of −1.30 and −1.75 V *vs*. Fc, while the first and second reductions of compound **Cu_{17b}** shifted to more positive potential, resulting in $E_{1/2}$ values of −1.05 and −1.52 V, which aligns with the effect of the β-lactone group as an electron-withdrawing substituent, thereby making **Cu_{17b}** more susceptible to reduction. The most significant anodic shift in reduction was observed for compound **Cu_{17d}**, with $E_{1/2}$ values of −0.78 and −1.29 V (Fig. 16b), confirming it as the most electron-deficient structure within this series.

These complexes were evaluated for HER in acetonitrile along with the reference complex **Cu_{17a}**, in presence of up to 70 mM trifluoroacetic acid (TFA) as the proton source (Fig. 16c–e). The investigation provided insights into the electrocatalytic hydrogen evolution pathways, which were found to be influenced by the

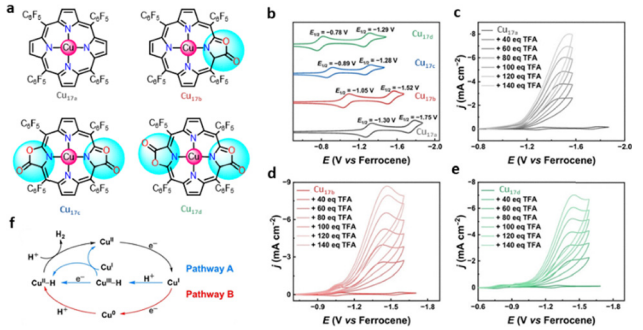

Fig. 16 (a) Chemical structure of the Cu-porphyrins (**Cu$_{17a–d}$**) with β-lactones substitutes, (b) CVs of 0.5 mM **Cu$_{17a–d}$** (c–e) CVs of 0.5 mM **Cu$_{17a}$**, **Cu$_{17b}$**, and **Cu$_{17d}$** with increasing TFA, respectively, (f) proposed HER pathways based on the electronic properties of the of the porphyrin ligands. Conditions: 0. M Bu_4NPF_6 acetonitrile, 100 mV s^{-1} scan rate, glassy carbon working electrode. Adapted from ref. 180 with permission from Wiley-VCH,[180] copyright 2024.

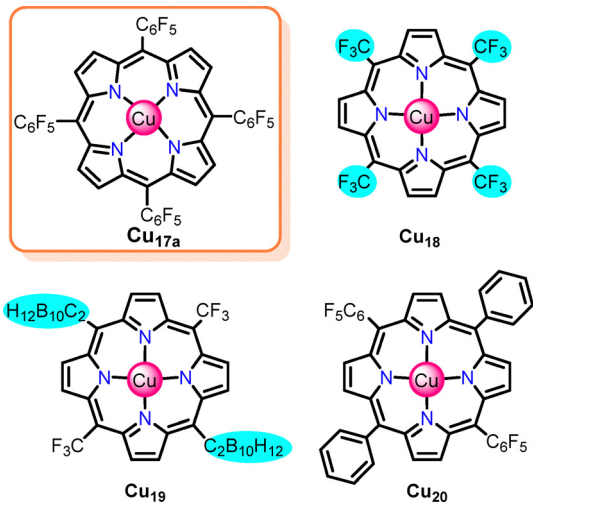

Fig. 17 Chemical structures of *meso* substituted Cu-porphyrins (**Cu$_{17a}$–Cu$_{20}$**).

electronic properties of the porphyrin framework. It was observed that the β-lactone groups in **Cu$_{17c–d}$** facilitated a more efficient reduction compared to the Cu-porphyrin with a single lactone group (**Cu$_{17b}$**); however, the overpotentials for HER exhibited by all four complexes, including the reference **Cu$_{17a}$**, remained within a similar range. The overall findings suggest that utilizing a more electron-deficient macrocycle leads to a transition in the catalytically active species for HER from a formal Cu^I species (Fig. 16f) in **Cu$_{17a}$** to a formal Cu^0 species in **Cu$_{17d}$**. This indicates that the proton transfer step (PC) occurs on the mono-reduced copper species (Cu^I, pathway A, Fig. 16f) in the former case, while it occurs on the doubly-reduced species (Cu^0, pathway B, Fig. 16f) in the latter case. The activity of this series of catalysts was also confirmed by 1-hour electrolysis experiment carried out at applied potential of −1.35 V *vs.* Fc in acetonitrile with 0.1 M Bu_4NPF_6 in the presence of TFA (up to 70 mM), this resulted in H_2 production over one hour with FE measured at 97%. The UV-vis spectra of **Cu$_{17a–d}$** after electrolysis were identical to those before electrolysis. The rinse test of the glassy carbon electrode after electrolysis in TFA showed no activity, suggesting the homogeneity of the catalytic system. Overall, this study represents a distinctive modern example in which tuning the ligand framework of a copper-based molecular catalyst administers the HER mechanism. Highlighting the potential of the copper-macrocyclic molecular catalysts to control the activity and pathways for HER.

Using the same porphyrin scaffold, Li *et al.* (2024) demonstrated that the presence of a trifluoromethyl substituent at the *meso* position of the porphyrin-Cu HER catalyst, **Cu$_{18}$** (Fig. 17), resulted in enhanced activity compared to its pentafluorophenyl counterpart, **Cu$_{17a}$**.[181] When trifluoroacetic acid was utilized as a proton source in acetonitrile, **Cu$_{18}$** exhibited an i_{cat}/i_p ratio of 97, in contrast to just 53 for the pentafluorophenyl counterpart (**Cu$_{17a}$**). Furthermore, the **Cu$_{18}$** achieved a HER catalytic activity overpotential that was 220 mV more positive than that of the pentafluorophenyl **Cu$_{17a}$**, as determined from the onset potential of both catalysts at a current density of −0.30 mA cm^{-2}. The turnover frequency (TOF) for the HER with both catalysts was assessed using foot-of-the-wave analysis (FOWA),[149,213] yielding a TOF_{max} of 6.8×10^4 s^{-1} for **Cu$_{18}$** and 4.3×10^4 s^{-1} for **Cu$_{17a}$**. Controlled potential electrolysis of **Cu$_{18}$** conducted at −1.25 V in acetonitrile in the presence of TFA demonstrated Faradaic efficiency exceeding 95%.

The molecular characteristics of the catalysts were validated by demonstrating that catalytic activity is dependent upon the concentration of the catalyst; specifically, the catalytic peak current was directly proportional to the catalyst's concentration. Furthermore, the group indicated that the UV-vis spectra of both catalysts after electrolysis exhibited minimal alterations in comparison to their UV-vis spectra prior to electrolysis. Additionally, rinse test in which the glassy carbon working electrode used in the electrolysis experiment of the catalyst is re-tested in TFA fresh electrolyte in the absence of the catalyst showed minimum activity under same applied conditions.

Similarly, a comparable finding was reported by the same group a year prior.[182] This time the group reported the synthesis and electrocatalytic performance of a novel copper porphyrin complex bearing *meso*-(*o*-carborane) substituents (**Cu$_{19}$**, Fig. 17). The incorporation of *o*-carborane groups into the porphyrin framework was hypothesized to enhance electron-transfer properties and stabilize reactive intermediates during the hydrogen evolution reaction (HER).

Electrochemical characterization in acetonitrile in the presence of trifluoroacetic (TFA) demonstrated that the *o*-carborane-substituted copper porphyrin (**Cu$_{19}$**) exhibits significantly improved HER performance compared to the pentafluorophenyl substituted catalyst (**Cu$_{20}$**), as inferred from the CV of both catalysts, where the onset potential was determined by the authors to be −1.07 and −1.26 V for **Cu$_{19}$** and **Cu$_{20}$**, respectively. Notably, **Cu$_{19}$** showed a positive shift of approximately 190 mV in the catalytic wave, indicating a lower overpotential for hydrogen evolution. CPE performed in acetonitrile containing 100 mM TFA at a glassy carbon electrode (1 cm^2) demonstrated that **Cu$_{19}$** catalyzes hydrogen evolution at an applied potential of −1.20 V. In comparison, **Cu$_{20}$** generates a

comparable amount of hydrogen with a similar Faradaic efficiency (≈95%), albeit requiring a more negative applied potential of −1.40 V. Additionally, higher current densities were observed at comparable potentials in aqueous solution, consistent with enhanced catalytic efficiency. Furthermore, **Cu$_{19}$** also outperformed the catalytic performance of the tetrakis(pentafluorophenyl)porphyrin (**Cu$_{17a}$**, Fig. 17) and surpassing many Cu-porphyrin-based catalysts. The results suggest that the electron-withdrawing nature of the *meso-o*-carborane substituents plays a critical role in facilitating proton reduction by modulating the electronic environment of the copper center and shifting the catalytic potential needed for catalysis to more positive values. These findings underscore the utility of molecular functionalization in tuning electrocatalytic activity of copper-based HER catalysts.

Zhang *et al*. reported a systematic investigation of through-space electrostatic effects on the electrocatalytic HER using a series of structurally well-defined copper porphyrins bearing charged pyridinium substituents (Fig. 18, **Cu$_{21a–d}$**).[183] By varying both the number and spatial proximity of positively charged *N*-methylpyridyl groups relative to the Cu center, the authors established a clear structure–activity relationship governing HER performance. Electrochemical studies carried out in aprotic organic media (acetonitrile, DMF, and THF) using TFA as a proton source revealed that increasing the number of cationic substituents, particularly those positioned closer to the Cu ion, led to a pronounced decrease in catalytic activity as reflected by i_{cat}/i_p values, which decreased from 38 for a neutral Cu porphyrin (**Cu$_{17a}$**) to 15 for a tetracationic analogue (**Cu$_{21d}$**) with proximal charged groups (Fig. 18). Notably, this activity suppression occurred despite positive shifts in the reduction potentials, indicating that diminished HER performance was not governed by thermodynamics alone. The disfavored activity effect was attributed to unfavorable electrostatic interactions between positively charged substituents and key proton-coupled electron transfer intermediates, effectively destabilizing proton binding and increasing the kinetic barrier for hydrogen formation. To validate this hypothesis, the authors synthesized a Cu porphyrin bearing sulfonate groups. This catalyst exhibited enhanced HER activity relative to all cationic analogues, indicting that negatively charged second-sphere functionalities can promote HER by facilitating proton delivery and stabilizing reactive intermediates. Importantly, all Cu porphyrins demonstrated high Faradaic efficiencies (>90%) and excellent molecular stability under 1h electrolysis, suggesting their robustness as homogeneous HER catalysts. The authors demonstrated that post-electrolysis UV-vis spectra of the catalyst solutions were essentially unchanged compared to pre-electrolysis spectra, suggesting the molecular integrity of the Cu porphyrins was preserved. This study therefor provides a compelling example that local electrostatic environments, independent of the primary coordination sphere, play a decisive role in governing HER activity in copper-based molecular systems, which underscores the importance of second-sphere and through-space electrostatic engineering in the rational design of copper HER catalysts.

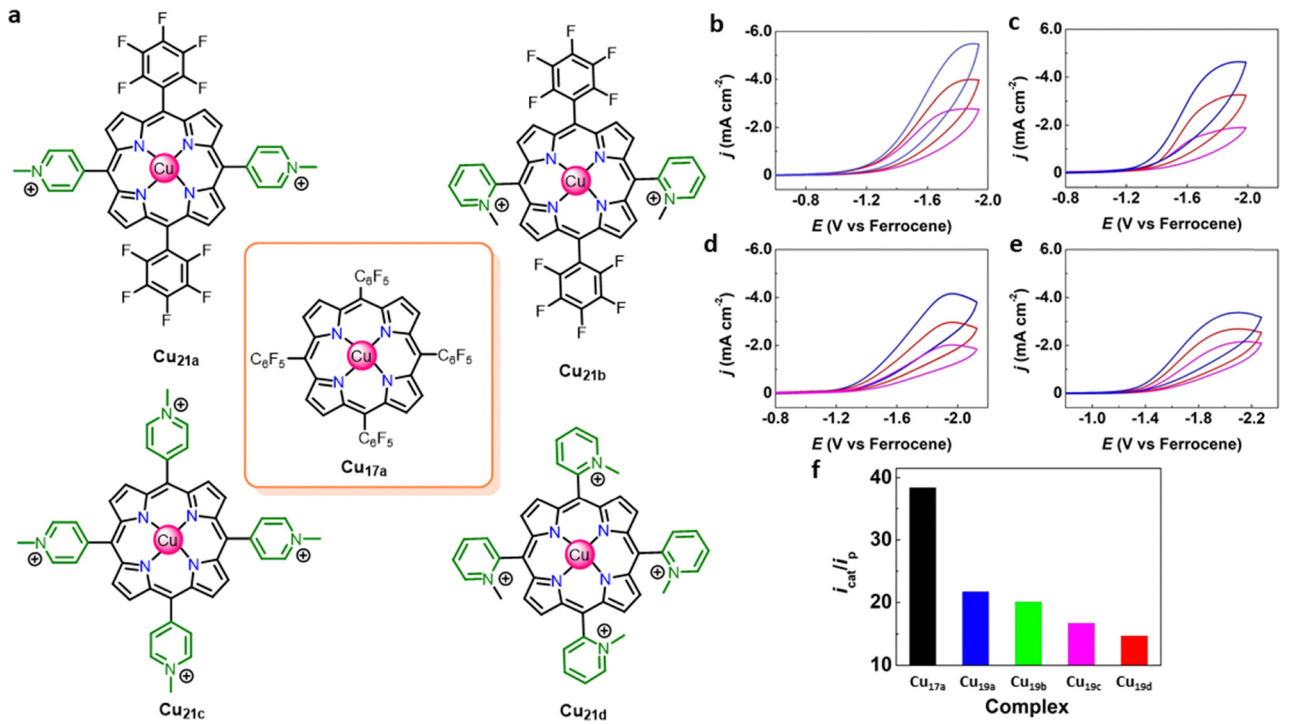

Fig. 18 (a) Chemical structures of copper porphyrins with *N*-methylpyridyl groups (**Cu$_{21a–d}$**) along with the neutral reference catalyst (**Cu$_{17a}$**) studied by Zhang *et al*. for HER, (b) CVs of **Cu$_{21a}$** (b), **Cu$_{21b}$** (c), **Cu$_{21c}$** (d), and **Cu$_{21d}$** (e) in acetonitrile of 0.50 mM with increasing TFA (pink) 20 equiv. (red) 40 equiv. and (blue) 60 equiv. Conditions: 0.1 M nBu$_4$NPF$_6$, GC electrode, 100 mV s^{-1} scan rate, 20 °C. (f) i_{cat}/i_p plot of the catalysts. Adapted from ref. 183 with permission from Wiley-VCH,[183] copyright 2022.

In 2023, Chandra *et al*. described a triply fused bimetallic copper(II) porphyrin complex (**Cu$_{22}$**, Fig. 19) as a an active molecular electrocatalyst for the HER.[184] Cyclic voltammetry of the dinuclear complex **Cu$_{22}$** shows multiple redox processes within the potential window of −0.35 to −2.35 V, displaying three reversible waves at $E_{1/2}$ = −0.86, −1.16, and −2.06 V *vs*. Fc/Fc$^+$ (Fig. 19c). In contrast, the monomeric complex **Cu$_{23}$** exhibited only two reduction processes at −1.66 and −2.12 V under identical conditions. Notably, the first reduction of **Cu$_{23}$** is shifted cathodically by 802 and 302 mV, relative to those of **Cu$_{22}$**.

Compared to a monomeric copper porphyrin analogue **Cu$_{23}$**, the fused system exhibited an enhanced catalytic performance, attributed to extended π-electron delocalization across the fused porphyrin framework. Notably, despite the very low catalyst's concentration employed, under identical conditions (0.01 mM catalyst, 15 mM acid), complex **Cu$_{22}$** exhibited an irreversible catalytic wave with a substantial cathodic shift (≈600 mV) (Fig. 19d) in the onset potential relative to **Cu$_{23}$**, indicating the superior activity of **Cu$_{23}$**. Further Electrochemical studies showed that the fused complex (**Cu$_{22}$**) underwent reduction at less negative potentials, resulting in a ∼320 mV lower overpotential for HER. CPE experiment in DMF using 100 mM TFA as a proton source with an applied potential of −1.05 V *vs*. Fc/Fc$^+$ using only 0.06 mM of **Cu$_{22}$** or 0.12 mM of **Cu$_{23}$** for 30 minutes confirms efficient hydrogen production, with Faradaic efficiency of ∼97% and a turnover number of 102, markedly outperforming the monomeric analogue (**Cu$_{23}$**, FE: 71%, TON: 18). Kinetic analysis reveals an exceptionally high observed rate constant ($k_{obs} \approx 0.5 \times 10^7$ s^{-1}), among the highest reported for first-row transition-metal molecular HER catalysts. Additionally, mechanistic evidence suggests that two-electron reduction to a doubly reduced species is required prior to proton reduction. Although the authors present several control experiments to support homogeneous catalysis, most notably rinse tests after electrolysis, and post-electrolysis spectroscopic EDX analyses, these assessments are largely confined to short-duration (30 min) controlled potential electrolysis. While such tests effectively exclude rapidly formed electrode-bound species, metal nanoparticle deposition, and significant catalyst decomposition, they do not fully rule out slow catalyst degradation, gradual metal leaching, or delayed nanoparticle formation under prolonged electrolysis.

Most recently, in 2025 Jiang *et al.* reported the synthesis and electrocatalytic evaluation of a series of wave-shaped mono-, di-, and trinuclear Cu(II) porphyrin "arrays" (**Cu$_{24a–c}$**, Fig. 20) as HER catalysts under alkaline conditions.[185] The tricpopper porphyrin array feature a non-planar, curved architecture that

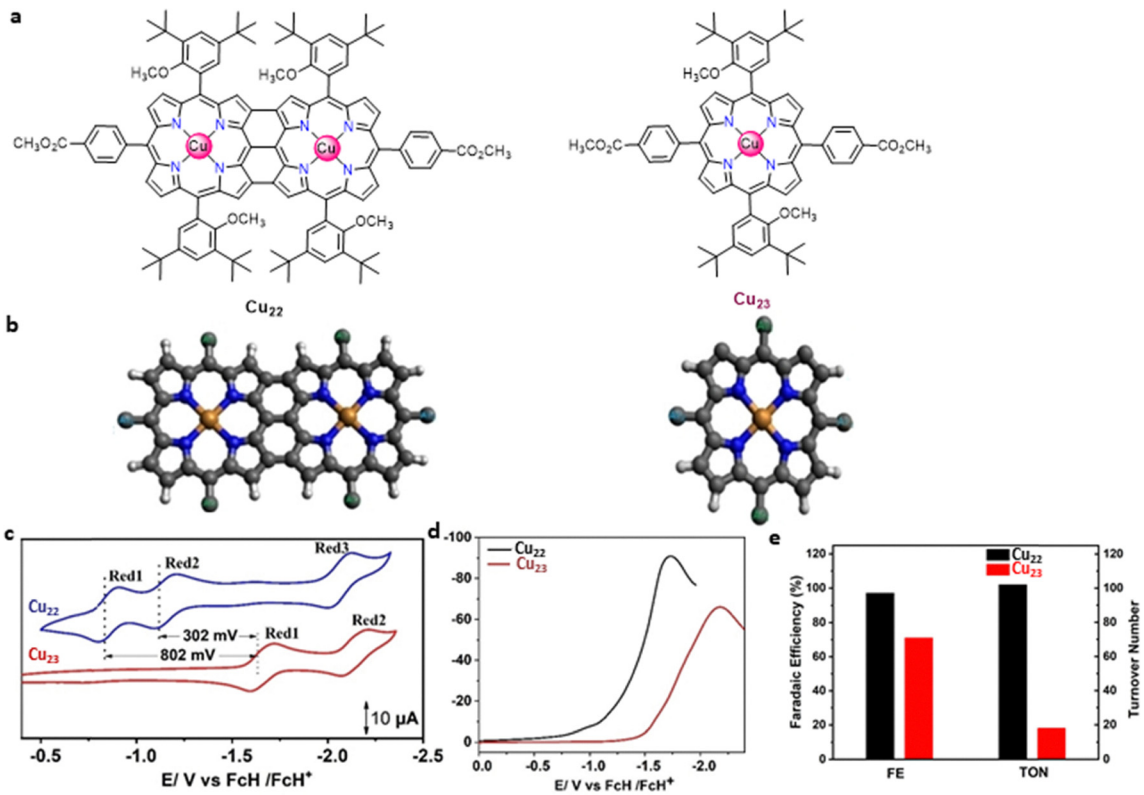

Fig. 19 (a) Chemical structure and (b) Ball-stick model crystal structure of porphyrin-fused copper catalyst **Cu$_{22}$** and its mono-copper analogue **Cu$_{23}$** studied for HER by Chandra *et al*., (c) CVs of 0.25 mM fused metalloporphyrin **Cu$_{22}$** (blue) and monomeric analogue **Cu$_{23}$** (red) in DMF, (d) LSV at 100 mV s^{-1} scan rate in presence of 100 mM TFA indicating proton reduction activity and (e) Faradaic efficiency of DMF solution (0.06 mM **Cu$_{22}$**, black) and (0.12 mM **Cu$_{23}$**, red) with nBu$_4$PF$_6$ (0.1 M) in the presence of 100 mM of TFA at applied potential of −1.05 V *vs*. Fc. Reproduced from ref. 184 with permission from Wiley-VCH,[184] copyright 2022.

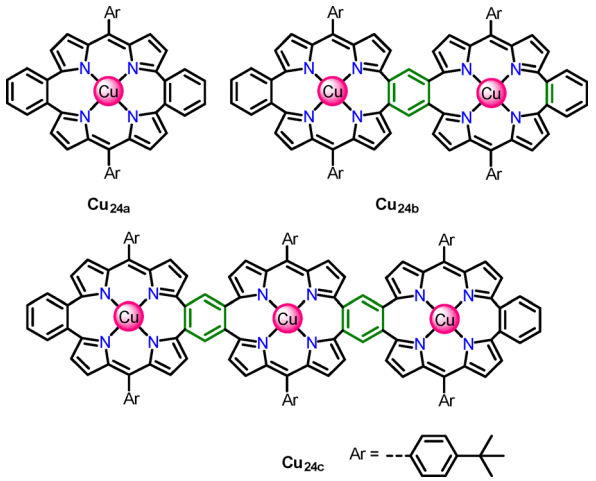

Fig. 20 Chemical structure of trinuclear Cu(II)-porphyrin array complexes (**Cu$_{24a-c}$**).

enables electronic communication between adjacent Cu centers and promotes charge delocalization across the π-conjugated framework. However, this array architecture exhibited limited solubility in common electrochemical solvents. To enable electrocatalytic testing, the Cu porphyrin arrays were immobilized onto carbon nanotubes (CNTs), forming hybrid heterogeneous catalysts.

Electrochemical HER studies were conducted in 1.0 M KOH using a standard three-electrode configuration. Among the catalysts examined, the trinuclear system (**Cu$_{24c}$**) exhibited the highest HER activity, achieving a current density of 10 mA cm^{-2} at an overpotential that was 137 mV and 95 mV lower than those required for the mononuclear and dinuclear analogues, respectively.

Although absolute overpotential values were not clearly tabulated, the systematic activity enhancement extracted form LSV data correlates with increasing nuclearity of the Cu centers. Tafel slope analysis revealed relatively sluggish kinetics for most catalysts, with values as high as 301 mV dec^{-1}, suggesting that the HER proceeds *via* a kinetically limited Volmer step under alkaline conditions. **Cu$_{24c}$** exhibited the smallest Tafel slope (265 mV dec^{-1}), indicating its fastest HER kinetics. Electrochemical impedance spectroscopy further showed also that **Cu$_{24c}$** possesses the lowest charge-transfer resistance, indicative of more efficient interfacial electron transport. Although the study provides a thorough account of the synthesis and characterization of these novel arrays, key catalytic performance metrics, including turnover number (TON), turnover frequency (TOF), and the applied potential under electrocatalytic conditions remain hardly defined.

Lei *et al.* reported the first series of copper macrocyclic electrocatalysts for the hydrogen evolution reaction (HER) based on corrole ligands (**Cu$_{25a}$**–**Cu$_{25d}$**, Fig. 21),[186] featuring systematic variation of substituents at the *meso* positions of the corrole framework. Cyclic voltammetry in acetonitrile revealed two quasi-reversible reduction processes for all complexes, with the first reduction likely to be Cu-centered redox event, and half-wave potentials at approximately $E_{1/2}$ = −0.12 V and −1.42 V *versus* Fc^{+}/Fc. Upon addition of trifluoroacetic acid (TFA), a pronounced catalytic wave associated with proton reduction emerged, with an onset potential near −0.95 V.

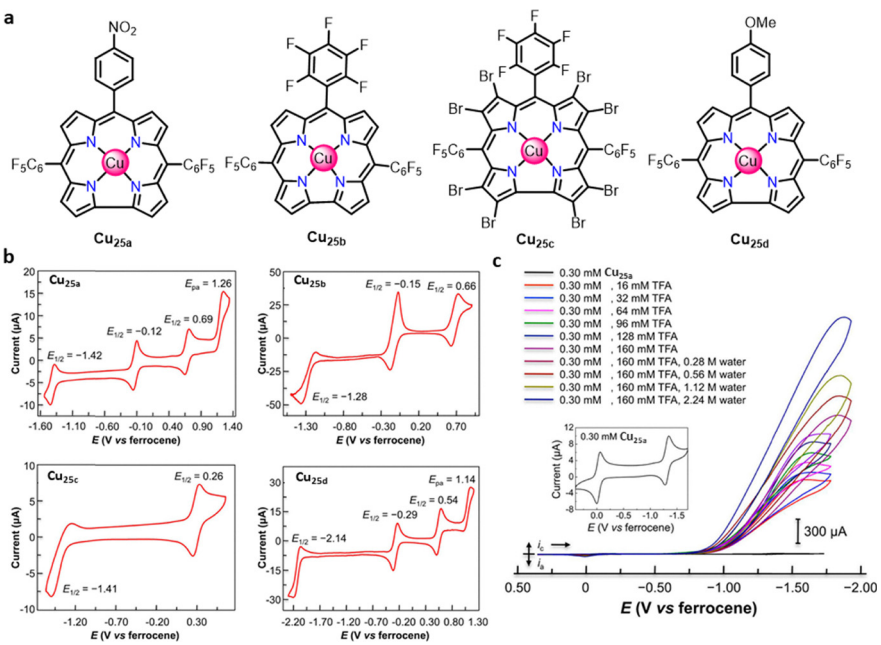

Fig. 21 (a) Chemical structure of Cu(II)-corrole complexes (**Cu$_{25a-d}$**), (b) CVs in acetonitrile solution of **Cu$_{25a}$** (0.30 mM), **Cu$_{25b}$** (1 mM), **Cu$_{25c}$** (0.13 mM), **Cu$_{25d}$** (0.75 mM), measurements were performed using 0.1 M (nBu$_4$N)PF$_6$ electrolyte with a scan rate of 100 mV s^{-1} on a glassy carbon electrode. (c) successive CVs of the active catalyst (**Cu$_{25a}$**, 0.30 mM) in acetonitrile with increasing concentrations of TFA followed by addition of small aliquots of water. Adapted from ref. 186 with permission from American Chemical Society,[186] copyright 2022.

The catalytic current reached a maximum at −1.65 V, while the half-wave catalytic potential ($E_{cat/2}$) was observed at −1.35 V. Based on this value, the overpotential for HER mediated by **Cu_{25a}** was estimated to be approximately 450 mV.

Control experiments carried by the authors using free Cu(II) ions resulted in copper film deposition on the electrode surface and electrochemical behavior markedly different from that of **Cu_{25a}**, highlighting the molecular nature of the corrole-based catalyst. Comparative studies within the series revealed distinct structure–performance relationships. Although **Cu_{25b}** exhibited reduction potentials similar to **Cu_{25a}**, it underwent rapid degradation under acidic conditions, consistent with known oxidative dimerization pathways of related corrole systems and the influence of axial ligation. **Cu_{25c}** displayed diminished catalytic activity, primarily attributed to its lower solubility and reduced catalytic current. In contrast, **Cu_{25d}**, bearing electron-donating methoxy substituents, was inactive toward proton reduction, as generation of the catalytically active species required access to a much more negative potential (−2.14 V). Among the series, **Cu_{25a}** demonstrated superior stability and activity. In the presence of 2.24 M water, **Cu_{25a}** achieved an exceptionally high catalytic-to-peak current ratio (i_{cat}/i_p) of 303 at an overpotential of 950 mV, recorded at a scan rate of 100 mV s^{-1}. CPE performed at −1.50 V for 2 h in acetonitrile containing 150 mM TFA resulted in sustained hydrogen evolution, affording a turnover number (TON) of 23 with a faradaic efficiency reaching 99%.

The molecular integrity and stability of **Cu_{25a}** during catalysis were confirmed through comprehensive post-electrolysis analyses. UV-visible and NMR spectroscopy conducted before and after CPE showed minimal changes, with more than 95% of the catalyst recovered following electrolysis. No significant loss of absorbance was observed in the UV-visible spectra after 2 h CPE. Furthermore, SEM and EDX were used by the group to examine the CPE glassy carbon working electrode and revealed no evidence of copper deposition. Collectively, these findings conclusively demonstrate that **Cu_{25a}** operates as a stable, homogeneous molecular electrocatalyst for hydrogen evolution.

Brooker and co-workers have systematically expanded what was a relatively small pool of known molecular copper catalysts at that time through the development of complexes (**Cu_{26}–Cu_{28}**, Fig. 22).[100,187,214] In their 2021 study, the group synthesized and characterized three copper(II) complexes supported by multidentate N_4 and N_5-donor macrocyclic and acyclic ligands that enforce distinct coordination geometries: square-planar (**Cu_{26}**), square-pyramidal (**Cu_{27}**), and acyclic trigonal-bipyramidal (**Cu_{28}**).

The N_4-macrocyclic ligand was synthesized *via* a Schiff base condensation between 2,2′-iminobisbenzaldehyde (dpa) and diethylenetriamine, following established literature procedures (Fig. 22).[215] The resulting macrocycle was subsequently transformed into the corresponding N_5-donor analogue through *N*-alkylation with 2-(bromomethyl)pyridine in dry THF at room temperature, using excess triethylamine (TEA) as base. The second N_5 acyclic ligand required for **Cu_{28}** was prepared directly by condensation of the dpa dialdehyde with 2-aminoethylpyridine

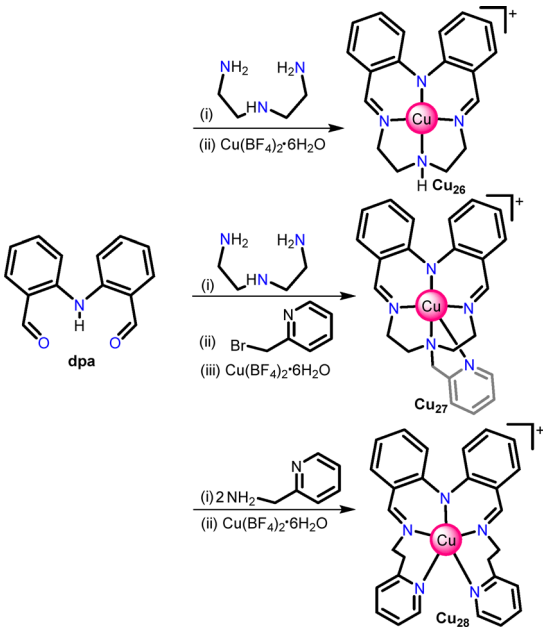

Fig. 22 Chemical structures of N_4 macrocycle and N_5 macrocyclic and noncyclic **Cu_{26}–Cu_{28}** studied as catalysts/pre-catalysts for HER by Brooker group.

in a 1 : 2 ratio under reflux in acetonitrile, affording the product in quantitative yield. The corresponding Cu(II) complexes ware then readily obtained at room temperature *via* a 1 : 1 : 1 reaction of the ligand, triethylamine (TEA), and $Cu(BF_4)_2{\cdot}H_2O$.

All three complexes exhibit reversible $Cu^{II/I}$ redox couples in dry acetonitrile with $E_{1/2}$ (*vs.* $AgNO_3/Ag$) = −1.39 V for the cyclic complexes **Cu_{26}** & **Cu_{27}** but −0.89 V for **Cu_{28}** with diffusion-controlled behavior evident from linear current *vs.* the square root of scan rate plots. Photocatalytic HER tests using a $[Ru(bpy)_3]^{2+}$ photosensitizer and triethanol amine (TEOA) sacrificial donor in DMF using blue LED (455 nm) produced modest turnover numbers (TON = 460–620), but control experiments revealed that simple copper salts and blanks often exhibited comparable or higher activity, underscoring the necessity of rigorous control tests and caution in interpreting apparent molecular photocatalysis. Consequently, attention shifted to electrocatalytic HER testing in MeCN with acetic acid (80 mM) as the proton source. Under steady-state conditions at −1.6 V *vs.* $AgNO_3/Ag$, the porphyrin like square-planar complex **Cu_{26}** displayed sustained catalytic activity (TON ≈ 12.5 over 6 h), whereas complexes **Cu_{27}** and **Cu_{28}** showed much lower activity, highlighting the influence of coordination geometry on electrocatalytic performance. Rinse-and-repeat and mercury drop tests were consistent with homogeneous catalysis for **Cu_{26}**, though small stripping waves suggest that the possibility of metastable heterogeneous species cannot be fully excluded.

Building on this, more recent work of the group in 2024 demonstrated that the square-planar **Cu_{26}** forms a catalytically active heterogeneous deposit under strictly aqueous conditions.[102] During controlled potential electrolysis (CPE) in pH 7 phosphate buffer at −1.10 V *vs.* Ag/AgCl, the complex

undergoes in *situ* transformation to a copper/oxygen-containing deposit (likely copper and Cu_2O) on a glassy carbon electrode. Characterization by EDX, PXRD, and SEM confirms that the deposit's composition and morphology differ from simple copper salt controls, and this heterogeneous phase exhibits robust and long-lived HER activity, with a TON of 2628 after 2.6 days, with FE = 93%. Interestingly and somewhat surprisingly, the rinse test performed on the working electrode revealed sustained activity even in the absence of dissolved catalyst in the solution (See Section 3, Fig. 7). This delivered a clear message to the authors, which was further supported by additional analysis, that the observed activity arises from heterogeneous species deposited on the electrode rather than solely from the homogeneous catalyst. The results highlight the dual role of the precursor complex: as an easily reducible molecular species under non-aqueous conditions, and as a precursor to a heterogeneous copper-based HER catalyst when operated in water. Collectively, these studies illustrate the transition from discrete molecular copper HER catalysts to heterogeneous active phases depending on the operational electrocatalytic conditions, emphasizing that molecular design can influence both intrinsic catalytic properties and the nature of *in situ* formed active species.

4.4.1. Design lessons from copper-macrocycles systems. Despite the relatively small number of reported copper macrocyclic HER catalysts compared with their Fe, Co, and Ni counterparts and beyond comparing individual catalytic performances, the macrocyclic systems discussed above provide several valuable emerging lessons for the rational design of future molecular copper HER catalysts. First, the rigid macrocyclic framework provides a robust platform capable of stabilizing multiple copper oxidation states and accommodating the geometric changes associated with Cu(II)/Cu(I)/Cu(0) redox processes. This feature is exemplified by porphyrin and corrole systems such as $\mathbf{Cu_{17}}$ and $\mathbf{Cu_{25}}$, which generally exhibit high Faradaic efficiencies (>95%) and retain their molecular integrity during electrolysis as confirmed by UV-vis, rinse-test, and post-electrolysis surface analyses.

Second, subtle electronic modifications of the macrocyclic framework can profoundly influence catalytic activity and even alter the HER mechanism. For example, β-lactone functionalization in the porphyrin series $\mathbf{Cu_{17a-d}}$ progressively shifted reduction potentials to more positive values and switched the catalytically active intermediate from a formal Cu(I) species to a Cu(0) species, demonstrating that ligand electronics can directly control the catalytic pathway. Likewise, *meso*-substitution of porphyrins resulted in substantial activity enhancement, with $\mathbf{Cu_{18}}$ achieving a TOF of $6.8 \times 10^4\ s^{-1}$ compared with $4.3 \times 10^4\ s^{-1}$ for the related $\mathbf{Cu_{17a}}$ catalyst while maintaining Faradaic efficiencies above 95%.

Third, several studies demonstrate the beneficial role of electronic communication between multiple copper centers. The fused bimetallic porphyrin $\mathbf{Cu_{16a}}$ and $\mathbf{Cu_{22}}$ displayed an exceptionally high TOF of $2 \times 10^6\ s^{-1}$ and $5 \times 10^6\ s^{-1}$, among the highest reported values for molecular copper HER catalysts, highlighting the advantages of metal–metal cooperativity and charge delocalization within conjugated macrocyclic frameworks. Similarly, increasing the nuclearity of wave-shaped copper porphyrin arrays from mono- to trinuclear architectures ($\mathbf{Cu_{24a}}$–$\mathbf{Cu_{24c}}$) systematically improved HER activity and lowered the overpotential required to achieve 10 mA cm^{-2} current density.

Fourth, the studies reveal that second-sphere effects can be as important as primary coordination-sphere modifications. Electrostatic engineering around copper porphyrins showed that negatively charged peripheral groups enhance HER activity as manifested in the series of the copper catalysts ($\mathbf{Cu_{21a-d}}$), whereas proximal cationic substituents suppress catalysis despite favorable redox potentials. These observations emphasize the importance of controlling proton delivery and intermediate stabilization through the local electrostatic environment.

Finally, macrocyclic systems provide valuable insight into the delicate balance between homogeneous catalysis and catalyst reconstruction. While corrole $\mathbf{Cu_{25a}}$ represents one of the most convincing examples of a stable homogeneous copper HER catalyst, exhibiting sustained electrolysis with FE = 99% and no detectable copper deposition, the $\mathbf{Cu_{26}}$ system illustrates how a molecular catalyst can act as a precursor to a highly active heterogeneous Cu/Cu_2O phase under aqueous conditions, ultimately reaching TON values as high as 2628 after 2.6 days of electrolysis. These contrasting cases underscore the necessity of rigorous homogeneity testing and highlight that catalyst stability remains one of the foremost challenges in the development of molecular copper HER systems.

4.5. Photocatalytic HER copper-based systems

Photocatalytic hydrogen generation driven by light represents a fundamental step toward solar fuel production. Despite recent advances in molecular catalysts operating under photocatalytic HE conditions,[56,58,193,216–223] examples based on copper remain relatively scarce. This section highlights and discusses representative recent work in copper-based photocatalytic hydrogen evolution systems. In addition to $\mathbf{Cu_{26}}$–$\mathbf{Cu_{28}}$ catalysts studied under photocatalytic conditions (see previous section), Yuan *et al.* reported in 2024 a series of square planar Cu(II)−anthraquinone molecular photocatalysts ($\mathbf{Cu_{29}}$–$\mathbf{Cu_{31}}$, Fig. 23) for hydrogen production.[224] The complexes were all active for photocatalytic hydrogen production without the use of additional catalyst or photosensitizer in 4 : 1 DMF/H_2O mixture with 2,3-dihydro-1,3-dimethyl-2-phenylbenzimidazole (BIH) as the sacrificial electron donor (SED) and irradiation with blue LED at λ_{max} of 450 nm (100 mW cm^{-2}). Cyclic voltammetry data also confirmed the electrocatalytic features of these catalysts in DMF in the presence of acetic acid as the proton source.

Under photocatalytic conditions the three complexes exhibited similar TOF_{max} of 11.7–13.5 h^{-1} $\mathbf{Cu_{31}}$ demonstrated the shortest stability, scoring an overall turnover number (TON) of 2240, whereas $\mathbf{Cu_{30}}$ exhibited enhanced longevity, achieving a TON of 3738. In contrast, $\mathbf{Cu_{29}}$ showed significantly superior long-term activity, sustaining consistent performance for over 20 days and reaching a TON of 6820 during this interval. The quantum yields for these systems were associated with the

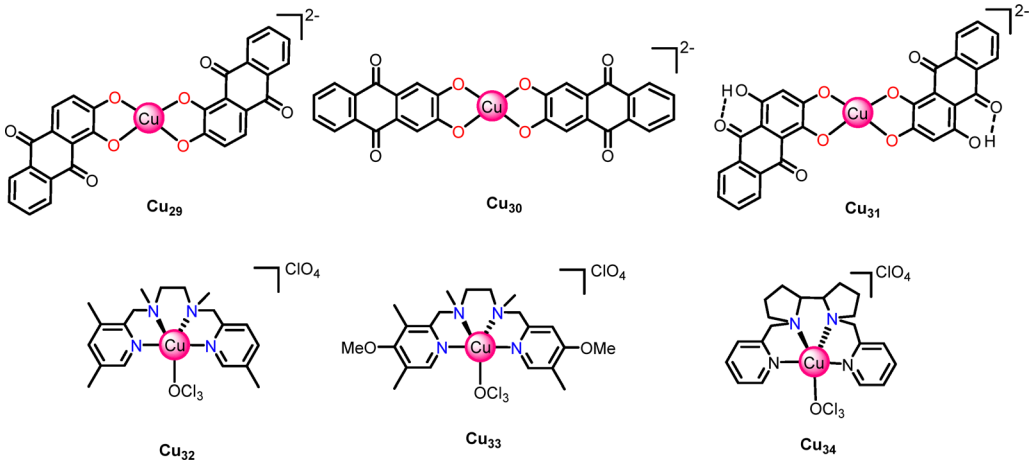

Fig. 23 Chemical structures of the Cu-complexes (**Cu$_{29}$–Cu$_{34}$**) used for photocatalytic HER.

observed activity, measured at 1.4×10^{-4} for **Cu$_{29}$**, 7.1×10^{-5} for **Cu$_{30}$**, and 2.2×10^{-4} for **Cu$_{29}$** at a wavelength of 450 nm. Dynamic light scattering (DLS) analysis conducted before and after irradiation of the system indicated the absence of nanoparticle formation and confirmed the homogeneity of the catalytic system. Additionally, a photolysis study conducted on the catalytic system over a 24-hour period in air revealed a 70% recovery of the Cu complex, as confirmed by UV-visible analysis.

Botcha *et al.* reported the synthesis and characterization of three water soluble copper complexes (**Cu$_{32}$–Cu$_{34}$**, Fig. 23) featuring diamine-dipyridine tetradentate ligands (N_2–Py_2) and evaluated their ability to mediate proton reduction under photocatalytic conditions.[178] The experiments were conducted in aqueous solution using mercaptopropionic acid-CdTe quantum dots (MPA-CdTe-QDs) as a photosensitizer due their superior photophysical properties. The authors employed quantum dots exclusively in photoluminescence quenching experiments to probe photoinduced electron-transfer capabilities of the Cu complexes. Photoluminescence studies of MPA–CdTe quantum dots in the presence of copper complexes revealed limited potential for photoinduced electron transfer (PET). **Cu$_{32–33}$** showed only minor quenching effects, attributed to static quenching or energy transfer rather than productive PET, while modification to a more rigid ligand framework **Cu$_{33}$** altered QD lifetimes but could not be conclusively quantified neither completely confirmed due to lack of ultrafast lifetime measurements. Overall, MPA–CdTe QDs were found to be unsuitable photosensitizers for these Cu complexes, highlighting that energetic alignment alone is insufficient to guarantee effective PET in Cu–QD systems.

4.5.1. Design lessons from photocatalytic copper HER systems. Although molecular copper photocatalysts for hydrogen evolution remain comparatively underdeveloped, the examples discussed above reveal several important design principles. First, ligand-centered photoactivity can be exploited to construct catalyst-only systems that operate without the need for an additional photosensitizer. The anthraquinone-containing complexes **Cu$_{29}$–Cu$_{31}$** demonstrate this concept effectively, achieving photocatalytic hydrogen production under visible-light irradiation using only a sacrificial electron donor. Among these systems, catalyst longevity rather than intrinsic activity proved to be the primary differentiating factor, as all three complexes exhibited comparable TOF values (11.7–13.5 h^{-1}), while their TONs varied substantially from 2240 (**Cu$_{31}$**) to 6820 (**Cu$_{29}$**). This observation highlights the importance of catalyst stability as a key determinant of long-term photocatalytic performance.

Second, the study of **Cu$_{29}$–Cu$_{31}$** illustrates that subtle ligand modifications can have a profound impact on catalyst durability. Despite exhibiting similar initial activities, **Cu$_{29}$** maintained hydrogen production for more than 20 days, significantly outperforming its analogues. Furthermore, DLS measurements and UV-vis analyses provided no evidence for nanoparticle formation, suggesting that the observed activity originated from a genuinely homogeneous molecular system. These results emphasize the value of incorporating structural motifs capable of stabilizing reduced copper intermediates while suppressing catalyst decomposition pathways.

A further lesson arises from the **Cu$_{32}$–Cu$_{34}$** systems, where photocatalytic performance was found to depend strongly on the compatibility between the copper catalyst and the photosensitizer. Although the redox potentials suggested favorable electron-transfer thermodynamics, photoluminescence studies revealed inefficient photoinduced electron transfer between the copper complexes and MPA–CdTe quantum dots. This finding demonstrates that energetic alignment alone is insufficient to ensure efficient photocatalysis and highlights the importance of optimizing electronic coupling, excited-state lifetimes, and interfacial charge transfer kinetics when designing photocatalytic assemblies.

Generally, these studies suggest that future advances in molecular copper photocatalysis will likely require the integration of three key features: robust ligand frameworks capable of stabilizing catalytically relevant copper species, efficient photosensitizer–catalyst communication pathways, and suppression

of decomposition processes that limit long-term operation. Such developments could enable molecular copper systems to emerge as attractive and earth-abundant alternatives for solar-driven hydrogen production.

5. Challenges and emerging opportunities in copper HER catalysts

Despite significant advances, molecular catalysts for the hydrogen evolution reaction (HER), particularly those based on copper, face several intrinsic challenges that limit their practical implementation.

As previously mentioned, early studies on copper-based HER catalysts largely relied on conventional polydentate ligands commonly used for other transition metals. However, the geometrical constrains often associated with copper redox-state changes encouraged the development of macrocyclic frameworks and bis-chelating ligands with pendant functionalities, anticipating improved adaptivity to geometric changes while improving catalyst stability. Fig. 24 presents a timeline of milestone copper catalysts developed over the last ten years, highlighting their characteristic structural motifs together with the corresponding benchmarking metrics for each system.

The studies discussed throughout this review collectively demonstrate that significant progress has been made in the development of molecular copper catalysts for hydrogen evolution. Despite the structural diversity of the reported systems, several common design principles have emerged, including the importance of ligand rigidity, multidentate coordination environments, electronic tuning, and strategies aimed at stabilizing catalytically relevant Cu(I) intermediates. These advances have improved catalytic activity, selectivity, and operational stability, while also providing valuable insights into the factors governing catalyst performance. Fig. 25 summarizes the key design principles that have emerged from molecular copper HER research, together with the major challenges that continue to limit further progress. These include important questions that remain regarding pre-catalyst activation, identification of the true active species, catalyst reconstruction/transformation under operating conditions, benchmarking standardization, and long-term durability. Addressing these challenges will be essential for translating molecular copper catalysts into practically relevant hydrogen-production systems.

A take-home message is that beyond the development of increasingly active catalysts, future progress in molecular copper HER catalysis will vitally require advances in four interconnected frontiers: (i) enhancement of catalyst stability and molecular integrity under operating conditions, (ii) widespread implementation of operando characterization methods to identify active species and catalyst transformation pathways, (iii) establishment of standardized benchmarking protocols to enable meaningful comparison between studies, and (iv) integration of computational and data-driven approaches for predictive catalyst design. These priorities are summarized in Fig. 25 and discussed in the following subsections.

5.1. Molecular integrity and enhanced stability

The possibility that the observed HER activity originates from *in situ* generated copper-containing species rather than the

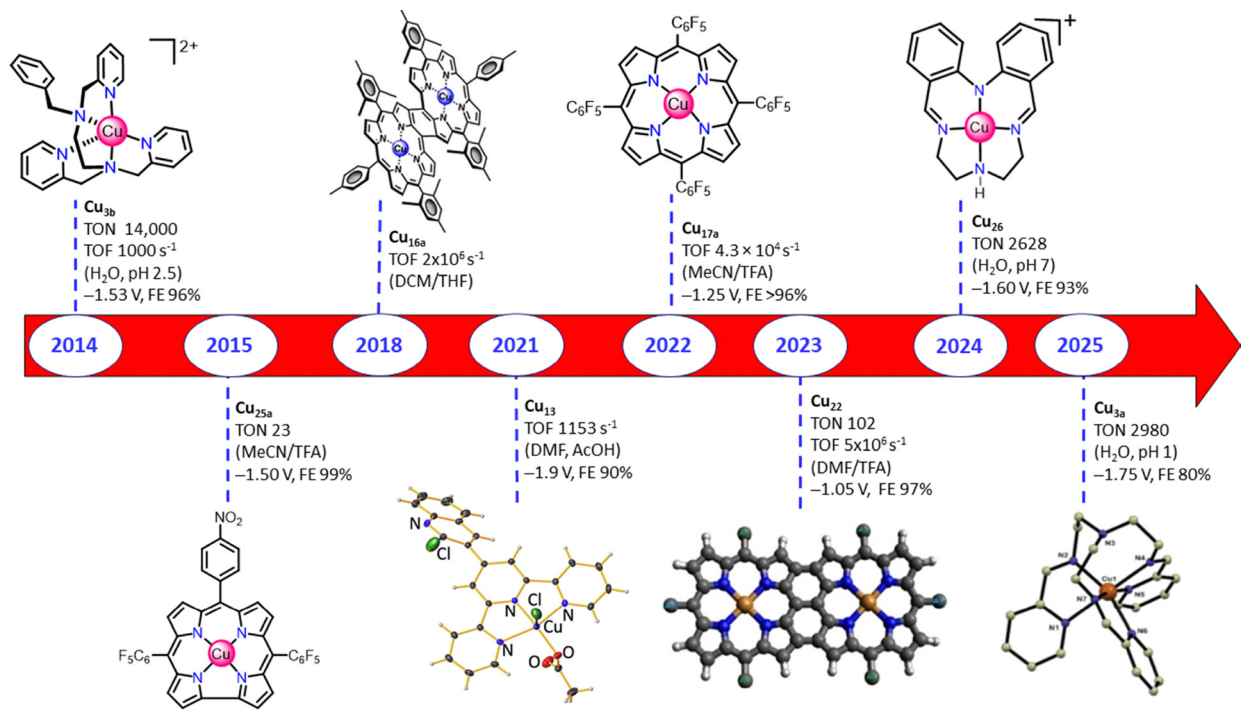

Fig. 24 Timeline highlighting the milestone structural motifs of copper-based catalysts/pre-catalysts for the hydrogen evolution reaction developed over the last decade.

Fig. 25 Schematic representation of emerging design principles, key challenges, and future research priorities for molecular copper HER catalysts.

initially designed molecular catalyst presents both a challenge and an opportunity for the molecular catalysis community. On one hand, the formation of nanoparticles, nanoclusters, or copper oxide species complicates the interpretation of structure–activity relationships and can obscure the true role of ligand design in governing catalytic performance. On the other hand, these observations provide valuable insight into catalyst activation processes and the dynamic nature of copper-based catalytic systems under operating conditions. Indeed, understanding when, how, and why molecular copper complexes retain their molecular identity or evolve into heterogeneous species was one of the primary motivations for undertaking this review. By critically examining catalyst activation pathways, catalyst integrity, and homogeneity diagnostics alongside catalytic performance, we aim to provide a more comprehensive framework for evaluating molecular copper HER systems and guiding the rational design of future catalysts.

A major challenge for molecular copper catalysts is their limited stability under operating conditions, where ligand degradation, demetallation, and irreversible reduction can occur, particularly at the negative potentials typically required for catalysis. These processes often lead to the formation of Cu(0), followed by aggregation or electrodeposition, and are further exacerbated in aqueous or acidic environments. Addressing these limitations requires rational molecular design strategies aimed at enhancing catalyst robustness. In this context, modification strategies already employed in other transition metal molecular catalyst such as but not limited to the incorporation of rigid, multidentate ligand frameworks, which can strengthen metal coordination and suppress structural degradation, while redox-active (non-innocent) ligands and metal–ligand cooperativity can help distribute the redox burden and reduce the likelihood of over-reduction.[225] The introduction of second-sphere functionalities, such as pendant proton relays or hydrogen-bonding groups, can facilitate proton-coupled electron transfer (PCET) and lower overpotentials, thereby minimizing catalyst stress. Additionally, steric protection around the metal center may inhibit bimolecular decomposition pathways and aggregation.[226–230]

A rational strategy to enhance the stability, and consequently the catalytic performance, of molecular copper catalysts for HER is to increase ligand hydrophobicity around the metal center, a strategy that is well used in CO_2 reduction catalysis, yet not in HER.[231–235] Introducing hydrophobic substituents (Fig. 26a) at the ligand periphery can limit excessive water access to the active site, which is often implicated in the formation of copper oxides or hydroxides that may lead to catalyst deactivation or the generation of heterogeneous species. In this context, it would be particularly interesting to apply such a strategy to copper corrole systems (Fig. 26a), where the *meso* and/or β-positions could be functionalized with long alkyl or perfluorinated chains to create a protective hydrophobic environment.

Corrole scaffolds, explored for copper-based HER in 2015,[186] represent promising platforms due to their N_4 macrocyclic framework. This ligand system can accommodate geometric changes associated with Cu(II)/Cu(I) redox cycling, while also

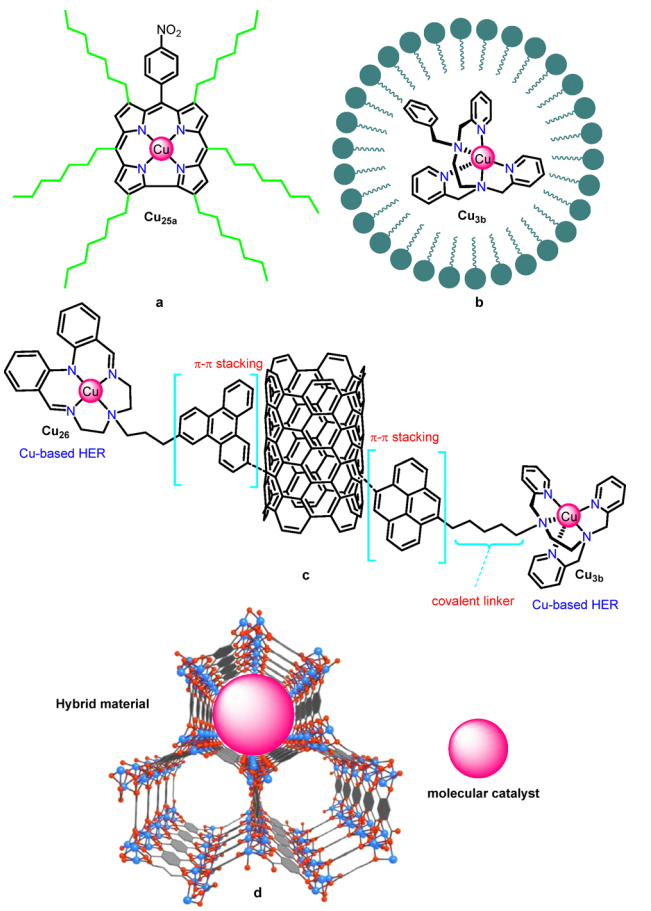

Fig. 26 Engineering approaches for enhanced HER performance: (a) surface modification with hydrophobic chains, (b) confined catalysis within micelle structures, (c) immobilization onto conductive CNT supports, and (d) hybridization with porous frameworks (COF/MOF).

exhibiting redox non-innocent behavior that enables electron storage and distribution during catalysis. Incorporating hydrophobic modifications into such systems may further enable operation in confined or nonpolar environments, such as micelles or liposome-like assemblies (Fig. 26b), which have already shown promise in other catalytic transformations, including CO_2 reduction.[231,232,234]

In addition to hydrophobic tuning, the introduction of electron-withdrawing substituents on the ligand framework represents another effective strategy to enhance catalytic performance. For example, copper corrole complexes bearing nitro substituents on *meso*-phenyl groups (**Cu_{25a}**) have demonstrated superior activity compared to their electron-donating analogues. A combined approach integrating hydrophobic shielding with electronic modulation is therefore anticipated to provide a powerful design strategy for developing next-generation molecular copper catalysts for hydrogen evolution.

Another important approach is catalyst immobilization or surface anchoring ideally onto conductive supports, such as carbon nanotubes, graphene, metal oxides, or electrodes modified with anchoring groups (Fig. 26c).[236–238] Immobilization can enhance catalyst lifetime, suppress decomposition and diffusion away from the electrode, and improve charge-transfer efficiency while retaining molecular-level control of the active site. The effectiveness of this strategy has recently been demonstrated in photocatalytic H_2 production using amine-functionalized CdS surfaces, suggesting its broader applicability to the design of next-generation molecular HER catalysts.[239] Effective strategy also involves integration into hybrid molecular–material architectures (Fig. 26d), including confinement within metal–organic frameworks (MOFs),[240–243] covalent organic frameworks (COFs),[219,244,245] or polymer matrices.[246,247] Recent studies on molecular HER catalysts have further highlighted the importance of secondary coordination sphere engineering, catalyst stability, and active-species identification as key determinants of catalytic performance.[248] Additionally, nanomaterials can serve as active surfaces for molecular catalysts, potentially resulting in hybrid materials that exhibit enhanced stability and activity. For instance, carbon nanotubes (CNTs) have recently been extensively utilized as supports for water reduction and oxidation catalysts.[249,250] Other supports, such as carbon nitrides, metal oxides and iron sulfides, are also recognized for their efficiency not only for HER but in overall water splitting as well.[251–253] These environments can protect molecular catalysts from degradation, enforce site isolation, and create local proton or electron transport pathways that enhance HER kinetics. Such confinement also helps bridge the gap between homogeneous molecular catalysis and heterogeneous electrode operation. Electronic tuning through ligand substitution represents a further route to improving HER performance. By modulating ligand donor strength, conjugation, or redox activity, the redox potentials, hydricity, and proton affinity of the metal center can be finely adjusted to lower overpotentials and accelerate proton-coupled electron transfer steps.[254,255] Closely related is the use of redox-active (non-innocent) ligands, which can serve as electron reservoirs and reduce the redox burden on the metal center, thereby stabilizing reactive intermediates.[256]

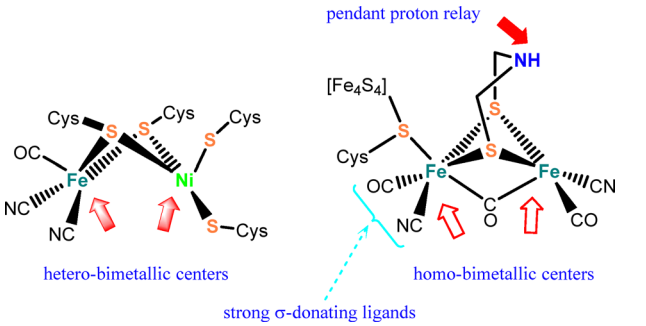

Fig. 27 Structural features of the active sites of two hydrogenase classes. Dashed and hollow red arrows denote bimetallic centers with unsaturated coordination sites, and the filled red arrow indicates the pendant proton relay (–NH–) group.

A further rational design strategy involves incorporating a second metal center such as Ni, Fe, or Co adjacent to the copper active site, inspired by the bimetallic architecture of hydrogenase cofactors (Fig. 27). Such an approach could introduce synergistic effects that enhance catalytic activity and facilitate multi-electron/proton transfer processes. Although the synthesis of heterobimetallic systems presents significant challenges, the potential benefits in terms of reactivity and stability make this a compelling direction for future research.

In parallel, the incorporation of pendant Lewis basic groups, such as primary or secondary amines, can serve as proton relays, mimicking the secondary coordination sphere of hydrogenases (Fig. 26). These functionalities can promote efficient proton-coupled electron transfer (PCET) and improve both catalytic efficiency and durability. Additionally, the use of strong σ-donating co-ligands, such as carbonyl (CO) or cyanide (CN^-), may help stabilize low-valent copper intermediates, provided that sufficient coordination flexibility is retained. Maintaining a labile coordination site—through weakly bound ligands such as H_2O, MeCN, or halides can further facilitate substrate binding and turnover following initial reduction steps.

Collectively, integrating bimetallic design, second-sphere proton relays, and electronic tuning through strong donor ligands represents a promising strategy for developing more efficient and robust copper-based catalysts for hydrogen evolution.

Finally, reaction-environment engineering including solvent selection, buffer identity, proton donor strength, and electrolyte composition plays a critical yet often underappreciated role in molecular HER catalysis. Optimizing these parameters can dramatically influence catalytic rates, selectivity, and apparent stability, underscoring the importance of full catalyst–environment design rather than catalyst structure alone.[257–259] It also of greatly wise to be aware that the development of homogeneous transition-metal catalysts capable of driving hydrogen evolution directly from water remains unmet goal in the pursuit of sustainable green hydrogen production. For large-scale and environmentally benign applications, catalysts must be

water-soluble, stable, and operationally robust. From an industrial standpoint, however, heterogeneous catalysts are often favoured due to their ease of separation, recyclability and resilience under harsh acidic or alkaline conditions, which translate into reduced operational costs. In this context, the realization of molecular catalysts that combine water solubility, stability, high activity, and long-term durability represents a significant milestone. Over the past two decades, several water-soluble molecular HER catalysts based on cobalt,[57,59,62,140,218,230,260–262] nickel,[263–265] and molybdenum[266,267] have been reported, whereas analogous copper-based systems remain comparatively rare.[102,110,268] As a consequence, emergence of copper-based molecular catalysts or pre-catalysts are expected to incline more than before in the coming future especially those which are soluble and water compatible.

Future catalyst development should prioritize systems capable of maintaining molecular integrity and catalytic activity during prolonged electrolysis under aqueous conditions while suppressing Cu(I) disproportionation, catalyst decomposition, and molecular-to-heterogeneous transformation.

5.2. *In situ* characterization

Determining the structure and composition of the true active species during catalysis presents significant challenges. This is likely due to insufficient characterization of the catalyst while it is operational. Operando techniques address this issue by simultaneously investigating the catalyst's structure during operation and correlating these observations with its catalytic performance.[269,270]

A variety of operando techniques applicable to electro- or photocatalytic processes range from traditional photo-spectroscopic methods to more complex methodologies. Spectroscopic techniques, such as infrared spectroscopy, serve as powerful instruments for examining chemical transformations induced by reactant interactions and alterations in the surrounding environment.[271] In addition to these methods, neutron scattering, though less commonly utilized, provides exceptional sensitivity to light elements, yielding structural information that is often unattainable through photon or X-ray-based approaches.[272] Concurrently, reactions occurring at solid–liquid interfaces have emerged as a central focus in contemporary electrocatalysis. Advanced characterization methods, including liquid-cell transmission electron microscopy,[273] scanning electrochemical probe microscopy,[274] X-ray scattering,[275] and X-ray computed tomography,[276] as well as operando electrochemical impedance spectroscopy (EIS) and surface-enhanced Raman spectroscopy[277] facilitate detailed analyses of both surface and bulk characteristics, enabling quantitative assessments of electrode morphology, texture, and internal transport pathways. Finally, it is not surprising to introduce a hybrid ultrahigh-vacuum–electrochemistry (UHV–EC) approach to probe the otherwise buried electrode–electrolyte interface.[278] By transferring electrodes from electrolyte to UHV after electrochemical control, surface-science techniques such as XPS and STM can be applied to analyze potential-dependent interfacial structure and electronic states. This methodology provides unique molecular-level insight into electrochemical interfaces that is inaccessible to conventional *in situ* techniques.

Moving forward, operando characterization should become a routine component of catalyst evaluation, enabling direct correlation between catalyst structure, activation pathways, and catalytic performance under realistic operating conditions.

5.3. Benchmarking and comparability

like other molecular catalytic systems, comparability between molecular catalysts for HER across studies remain inconsistent, owing to variations in solvents, proton sources, reference electrodes, and kinetic metrics (*e.g.*, k_{obs}, TOF, TON). The absence of standardized testing protocols complicates objective performance evaluation. For example, Appel and Helm discuss the importance of consistent determination of overpotentials for molecular electrocatalysts,[143] noting that inconsistent definitions (*e.g.*, onset *vs.* $E_{cat/2}$, see Section 1) can lead to misleading comparisons between studies.[279]

Critical reviews highlighted that current HER/OER research suffers from inconsistent benchmarking,[280,281] where variations in electrolyte purity, electrode preparation, normalization methods and data analysis lead to poor comparability between reported performances. A useful review by Bligaard *et al.* emphasizes that objective comparisons of electrocatalytic activity require standardized testing under identical conditions; without such protocols, reported overpotentials and activities cannot be fairly compared across different catalyst systems.[282] Greater adoption of unified benchmarking criteria, transparent reporting of experimental conditions, and the combined use of electrochemical and bulk electrolysis metrics would significantly improve cross-comparison and accelerate rational catalyst design.

In addition, future studies should incorporate standardized electrochemical metrics, including Tafel analysis and long-term stability testing, to enable meaningful comparison of molecular copper HER catalysts and facilitate the identification of robust structure–activity relationships.

The establishment of community-wide benchmarking practices, including consistent reporting of TON, TOF, overpotential, Faradaic efficiency, electrolysis duration, catalyst concentration, and proton source, will be essential for meaningful comparison and accelerated catalyst development.

5.4. Computational and data-driven challenges

Despite rapid advances in experimental synthesis and mechanistic studies of copper-based HER catalysts, the limited integration of computational modelling and modern Artificial Intelligence (AI) tools has constrained rational catalyst design.[283–286] yet their application to molecular electrocatalysis,[287] including copper complexes, remains nascent.[288] Based on the diverse cases discussed in this review and elsewhere copper complexes has demonstrated the capability to exhibit a rich landscape of accessible electronic states, proton-coupled electron transfer pathways, and secondary-sphere effects that profoundly influence catalytic activity and stability, yet these multiscale phenomena are challenging to capture with

traditional, manually driven theory alone, particularly when explore ligand space, predict overpotentials, or anticipate degradation pathways. Consequently, catalyst development often remains empirical and incremental rather than predictive, slowing progress toward optimally tuned Cu complexes with low overpotentials and high turnover frequencies. The integration of *in silico* approaches,[289,290] including advanced DFT benchmarking, automated reaction network exploration, and AI-driven optimization promises to accelerate discovery, improve mechanistic understanding, and guide experimental efforts toward targeted performance objectives in copper-based HER catalysis.

The integration of machine learning, automated reaction-network analysis, and high-throughput computational screening offers a promising pathway toward predictive catalyst design and accelerated discovery of next-generation molecular copper HER catalysts.

6. Conclusions and outlook

Copper-based catalysts occupy a unique and increasingly important position in the landscape of hydrogen evolution catalysis. While copper has long been involved in fundamental studies of hydrogen evolution, only relatively recently has significant attention been directed toward the development of well-defined molecular copper complexes operating under electro- and photocatalytic conditions. The examples surveyed in this review demonstrate that rational ligand design, control over coordination geometry, and tuning of electronic structure can enable copper complexes to access catalytically competent redox states and promote proton-coupled electron transfer processes relevant to HER.

Despite these advances, the performance of molecular copper HER catalysts remain less mature compared to analogous systems based on cobalt, nickel, or iron. In many reported studies, catalytic activity is demonstrated, yet key benchmarking parameters, such as turnover numbers, turnover frequencies, overpotentials, and long-term durability are not always reported in a consistent or comprehensive manner. Moreover, distinguishing true homogeneous molecular catalysis from *in situ* formation of heterogeneous copper deposits continues to represent a critical challenge, underscoring the need for rigorous control experiments, including rinse tests, spectroelectrochemical monitoring, and post-electrolysis electrode characterization.

Looking ahead, several promising directions emerge. Incorporation of second-sphere proton relays, multidentate and redox-active ligand frameworks, and metal–ligand cooperativity offers clear pathways to lowering overpotentials and enhancing catalytic rates. Hybrid approaches, such as immobilization of molecular copper catalysts on conductive supports or within polymeric and porous matrices, may further improve stability while retaining molecular-level control. In parallel, greater integration of computational modeling and data-driven approaches could accelerate catalyst discovery and provide mechanistic insight that is currently underdeveloped for copper systems. A broader challenge facing molecular copper HER catalysts is their translation from proof-of-concept systems to technologically relevant hydrogen-production platforms. Despite substantial progress in catalyst design, many reported molecular copper systems still operate at higher overpotentials and exhibit lower long-term stability than state-of-the-art heterogeneous catalysts based on noble metals or optimized earth-abundant materials. Consequently, direct industrial implementation of molecular copper catalysts remains a long-term objective rather than an immediate prospect. Nevertheless, molecular catalysts provide unique advantages that are difficult to access in heterogeneous systems, including atomically defined active sites, precise control over the coordination environment, tunable electronic structures, and unparalleled opportunities for mechanistic investigation. Future industrial relevance will likely emerge through hybrid molecular–material architectures in which molecular copper catalysts are immobilized on conductive supports, incorporated into porous frameworks, or integrated into photoelectrochemical and electrolyzer devices. Such approaches could combine the robustness and scalability of heterogeneous materials with the selectivity and tunability of molecular catalysts. In this context, advances in catalyst stability, operation in aqueous media, and long-term durability will be essential prerequisites for translating molecular copper HER systems from laboratory studies toward practical hydrogen-production technologies. In summary, while molecular copper catalysts for hydrogen evolution are still at an early stage of development, the progress achieved to date demonstrates their viability and potential. With improved benchmarking practices, rigorous assessment of catalytic homogeneity, and continued advances in molecular design and reaction engineering, copper-based HER catalysts may evolve into competitive, earth-abundant alternatives for sustainable hydrogen production.

Conflicts of interest

There are no conflicts to declare.

Data availability

No data was used for the research described in the article.

Acknowledgements

A. M. A gratefully acknowledges the ASU for financial support within DRGS-20268 research grant. L. T.-G. is a Chercheur Qualifié of the Fonds de la Recherche Scientifique – FNRS. ChatGPT (OpenAI) was used solely as an auxiliary tool during the preparation of Fig. 1. The authors reviewed, modified, and verified all generated content and take full responsibility for the accuracy and integrity of the manuscript.

References

1 A. L. Hammond, Solar energy: the largest resource, *Science*, 1972, **177**(4054), 1088–1090.
2 (UNFCCC), C. C., Paris Agreement to the United Nations Framework Convention on Climate Change. In T.I.A.S. No. 16-1104, Convention, T. U. N. F., Ed. Paris-France, December 12, 2015.
3 Decision, U. C. United Nations Framework Convention on Climate Change; https://unfccc.int/documents/628660, Dec 2023.
4 C. Nature, Editorial, A future for hydrogen in European transportation, *Nat. Catal.*, 2020, **3**(2), 91.
5 N. Armaroli and V. Balzani, The Hydrogen Issue, *ChemSusChem*, 2011, **4**(1), 21–36.
6 J. A. Turner, Sustainable hydrogen production, *Science*, 2004, **305**, 972–974.
7 B. Pivovar, Catalysts for fuel cell transportation and hydrogen related uses, *Nat. Catal.*, 2019, **2**(7), 562–565.
8 V. Andrei, B. Reuillard and E. Reisner, Bias-free syngas production by integrating a molecular cobalt catalyst with perovskite-$BiVO_4$ tandems, *Nat. Mater.*, 2020, **19**, 189–194.
9 Energy, U. S. D. o., How Do Fuel Cell Electric Vehicles Work Using Hydrogen? Energy, A.-O. o. E. E. a. R., Ed. retrieved 26-08-2025.
10 N. Ma, W. Zhao, W. Wang, X. Li and H. Zhou, Large scale of green hydrogen storage: Opportunities and challenges, *Int. J. Hydrogen Energy.*, 2024, **50**, 379–396.
11 J. G. Segovia-Hernández, S. Hernández, E. Cossío-Vargas, M. Juarez-García and E. Sánchez-Ramírez, Green hydrogen production for sustainable development: a critical examination of barriers and strategic opportunities, *RSC Sustainability*, 2025, **3**(1), 134–157.
12 S. Shiva Kumar and H. Lim, An overview of water electrolysis technologies for green hydrogen production, *Energy Rep*, 2022, **8**, 13793–13813.
13 J. Li, Y. Ma, X. Mu, X. Wang, Y. Li, H. Ma and Z. Guo, Recent Advances and Perspectives on Coupled Water Electrolysis for Energy-Saving Hydrogen Production, *Adv. Sci.*, 2025, **12**(7), 2411964.
14 P. Phogat and B. Chand, Shreya, Hydrogen economy: Pathways, production methods, and applications for a sustainable energy future, *Sustain. Mater. Technol.*, 2025, **45**, e01550.
15 M. Chatenet, B. G. Pollet, D. R. Dekel, F. Dionigi, J. Deseure, P. Millet, R. D. Braatz, M. Z. Bazant, M. Eikerling, I. Staffell, P. Balcombe, Y. Shao-Horn and H. Schäfer, Water electrolysis: from textbook knowledge to the latest scientific strategies and industrial developments, *Chem. Soc. Rev.*, 2022, **51**(11), 4583–4762.
16 Association, I. E. The Future of Hydrogen; IEA, Paris: https://www.iea.org/reports/the-future-of-hydrogen, June 2019, 2019.
17 H. Vrubel and X. Hu, Molybdenum Boride and Carbide Catalyze Hydrogen Evolution in both Acidic and Basic Solutions, *Angew. Chem., Int. Ed.*, 2012, **51**(51), 12703–12706.
18 W.-F. Chen, J. T. Muckerman and E. Fujita, Recent developments in transition metal carbides and nitrides as hydrogen evolution electrocatalysts, *Chem. Commun.*, 2013, **49**(79), 8896–8909.
19 H.-M. Zhang, J.-J. Wang, Y. Meng, F. Lu, M. Ji, C. Zhu, J. Xu and J. Sun, Review on Intrinsic Electrocatalytic Activity of Transition Metal Nitrides on HER, *Energy Mater. Adv.*, 2022, **2022**, 0006.
20 M. S. A. Sher Shah, G. Y. Jang, K. Zhang and J. H. Park, Transition EcoEnergy metal carbide-based nanostructures for electrochemical hydrogen and oxygen evolution reactions, *EcoEnergy*, 2023, **1**(2), 344–374.
21 Q. Lu, G. S. Hutchings, W. Yu, Y. Zhou, R. V. Forest, R. Tao, J. Rosen, B. T. Yonemoto, Z. Cao, H. Zheng, J. Q. Xiao, F. Jiao and J. G. Chen, Highly porous non-precious bimetallic electrocatalysts for efficient hydrogen evolution, *Nat. Commun.*, 2015, **6**(1), 6567.
22 C. C. L. McCrory, S. Jung, I. M. Ferrer, S. M. Chatman, J. C. Peters and T. F. Jaramillo, Benchmarking Hydrogen Evolving Reaction and Oxygen Evolving Reaction Electrocatalysts for Solar Water Splitting Devices, *J. Am. Chem. Soc.*, 2015, **137**(13), 4347–4357.
23 Z. Xing, Q. Liu, A. M. Asiri and X. Sun, High-Efficiency Electrochemical Hydrogen Evolution Catalyzed by Tungsten Phosphide Submicroparticles, *ACS Catal.*, 2015, **5**(1), 145–149.
24 E. J. Popczun, J. R. McKone, C. G. Read, A. J. Biacchi, A. M. Wiltrout, N. S. Lewis and R. E. Schaak, Nanostructured Nickel Phosphide as an Electrocatalyst for the Hydrogen Evolution Reaction, *J. Am. Chem. Soc.*, 2013, **135**(25), 9267–9270.
25 E. J. Popczun, C. G. Read, C. W. Roske, N. S. Lewis and R. E. Schaak, Highly Active Electrocatalysis of the Hydrogen Evolution Reaction by Cobalt Phosphide Nanoparticles, *Angew. Chem., Int. Ed.*, 2014, **53**(21), 5427–5430.
26 T. F. Jaramillo, K. P. Jørgensen, J. Bonde, J. H. Nielsen, S. Horch and I. Chorkendorff, Identification of Active Edge Sites for Electrochemical H2 Evolution from MoS_2 Nanocatalysts, *Science*, 2007, **317**(5834), 100–102.
27 B. Hinnemann, P. G. Moses, J. Bonde, K. P. Jørgensen, J. H. Nielsen, S. Horch, I. Chorkendorff and J. K. Nørskov, Biomimetic Hydrogen Evolution: MoS2 Nanoparticles as Catalyst for Hydrogen Evolution, *J. Am. Chem. Soc.*, 2005, **127**(15), 5308–5309.
28 X. Hu, Y. Gao, X. Luo, J. Xiong, P. Chen and B. Wang, Insight into the intrinsic activity of various transition metal sulfides for efficient hydrogen evolution reaction, *Nanoscale*, 2024, **16**(9), 4909–4918.
29 M. Li, H. Li, H. Fan, Q. Liu, Z. Yan, A. Wang, B. Yang and E. Wang, Engineering interfacial sulfur migration in transition-metal sulfide enables low overpotential for durable hydrogen evolution in seawater, *Nat. Commun*, 2024, **15**(1), 6154.
30 J.-D. Xiao, Q. Shang, Y. Xiong, Q. Zhang, Y. Luo, S.-H. Yu and H.-L. Jiang, Boosting Photocatalytic Hydrogen Production of a Metal–Organic Framework Decorated with

Platinum Nanoparticles: The Platinum Location Matters, *Angew. Chem., Int. Ed.*, 2016, **55**(32), 9389–9393.
31 H. H. Do, T. H. C. Nguyen, T. V. Nguyen, C. Xia, D. L. T. Nguyen, P. Raizada, P. Singh, V.-H. Nguyen, S. H. Ahn, S. Y. Kim and Q. V. Le, Metal-organic-framework based catalyst for hydrogen production: Progress and perspectives, *Int. J. Hydrogen Energy.*, 2022, **47**(88), 37552–37568.
32 H. B. Wu and X. W. Lou, Metal-organic frameworks and their derived materials for electrochemical energy storage and conversion: Promises and challenges, *Sci. Adv.*, 2017, **3**(12), eaap9252.
33 L. Jimenez-Lopez, R. Morales Ospino, L. G. de Araujo, A. Celzard and V. Fierro, Latest developments in the synthesis of metal–organic frameworks and their hybrids for hydrogen storage, *Nanoscale*, 2025, **17**(11), 6390–6413.
34 Y. Choi, H.-i Kim, G.-h Moon, S. Jo and W. Choi, Boosting up the Low Catalytic Activity of Silver for H_2 Production on Ag/TiO_2 Photocatalyst: Thiocyanate as a Selective Modifier, *ACS Catal.*, 2016, **6**(2), 821–828.
35 T. Mondal, S. Patra, B. Mondal, P. Ghosh, I. W. Hamley and A. Banerjee, Silver-Containing Metallo Hydrogel as a Nanocatalyst for Hydrogen Evolution, *ACS Appl. Polym. Mater.*, 2024, **6**(18), 11383–11391.
36 Y. Zhang, J. Zhao, H. Wang, B. Xiao, W. Zhang, X. Zhao, T. Lv, M. Thangamuthu, J. Zhang, Y. Guo, J. Ma, L. Lin, J. Tang, R. Huang and Q. Liu, Single-atom Cu anchored catalysts for photocatalytic renewable H_2 production with a quantum efficiency of 56%, *Nat. Commun*, 2022, **13**(1), 58.
37 X.-H. Jiang, L.-S. Zhang, H.-Y. Liu, D.-S. Wu, F.-Y. Wu, L. Tian, L.-L. Liu, J.-P. Zou, S.-L. Luo and B.-B. Chen, Silver Single Atom in Carbon Nitride Catalyst for Highly Efficient Photocatalytic Hydrogen Evolution, *Angew. Chem., Int. Ed.*, 2020, **59**(51), 23112–23116.
38 L. Wang, X. Liu, L. Cao, W. Zhang, T. Chen, Y. Lin, H. Wang, Y. Wang and T. Yao, Active Sites of Single-Atom Iron Catalyst for Electrochemical Hydrogen Evolution, *J. Phys. Chem. Lett.*, 2020, **11**(16), 6691–6696.
39 K. L. Zhou, Z. Wang, C. B. Han, X. Ke, C. Wang, Y. Jin, Q. Zhang, J. Liu, H. Wang and H. Yan, Platinum single-atom catalyst coupled with transition metal/metal oxide heterostructure for accelerating alkaline hydrogen evolution reaction, *Nat. Commun*, 2021, **12**(1), 3783.
40 M. Kim, S. Kim, X. Wang, R. Q. Snurr, J. T. Hupp and D. Whang, Adjusting the Criteria for Hydrogen Evolution by Single-Atom Catalysts, *J. Am. Chem. Soc.*, 2025, **147**(36), 33281–33287.
41 J. Shan, C. Ye, Y. Jiang, M. Jaroniec, Y. Zheng and S.-Z. Qiao, Metal-metal interactions in correlated single-atom catalysts, *Sci. Adv.*, 2022, **8**(17), eabo0762.
42 R. L. H. Freire, H. A. B. Fonseca, P. I. R. Moraes, M. Mocelim, M. M. C. B. Neto and J. L. F. Da Silva, Defect-Engineered MoS2 Supported Transition Metal Clusters for Electrochemical Reactions, *ACS Catal.*, 2025, **15**(23), 20036–20048.
43 Y. Chen, L. Soler, C. Cazorla, J. Oliveras, N. G. Bastús, V. F. Puntes and J. Llorca, Facet-engineered TiO2 drives photocatalytic activity and stability of supported noble metal clusters during H2 evolution, *Nat. Commun*, 2023, **14**(1), 6165.
44 Y. Fan, J. Zhao, J. Zhou, W.-H. Huang, J. Zhu, C.-Y. Kuo, S. Zhang, C.-W. Pao, T.-S. Chan, Y. Zhang, S.-Y. Hsu, J.-M. Chen, C.-T. Chen, C. Jin, L. H. Tjeng, J.-Q. Wang, Z. Hu and L. Zhang, Self-assembled metal cluster/perovskite catalysts for efficient acidic hydrogen production with an ultra-low overpotential of 62 mV and over 1500 hours of stability at 1 A cm^{-2}, *Energy Environ. Sci.*, 2025, **18**(15), 7527–7540.
45 S. Yang, D. Rao, J. Ye, S. Yang, C. Zhang, C. Gao, X. Zhou, H. Yang and X. Yan, Mechanism of transition metal cluster catalysts for hydrogen evolution reaction, *Int. J. Hydrogen Energy.*, 2021, **46**(5), 3484–3492.
46 X.-Y. Liu, J.-W. Liu, G. Li and J.-X. Zhao, Transition metal clusters with precise numbers of atoms anchored on graphdiyne as multifunctional electrocatalysts for OER/ORR/HER: a computational study, *Rare Met.*, 2024, **43**(7), 3107–3117.
47 L. A. Berben and J. C. Peters, Hydrogen evolution by cobalt tetraimine catalysts adsorbed on electrode surfaces, *Chem. Commun.*, 2010, **46**(3), 398–400.
48 C. M. Lousada and A. M. Kotasthane, Hydrogen adsorption on fcc metal surfaces towards the rational design of electrode materials, *Sci. Rep.*, 2024, **14**(1), 20972.
49 W. Lubitz, H. Ogata, O. Rüdiger and E. Reijerse, Hydrogenases, *Chem. Rev.*, 2014, **114**, 4081–4148.
50 G. A. N. Felton, R. S. Glass, D. L. Lichtenberger and D. H. Evans, Iron-Only Hydrogenase Mimics. Thermodynamic Aspects of the Use of Electrochemistry to Evaluate Catalytic Efficiency for Hydrogen Generation, *Inorg. Chem.*, 2006, **45**(23), 9181–9184.
51 T. R. Simmons, G. Berggren, M. Bacchi, M. Fontecave and V. Artero, Mimicking hydrogenases: From biomimetics to artificial enzymes, *Coord. Chem. Rev.*, 2014, **270–271**, 127–150.
52 K. C. Gupta and A. K. Sutar, Catalytic activities of Schiff base transition metal complexes, *Coord. Chem. Rev.*, 2008, **252**(12–14), 1420–1450.
53 S. Losse, J. G. Vos and S. Rau, Catalytic hydrogen production at cobalt centres, *Coord. Chem. Rev.*, 2010, **254**, 2492–2504.
54 C. Costentin and D. G. Nocera, Self-healing catalysis in water, *Proc. Natl. Acad. Sci.*, 2017, **114**(51), 13380–13387.
55 D. Z. Zee, T. Chantarojsiri, J. R. Long and C. J. Chang, Metal–polypyridyl catalysts for electro- and photochemical reduction of water to hydrogen, *Acc. Chem. Res.*, 2015, **48**(7), 2027–2036.
56 N. Queyriaux, R. T. Jane, J. Massin, V. Artero and M. Chavarot-Kerlidou, Recent developments in H_2 evolving molecular cobalt(II)–polypyridyl catalysts, *Coord. Chem. Rev.*, 2015, **304–305**, 3–19.
57 Y. Sun, J. P. Bigi, N. A. Piro, M. L. Tang, J. R. Long and C. J. Chang, Molecular Cobalt Pentapyridine Catalysts for Generating Hydrogen from Water, *J. Am. Chem. Soc.*, 2011, **133**, 9212–9215.

58 W. M. Singh, T. Baine, S. Kudo, S. Tian, X. A. N. Ma, H. Zhou, N. J. DeYonker, T. C. Pham, J. C. Bollinger, D. L. Baker, B. Yan, C. E. Webster and X. Zhao, Electrocatalytic and Photocatalytic Hydrogen Production in Aqueous Solution by a Molecular Cobalt Complex, *Angew. Chem., Int. Ed.*, 2012, **51**, 5941–5944.

59 P. Zhang, M. Wang, F. Gloaguen, L. Chen, F. Quentel and L. Sun, Electrocatalytic hydrogen evolution from neutral water by molecular cobalt tripyridine–diamine complexes, *Chem. Commun.*, 2013, **49**, 9455–9457.

60 D. Basu, S. Mazumder, X. Shi, H. Baydoun, J. Niklas, O. Poluektov, H. B. Schlegel and C. N. Verani, Ligand Transformations and Efficient Proton/Water Reduction with Cobalt Catalysts Based on Pentadentate Pyridine-Rich Environments, *Angew. Chem., Int. Ed.*, 2014, **127**, 2133–2138.

61 B. B. Beyene, S. B. Mane and C.-H. Hung, Highly efficient electrocatalytic hydrogen evolution from neutral aqueous solution by a water-soluble anionic cobalt(ii) porphyrin, *Chem. Commun.*, 2015, **51**(81), 15067–15070.

62 B. B. Beyene, S. B. Mane and C.-H. Hung, Highly efficient electrocatalytic hydrogen evolution from neutral aqueous solution by a water-soluble anionic cobalt(II) porphyrin, *Chem. Commun.*, 2015, **51**(81), 15067–15070.

63 P. Zhang, M. Wang, Y. Yang, D. Zheng, K. Han and L. Sun, Highly efficient molecular nickel catalysts for electrochemical hydrogen production from neutral water, *Chem. Commun.*, 2014, **50**(91), 14153–14156.

64 A. D. Wilson, R. H. Newell, M. J. McNevin, J. T. Muckerman, M. Rakowski DuBois and D. L. DuBois, Hydrogen Oxidation and Production Using Nickel-Based Molecular Catalysts with Positioned Proton Relays, *J. Am. Chem. Soc.*, 2006, **128**(1), 358–366.

65 S. Wiese, U. J. Kilgore, M.-H. Ho, S. Raugei, D. L. DuBois, R. M. Bullock and M. L. Helm, Hydrogen Production Using Nickel Electrocatalysts with Pendant Amines: Ligand Effects on Rates and Overpotentials, *ACS Catal.*, 2013, **3**(11), 2527–2535.

66 A. L. Goff, V. Artero, B. Jousselme, P. D. Tran, N. Guillet, R. Métayé, A. Fihri, S. Palacin and M. Fontecave, From Hydrogenases to Noble Metal–Free Catalytic Nanomaterials for H2 Production and Uptake, *Science*, 2009, **326**, 1384–1387.

67 Z. Han, F. Qiu, R. Eisenberg, P. L. Holland and T. D. Krauss, Robust photogeneration of H_2 in water using semiconductor nanocrystals and a nickel catalyst, *Science*, 2012, **338**(6112), 1321–1324.

68 X. L. Ho, H. Shao, Y. Y. Ng, R. Ganguly, Y. Lu and H. S. Soo, Visible Light Driven Hydrogen Evolution by Molecular Nickel Catalysts with Time-Resolved Spectroscopic and DFT Insights, *Inorg. Chem.*, 2019, **58**(2), 1469–1480.

69 W. T. Eckenhoff, Molecular catalysts of Co, Ni, Fe, and Mo for hydrogen generation in artificial photosynthetic systems, *Coord. Chem. Rev.*, 2018, **373**, 295–316.

70 A. Barma, M. Chakraborty, S. K. Bhattacharya, P. Ghosh and P. Roy, Mononuclear nickel(ii) complexes as electrocatalysts in hydrogen evolution reactions: effects of alkyl side chain lengths, *Mater. Adv.*, 2022, **3**(20), 7655–7666.

71 P.-A. Jacques, V. Artero, J. Pécaut and M. Fontecave, Cobalt and nickel diimine-dioxime complexes as molecular electrocatalysts for hydrogen evolution with low overvoltages, *Proc. Natl. Acad. Sci. U. S. A.*, 2009, **106**(49), 20627–20632.

72 P. Zhang, M. Wang, Y. Yang, D. Zheng, K. Han and L. Sun, Highly efficient molecular nickel catalysts for electrochemical hydrogen production from neutral water, *Chem. Commun.*, 2014, **50**(91), 14153–14156.

73 S. Wiese, U. J. Kilgore, M.-H. Ho, S. Raugei, D. L. DuBois, R. M. Bullock and M. L. Helm, Hydrogen Production Using Nickel Electrocatalysts with Pendant Amines: Ligand Effects on Rates and Overpotentials, *ACS Catal.*, 2013, **3**(11), 2527–2535.

74 M. Nippe, R. S. Khnayzer, J. A. Panetier, D. Z. Zee, B. S. Olaiya, M. Head-Gordon, C. J. Chang, F. N. Castellano and J. R. Long, Catalytic proton reduction with transition metal complexes of the redox-active ligand bpy2PYMe, *Chem. Sci.*, 2013, **4**(10), 3934–3945.

75 L. L. Efros, H. H. Thorp, G. W. Brudvig and R. H. Crabtree, Toward a Functional Model of Hydrogenase: Electrocatalytic Reduction of Protons to Dihydrogen by a Nickel Macrocyclic Complex, *Inorg. Chem.*, 1992, **31**, 1722–1724.

76 D. Huang, B. He, Y. Zhao, M. Liu and L. Wang, Homogeneous electrocatalytic hydrogen evolution by a N2P2Fe(II) complex: Structural characterization of iron-hydride intermediate, *J. Mol. Struct.*, 2025, **1325**, 141021.

77 I. Bhugun, D. Lexa and J.-M. Savéant, Homogeneous Catalysis of Electrochemical Hydrogen Evolution by Iron(0) Porphyrins, *J. Am. Chem. Soc.*, 1996, **118**(16), 3982–3983.

78 J. R. McKone, S. C. Marinescu, B. S. Brunschwig, J. R. Winkler and H. B. Gray, Earth-abundant hydrogen evolution electrocatalysts, *Chem. Sci.*, 2014, **5**(3), 865–878.

79 J.-F. Capon, F. Gloaguen, F. Y. Pétillon, P. Schollhammer and J. Talarmin, Electron and proton transfers at diiron dithiolate sites relevant to the catalysis of proton reduction by the [FeFe]-hydrogenases, *Coord. Chem. Rev.*, 2009, **253**(9), 1476–1494.

80 J. A. Halfen, D. C. Fox, M. P. Mehn and L. Que Jr, Enhanced reactivity of copper catalysts for olefin aziridination by manipulation of ligand denticity, *Inorg. Chem.*, 2001, **40**, 5060–5061.

81 Y. Zhang, H.-C. Liang, L. N. Zakharov, S. K. Das, M. M. Hetu and A. L. Rheingold, Carboxyester hydrolysis promoted by Cu(II) complexes of pyridyl-amine carboxylate-pendant ligands, *Inorg. Chim. Acta.*, 2007, **360**, 1691–1701.

82 L. Liang and D. Astruc, The copper(I)-catalyzed alkyne-azide cycloaddition (CUAAC) ''click'' reaction and its applications. An overview, *Coord. Chem. Rev.*, 2011, **255**, 2933–2945.

83 J. E. Hein and V. V. Fokin, Copper-catalyzed azide–alkyne cycloaddition (CuAAC) and beyond: new reactivity of copper(I) acetylides, *Chem. Soc. Rev.*, 2010, **39**, 1302–1315.

84 R. Angamuthu, P. Byers, M. Lutz, A. L. Spek and E. Bouwman, Electrocatalytic CO_2 Conversion to Oxalate by a Copper Complex, *Science*, 2010, **327**(5963), 313–315.

85 Z. Chen and T. J. Meyer, Copper(II) Catalysis of Water Oxidation, *Angew. Chem., Int. Ed.*, 2013, **52**(2), 700–703.

86 S. M. Barnett, K. I. Goldberg and J. M. Mayer, A soluble copper–bipyridine water-oxidation electrocatalyst, *Nat. Chem.*, 2012, **4**, 498.

87 J. Du, Z. Chen, S. Ye, B. J. Wiley and T. J. Meyer, Copper as a Robust and Transparent Electrocatalyst for Water Oxidation, *Angew. Chem., Int. Ed.*, 2015, **54**, 2073–2078.

88 M.-T. Zhang, Z. Chen, P. Kang and T. J. Meyer, Electrocatalytic Water Oxidation with a Copper(II) Polypeptide Complex, *J. Am. Chem. Soc.*, 2013, **135**(6), 2048–2051.

89 T. Zhang, C. Wang, S. Liu, J.-L. Wang, W. Lin and A. Biomimetic Copper Water, Oxidation Catalyst with Low Overpotential, *J. Am. Chem. Soc.*, 2014, **136**(1), 273–281.

90 R.-Z. Xiong, H.-M. Xu, H.-R. Zhu, Z.-J. Zhang and G.-R. Li, Recent progress in Cu-based electrocatalysts for CO_2 reduction, *Chem. Eng. J.*, 2025, **505**, 159210.

91 N. Liu, W. Ju and R. Francke, Molecular copper catalysts for electro-reductive homocoupling of CO_2 towards C_2 compounds, *Curr. Opin. Electrochem.*, 2025, **49**, 101598.

92 H. A. Younus, Y. Zhang, M. Vandichel, N. Ahmad, K. Laasonen, F. Verpoort, C. Zhang and S. Zhang, Water Oxidation at Neutral pH using a Highly Active Copper-Based Electrocatalyst, *ChemSusChem*, 2020, **13**(18), 5088–5099.

93 J. Bandara, C. P. K. Udawatta and C. S. K. Rajapakse, Highly stable CuO incorporated TiO_2 catalyst for photocatalytic hydrogen production from H_2O, *Photochem. Photobiol. Sci.*, 2005, **4**(11), 857–861.

94 D. Praveen Kumar, M. V. Shankar, M. Mamatha Kumari, G. Sadanandam, B. Srinivas and V. Durgakumari, Nanosize effects on CuO/TiO_2 catalysts for highly efficient H_2 production under solar light irradiation, *Chem. Commun.*, 2013, **49**(82), 9443–9445.

95 H. Tian, X. L. Zhang, J. Scott, C. Ng and R. Amal, TiO2-supported copper nanoparticles prepared via ion exchange for photocatalytic hydrogen production, *J. Mater. Chem. A*, 2014, **2**(18), 6432–6438.

96 L. Ye and Z. Wen, Self-supported three-dimensional Cu/Cu_2O–CuO/rGO nanowire array electrodes for an efficient hydrogen evolution reaction, *Chem. Commun.*, 2018, **54**(49), 6388–6391.

97 C. Liu, X.-D. Zhang, J.-M. Huang, M.-X. Guan, M. Xu and Z.-Y. Gu, *In Situ* Reconstruction of Cu–N Coordinated MOFs to Generate Dispersive Cu/Cu_2O Nanoclusters for Selective Electroreduction of CO_2 to C_2H_4, *ACS Catal.*, 2022, **12**(24), 15230–15240.

98 C. G. Morales-Guio, S. D. Tilley, H. Vrubel, M. Grätzel and X. Hu, Hydrogen evolution from a copper(I) oxide photocathode coated with an amorphous molybdenum sulphide catalyst, *Nat. Commun.*, 2014, **5**(1), 3059.

99 X. Chen, H. Zhang, Z. Xia, S. Zhang and Y. Ma, Base-free hydrogen generation from formaldehyde and water catalyzed by copper nanoparticles embedded on carbon sheets, *Catal. Sci. Technol.*, 2019, **9**(3), 783–788.

100 A. M. Abudayyeh, O. Schott, G. S. Hanan and S. Brooker, Copper catalysts for photo- and electro-catalytic hydrogen production, *Inorg. Chem. Front.*, 2021, **8**, 1015–1029.

101 M. Kügler, J. Scholz, A. Kronz and I. Siewert, Copper complexes as catalyst precursors in the electrochemical hydrogen evolution reaction, *Dalton Trans.*, 2016, **45**(16), 6974–6982.

102 A. M. Abudayyeh, M. S. Bennington, J. Hamonnet, A. T. Marshall and S. Brooker, Copper-based electrocatalyst for hydrogen evolution in water, *Dalton Trans.*, 2024, **53**(14), 6207–6214.

103 J.-P. Cao, T. Fang, Z.-Q. Wang, Y.-W. Ren and S. Zhan, A dinuclear triazenido–copper complex: A new molecular electro-catalyst for generating hydrogen from acetic acid or water, *J. Mol. Catal. A. Chem.*, 2014, **391**, 191–197.

104 L.-L. Zhou, T. Fang, J.-P. Cao, Z.-H. Zhu, X.-T. Su and S.-Z. Zhan, A dinuclear copper(II) electrocatalyst both water reduction and oxidation, *J. Power Sources*, 2015, **273**, 298–304.

105 X. Liu, H. Zheng, Z. Sun, A. Han and P. Du, Earth-Abundant Copper-Based Bifunctional Electrocatalyst for Both Catalytic Hydrogen Production and Water Oxidation, *ACS Catal.*, 2015, **5**(3), 1530–1538.

106 S. Rai, S. S. Akhter and S. K. Padhi, Electrocatalytic hydrogen evolution by molecular Cu(II) catalysts, *Polyhedron*, 2021, **208**, 115425.

107 J.-P. Cao, T. Fang, L.-Z. Fu, L.-L. Zhou and S.-Z. Zhan, First mononuclear copper(II) electro-catalyst for catalyzing hydrogen evolution from acetic acid and water, *Int. J. Hydrog. Energy*, 2014, **39**(26), 13972–13978.

108 J. Du, J. Wang, L. Ji, X. Xu and Z. Chen, A Highly Active and Robust Copper-Based Electrocatalyst toward Hydrogen Evolution Reaction with Low Overpotential in Neutral Solution, *ACS Appl. Mater. Interfaces*, 2016, **8**(44), 30205–30211.

109 Z.-J. Xin, S. Liu, C.-B. Li, Y.-J. Lei, D.-X. Xue, X.-W. Gao and H.-Y. Wang, Hydrogen production in a neutral aqueous solution with a water-soluble copper complex, *Int. J. Hydrog. Energy*, 2017, **42**(7), 4202–4207.

110 P. Zhang, M. Wang, Y. Yang, T. Yao and L. Sun, A Molecular Copper Catalyst for Electrochemical Water Reduction with a Large Hydrogen-Generation Rate Constant in Aqueous Solution, *Angew. Chem., Int. Ed.*, 2014, **53**(50), 13803–13807.

111 H. A. Younus, H. Emam, N. Ahmad, M. Negm, M. Alomar, F. M. Elantabli, M. M. El-Rabiei, R. Al Hajri, S. Zhang and M. Al Abri, Dinuclear Copper Complex for High-Rate Hydrogen Evolution Under Neutral Aqueous Conditions, *ChemElectroChem*, 2024, **11**(10), e202300710.

112 K. C. Christoforidis and P. Fornasiero, Photocatalysis for Hydrogen Production and CO2 Reduction: The Case of Copper-Catalysts, *ChemCatChem*, 2019, **11**(1), 368–382.

113 J. O. M. Bockris and N. Pentland, The mechanism of hydrogen evolution at copper cathodes in aqueous solutions, *Trans. Faraday Soc.*, 1952, **48**(0), 833–839.

114 N. Pentland, J. O. M. Bockris and E. Sheldon, Hydrogen Evolution Reaction on Copper, Gold, Molybdenum, Palladium, Rhodium, and Iron Mechanism and Measurement Technique under High Purity Conditions, *J. Electrochem. Soc.*, 1957, **104**, 182–194.

115 D. J. Sconyers and J. D. Blakemore, Electrodeposition behavior of homoleptic transition metal acetonitrile complexes interrogated with piezoelectric gravimetry, *Analyst*, 2020, **145**, 466–477.

116 D. Grujicic and B. Pesic, Electrodeposition of copper: the nucleation mechanisms, *Electrochim. Acta*, 2002, **47**(18), 2901–2912.

117 E. Anxolabéhère-Mallart, C. Costentin, M. Fournier, S. Nowak, M. Robert and J.-M. Savéant, Boron-Capped Tris(glyoximato) Cobalt Clathrochelate as a Precursor for the Electrodeposition of Nanoparticles Catalyzing H_2 Evolution in Water, *J. Am. Chem. Soc.*, 2012, **134**(14), 6104–6107.

118 V. Artero and M. Fontecave, Solar fuels generation and molecular systems: is it homogeneous or heterogeneous catalysis?, *Chem. Soc. Rev.*, 2013, **42**(6), 2338–2356.

119 S. J. Folkman, J. Soriano-Lopez, J. R. Galán-Mascarós and R. G. Finke, Electrochemically Driven Water-Oxidation Catalysis Beginning with Six Exemplary Cobalt Polyoxometalates: Is It Molecular, Homogeneous Catalysis or Electrode-Bound, Heterogeneous CoO_x Catalysis?, *J. Am. Chem. Soc.*, 2018, **140**(38), 12040–12055.

120 M. A. Bhatti, L. Carrella, C. Streb, E. Rentschler and S. Sundaresan, Stability *vs.* Activity in Electrocatalytic Hydrogen Production and Magnetic Studies of Mononuclear Labile Cu(II) and Ni(II) Complexes, *Dalton Trans.*, 2026, **55**(11), 3866–3874.

121 J. Zhang, B. Xiao, X. Liu, P. Liu, P. Xi, W. Xiao, J. Ding, D. Gao and D. Xue, Copper dopants improved the hydrogen evolution activity of earth-abundant cobalt pyrite catalysts by activating the electrocatalytically inert sulfur sites, *J. Mater. Chem. A*, 2017, **5**(33), 17601–17608.

122 Q. Wu, M. Luo, J. Han, W. Peng, Y. Zhao, D. Chen, M. Peng, J. Liu, F. M. F. de Groot and Y. Tan, Identifying Electrocatalytic Sites of the Nanoporous Copper–Ruthenium Alloy for Hydrogen Evolution Reaction in Alkaline Electrolyte, *ACS Energy Lett.*, 2020, **5**(1), 192–199.

123 S. Cao, C.-J. Wang, G.-Q. Wang, Y. Chen, X.-J. Lv and W.-F. Fu, Visible light driven photo-reduction of Cu^{2+} to Cu_2O to Cu in water for photocatalytic hydrogen production, *RSC Adv.*, 2020, **10**(10), 5930–5937.

124 N. Kaeffer, A. Morozan, J. Fize, E. Martinez, L. Guetaz and V. Artero, The Dark Side of Molecular Catalysis: Diimine–Dioxime Cobalt Complexes Are Not the Actual Hydrogen Evolution Electrocatalyst in Acidic Aqueous Solutions, *ACS Catal.*, 2016, **6**(6), 3727–3737.

125 M. Fang, M. H. Engelhard, Z. Zhu, M. L. Helm and J. A. S. Roberts, Electrodeposition from Acidic Solutions of Nickel Bis(benzenedithiolate) Produces a Hydrogen-Evolving Ni–S Film on Glassy Carbon, *ACS Catal.*, 2014, **4**(1), 90–98.

126 A. Khan, M. Le Pivert, A. Ranjbari, D. Dragoe, D. Bahena-Uribe, C. Colbeau-Justin, C. Herrero, D. Rutkowska-Zbik, J. Deschamps and H. Remita, Cu-Based MOF/TiO_2 Composite Nanomaterials for Photocatalytic Hydrogen Generation and the Role of Copper, *Adv. Funct. Mater.*, 2026, **36**(21), 2501736.

127 J.-J. Long, H.-C. Wu, Y.-T. Liu, Y.-Y. Ding, Q.-L. Yao, O. Metin and Z.-H. Lu, Hydrogen production from chemical hydrogen storage materials over copper-based catalysts, *cMat*, 2024, **1**(1), e10.

128 A. S. Hashimi, M. A. N. M. Nohan, S. X. Chin, P. S. Khiew, S. Zakaria and C. H. Chia, Copper Nanowires as Highly Efficient and Recyclable Catalyst for Rapid Hydrogen Generation from Hydrolysis of Sodium Borohydride, *Nanomaterials*, 2020, **10**(6), 1153.

129 T. Kunikubo, R. Castañeda, M. Murugesu, J. L. Brusso, K. Yamauchi, H. Ozawa and K. Sakai, Enhanced red-light-driven hydrogen evolution by a diplatinum photocatalyst by the larger wavefunction leakage of iodide coordinated to the platinum center, *Chem. Sci.*, 2025, **16**(47), 22580–22587.

130 S. Samuei, S. Attar, D. N. Sredojevic, A. A. Ahmad, T. G. Ulusoy Ghobadi, M. Al-Hashimi and F. Karadaş, Covalently Linked Organic–Inorganic Hybrid Assemblies for Enhanced Photocatalytic Water Splitting, *Artif. Photosynth.*, 2025, **1**(6), 324–332.

131 A. Tombrink, M. Semwal, T. Maisuradze, A. K. Mengele, D. Straub, A. J. C. Kuehne, S. Rau, S. Kupfer, B. Dietzek-Ivanšić and B. Esser, A donor–acceptor photosensitizer-catalyst dyad for light-driven nicotinamide hydrogenation, *Chem. Sci.*, 2026, **17**(6), 3012–3022.

132 S. Kozuch and J. M. L. Martin, ''Turning Over'' Definitions in Catalytic Cycles, *ACS Catal.*, 2012, **2**(12), 2787–2794.

133 C. Costentin, S. Drouet, M. Robert and J.-M. Savéant, Turnover Numbers, Turnover Frequencies, and Overpotential in Molecular Catalysis of Electrochemical Reactions. Cyclic Voltammetry and Preparative-Scale Electrolysis, *J. Am. Chem. Soc.*, 2012, **134**(27), 11235–11242.

134 J. Schneider, M. Matsuoka, M. Takeuchi, J. Zhang, Y. Horiuchi, M. Anpo and D. W. Bahnemann, Understanding TiO_2 Photocatalysis: Mechanisms and Materials, *Chem. Rev.*, 2014, **114**(19), 9919–9986.

135 J. E. B. Randles, A cathode ray polarograph. Part II.—The current-voltage curves, *Trans. Faraday Soc.*, 1948, **44**(0), 327–338.

136 A. Ševčík, Oscillographic polarography with periodical triangular voltage, *Collect. Czechoslov. Chem. Commun.*, 1948, **13**, 349–377.

137 N. Elgrishi, K. J. Rountree, B. D. McCarthy, E. S. Rountree, T. T. Eisenhart and J. L. Dempsey, A Practical Beginner's Guide to Cyclic Voltammetry, *J. Chem. Ed.*, 2018, **95**(2), 197–206.

138 J. M. Saveant and E. Vianello, Potential-sweep chronoamperometry: Kinetic currents for first-order chemical reaction parallel to electron-transfer process (catalytic currents), *Electrochim. Acta*, 1965, **10**(9), 905–920.

139 J.-M. Savéant, Molecular Catalysis of Electrochemical Reactions. Mechanistic Aspects, *Chem. Rev.*, 2008, **108**(7), 2348–2378.

140 C. C. L. McCrory, C. Uyeda and J. C. Peters, Electrocatalytic Hydrogen Evolution in Acidic Water with Molecular Cobalt Tetraazamacrocycles, *J. Am. Chem. Soc.*, 2012, **134**(6), 3164–3170.

141 M. L. Helm, M. P. Stewart, R. M. Bullock, M. R. DuBois and D. L. DuBois, A Synthetic Nickel Electrocatalyst with a Turnover Frequency Above 100000 s^{-1} for H_2 Production, *Science*, 2011, **333**(6044), 863–866.

142 E. S. Rountree, B. D. McCarthy, T. T. Eisenhart and J. L. Dempsey, Evaluation of Homogeneous Electrocatalysts by Cyclic Voltammetry, *Inorg. Chem.*, 2014, **53**(19), 9983–10002.

143 A. M. Appel and M. L. Helm, Determining the Overpotential for a Molecular Electrocatalyst, *ACS Catal.*, 2014, **4**(2), 630–633.

144 Z. Chen, D. Cummins, B. N. Reinecke, E. Clark, M. K. Sunkara and T. F. Jaramillo, Core–shell MoO_3–MoS_2 Nanowires for Hydrogen Evolution: A Functional Design for Electrocatalytic Materials, *Nano Lett.*, 2011, **11**(10), 4168–4175.

145 V. Fourmond, P.-A. Jacques, M. Fontecave and V. Artero, H2 Evolution and Molecular Electrocatalysts: Determination of Overpotentials and Effect of Homoconjugation, *Inorg. Chem.*, 2010, **49**(22), 10338–10347.

146 B. D. McCarthy, D. J. Martin, E. S. Rountree, A. C. Ullman and J. L. Dempsey, Electrochemical reduction of Brønsted acids by glassy carbon in acetonitrile—implications for electrocatalytic hydrogen evolution, *Inorg. Chem.*, 2014, **53**(16), 8350–8361.

147 M. K. Chantooni Jr. and I. M. Kolthoff, Reevaluation of the formation constants of the hydrated proton in acetonitrile, *J. Am. Chem. Soc.*, 1970, **92**(8), 2236–2239.

148 L. Tong, L. Duan, A. Zhou and R. P. Thummel, First-row transition metal polypyridine complexes that catalyze proton to hydrogen reduction, *Coord. Chem. Rev.*, 2020, **402**, 213079.

149 V. Artero and J.-M. Saveant, Toward the rational benchmarking of homogeneous H_2-evolving catalysts, *Energy Environ. Sci.*, 2014, **7**(11), 3808–3814.

150 K. Izutsu, *Acid-Base Dissociation Constants in Dipolar Aprotic Solvents*, Blackwell Scientific Publications, USA, 1990.

151 P. De Vreese, K. Haerens, E. Matthijs and K. Binnemans, Redox reference systems in ionic liquids, *Electrochim. Acta*, 2012, **76**, 242–248.

152 L. Fabbrizzi, The ferrocenium/ferrocene couple: a versatile redox switch, *ChemTexts*, 2020, **6**(4), 22.

153 V. V. Pavlishchuk and A. W. Addison, Conversion constants for redox potentials measured *versus* different reference electrodes in acetonitrile solutions at 25 °C, *Inorg. Chim. Acta*, 2000, **298**(1), 97–102.

154 D. A. Bohling, J. F. Evans and K. R. Mann, Inductive, steric, and environmental effects in the nonaqueous electrochemistry of hexakis(aryl isocyanide)chromium complexes, *Inorg. Chem.*, 1982, **21**(9), 3546–3551.

155 K. J. Lee, B. D. McCarthy and J. L. Dempsey, On decomposition, degradation, and voltammetric deviation: the electrochemist's field guide to identifying precatalyst transformation, *Chem. Soc. Rev.*, 2019, **48**(11), 2927–2945.

156 J. A. Widegren and R. G. Finke, A review of the problem of distinguishing true homogeneous catalysis from soluble or other metal-particle heterogeneous catalysis under reducing conditions, *J. Mol. Catal. A: Chem.*, 2003, **198**(1), 317–341.

157 C. M. Hagen, J. A. Widegren, P. M. Maitlis and R. G. Finke, Is It Homogeneous or Heterogeneous Catalysis? Compelling Evidence for Both Types of Catalysts Derived from $[Rh(\eta^5\text{-}C_5Me_5)Cl_2]_2$ as a Function of Temperature and Hydrogen Pressure, *J. Am. Chem. Soc.*, 2005, **127**(12), 4423–4432.

158 Y. Lin and R. G. Finke, A More General Approach to Distinguishing ''Homogeneous'' from ''Heterogeneous'' Catalysis: Discovery of Polyoxoanion- and Bu4N + -Stabilized, Isolable and Redissolvable, High-Reactivity Ir.apprx.190-450 Nanocluster Catalysts, *Inorg. Chem.*, 1994, **33**(22), 4891–4910.

159 A. Economou and C. Kokkinos, Advances in Stripping Analysis of Metals, in *Electrochemical Strategies in Detection Science*, ed. D. W. M. Arrigan, Detection Science Series, Royal Society of Chemistry, 2015, vol. 6, pp. 1–18.

160 J. Du, J. Wang, L. Ji, X. Xu and Z. Chen, A Highly Active and Robust Copper-Based Electrocatalyst toward Hydrogen Evolution Reaction with Low Overpotential in Neutral Solution, *ACS Appl. Mater. Interfaces*, 2016, **8**(44), 30205–30211.

161 M. Fang, M. H. Engelhard, Z. Zhu, M. L. Helm and J. A. S. Roberts, Electrodeposition from Acidic Solutions of Nickel Bis(benzenedithiolate) Produces a Hydrogen-Evolving Ni–S Film on Glassy Carbon, *ACS Catal.*, 2014, **4**(1), 90–98.

162 D. J. Martin, B. D. McCarthy, C. L. Donley and J. L. Dempsey, Electrochemical hydrogenation of a homogeneous nickel complex to form a surface adsorbed hydrogen-evolving species, *Chem. Commun.*, 2015, **51**(25), 5290–5293.

163 G. M. Whitesides, M. Hackett, R. L. Brainard, J. P. P. M. Lavalleye, A. F. Sowinski, A. N. Izumi, S. S. Moore, D. W. Brown and E. M. Staudt, Suppression of unwanted heterogeneous platinum(0)-catalyzed reactions by poisoning with mercury(0) in systems involving competing homogeneous reactions of soluble organoplatinum compounds: thermal decomposition of bis(triethylphosphine)-3,3,4,4-tetramethylplatinacyclopentane, *Organometallics*, 1985, **4**(10), 1819–1830.

164 K. S. Weddle, J. D. Aiken Iii and R. G. Finke, Rh(0) nanoclusters in benzene hydrogenation catalysis: Kinetic and mechanistic evidence that a putative $[(C_8H_{17})_3NCH_3]$ + $[RhCl_4]$- ion- pair catalyst is actually a distribution of Cl- and [(C8H17)3NCH_3]+ stabilized Rh(0) nanoclusters, *J. Am. Chem. Soc.*, 1998, **120**(23), 5653–5666.

165 J. C. Yang, M. W. Small, R. V. Grieshaber and R. G. Nuzzo, Recent developments and applications of electron

microscopy to heterogeneous catalysis, *Chem. Soc. Rev.*, 2012, **41**(24), 8179–8194.
166 D. N. G. Krishna and J. Philip, Review on surface-characterization applications of X-ray photoelectron spectroscopy (XPS): Recent developments and challenges, *Appl. Surf. Sci. Adv.*, 2022, **12**, 100332.
167 Y. Surendranath, D. A. Lutterman, Y. Liu and D. G. Nocera, Nucleation, Growth, and Repair of a Cobalt-Based Oxygen Evolving Catalyst, *J. Am. Chem. Soc.*, 2012, **134**(14), 6326–6336.
168 A. J. Bard and M. V. Mirkin, *Scanning Electrochemical Microscopy*, 3rd edn, CRC Press, Boca Raton, FL, USA, 2022.
169 O. Pantani, S. Naskar, R. Guillot, P. Millet, E. Anxolabéhère-Mallart and A. Aukauloo, Cobalt Clathrochelate Complexes as Hydrogen-Producing Catalysts, *Angew. Chem., Int. Ed.*, 2008, **47**(51), 9948–9950.
170 A. J. Bard, L. R. Faulkner and H. S. White, *Electrochemical Methods: Fundamentals and Applications*, 2nd edn, John Wiley & Sons: Inc, Hoboken, NJ, USA, 2001.
171 L. Chen, G. Chen, C.-F. Leung, S.-M. Yiu, C.-C. Ko, E. Anxolabéhère-Mallart, M. Robert and T.-C. Lau, Dual Homogeneous and Heterogeneous Pathways in Photo- and Electrocatalytic Hydrogen Evolution with Nickel(II) Catalysts Bearing Tetradentate Macrocyclic Ligands, *ACS Catal.*, 2015, **5**(1), 356–364.
172 Z. Jia, J. Li, L. Gao, D. Yang and A. Kanaev, Dynamic Light Scattering: A Powerful Tool for *In Situ* Nanoparticle Sizing, *Colloids Interfaces*, 2023, **7**(1), 15.
173 M. C. Iannaco, S. Mottola, V. Vaiano, G. Iervolino and I. De Marco, CeO_2-CuO composites prepared via supercritical antisolvent precipitation for photocatalytic hydrogen production from lactic acid aqueous solution, *J. CO2 Util.*, 2024, **85**, 102878.
174 G.-S. Chen, C. Liu, X.-J. Yang, Z.-H. Zhan, T.-S. Wang and H.-X. Zhang, Effect of proton sources on the electrocatalytic hydrogen evolution reaction mediated by a copper complex of bistriazolylpyridine, *Dalton Trans.*, 2025, **54**(11), 4761–4771.
175 N. A. Shah, T. Dolkar, S. Karim, J. Ishrat, C. Das, S. Das, A. Sinha Roy, K. Bhattacharyya and A. Dutta, pH-Modulated activation of a pendant amine leading to rapid electrocatalytic H_2 production by a molecular copper complex in acidic water, *Inorg. Chem. Front.*, 2025, **12**(20), 6178–6190.
176 S. Diyali, S. Saha, N. Diyali, A. Bhattacharjee, A. Mallick, S. K. Agrawalla, C. S. Purohit and B. Biswas, Deciphering Electrocatalytic Hydrogen Production in Water Through a Bioinspired Water-Stable Copper(II) Complex Adorned with (N_2S_2)-Donor Sites, *ChemSusChem*, 2025, **18**(4), e202401089.
177 S. Rai and S. K. Padhi, Effectual electrocatalytic proton and water reduction by CuII terpyridine scaffolds, *Electrochim. Acta*, 2020, **364**, 137277.
178 N. K. Botcha, R. R. Gutha, S. M. Sadeghi and A. Mukherjee, Exploring the Potential of Water-Soluble Cu(II) Complexes with MPA–CdTe Quantum Dots for Photoinduced Electron Transfer, *Catalysts*, 2022, **12**(4), 422.
179 D. Khusnutdinova, B. L. Wadsworth, M. Flores, A. M. Beiler, E. A. Reyes Cruz, Y. Zenkov and G. F. Moore, Electrocatalytic Properties of Binuclear Cu(II) Fused Porphyrins for Hydrogen Evolution, *ACS Catal.*, 2018, **8**(10), 9888–9898.
180 X. Peng, M. Zhang, H. Qin, J. Han, Y. Xu, W. Li, X.-P. Zhang, W. Zhang, U.-P. Apfel and R. Cao, Switching Electrocatalytic Hydrogen Evolution Pathways through Electronic Tuning of Copper Porphyrins, *Angew. Chem., Int. Ed.*, 2024, **63**(13), e202401074.
181 W. Li, X. Peng, H. Qin, Y. Xu, J. Han, H. Lei and R. Cao, Electrocatalytic hydrogen evolution reaction with a Cu porphyrin bearing meso-CF(3) substituents, *Dalton Trans*, 2024, **53**(48), 19121–19125.
182 X. Peng, J. Han, X. Li, G. Liu, Y. Xu, Y. Peng, S. Nie, W. Li, X. Li, Z. Chen, H. Peng, R. Cao and Y. Fang, Electrocatalytic hydrogen evolution with a copper porphyrin bearing meso-(o-carborane) substituents, *Chem. Commun.*, 2023, **59**(72), 10777–10780.
183 Q. Zhang, H. Lei, H. Guo, Y. Wang, Y. Gao, W. Zhang and R. Cao, Through-Space Electrostatic Effects of Positively Charged Substituents on the Hydrogen Evolution Reaction, *ChemSusChem*, 2022, **15**(10), e202200086.
184 S. Chandra, A. S. Hazari, Q. Song, D. Hunger, N. I. Neuman, J. van Slageren, E. Klemm and B. Sarkar, Remarkable Enhancement of Catalytic Activity of Cu-Complexes in the Electrochemical Hydrogen Evolution Reaction by Using Triply Fused Porphyrin, *ChemSusChem*, 2023, **16**(1), e202201146.
185 T. Jiang, Y. Zhou, T. Ye, S. Liu, K. Li, X. Zhao, Z. Sun, N. Aratani, H. Yamada, F. Qiu, J. Pan, T. Teranishi and S. Xue, Synthesis of wave-shaped Cu(ii) porphyrin arrays and their electrocatalytic hydrogen evolution activity, *Chem. Sci.*, 2025, **16**(47), 22498–22503.
186 H. Lei, H. Fang, Y. Han, W. Lai, X. Fu and R. Cao, Reactivity and Mechanism Studies of Hydrogen Evolution Catalyzed by Copper Corroles, *ACS Catal.*, 2015, **5**(9), 5145–5153.
187 V. Singh, A. M. Abudayyeh, M. G. Robb and S. Brooker, Mono-copper far more active than analogous di-copper complex for electrocatalytic hydrogen evolution, *Dalton Trans.*, 2022, **51**(10), 4166–4172.
188 S. Ghorai, G. Afshan, S. Saha, A. Saini, C. Das, Y. P. Kharwar, A. Sinha Roy and A. Dutta, Oxygen-tolerant hydrogen evolution in water using Schiff base copper complexes with tuneable secondary coordination environments, *Dalton Trans.*, 2025, **54**(38), 14505–14512.
189 D. K. Bediako, B. H. Solis, D. K. Dogutan, M. M. Roubelakis, A. G. Maher, C. H. Lee, M. B. Chambers, S. Hammes-Schiffer and D. G. Nocera, Role of pendant proton relays and proton-coupled electron transfer on the hydrogen evolution reaction by nickel hangman porphyrins, *Proc. Natl. Acad. Sci.*, 2014, **111**(42), 15001–15006.
190 R. M. Bullock and M. L. Helm, Molecular electrocatalysts for oxidation of hydrogen using earth-abundant metals: shoving protons around with proton relays, *Acc. Chem. Res.*, 2015, **48**(7), 2017–2026.

191 G. M. Jacobsen, J. Y. Yang, B. Twamley, A. D. Wilson, R. M. Bullock, M. Rakowski DuBois and D. L. DuBois, Hydrogen production using cobalt-based molecular catalysts containing a proton relay in the second coordination sphere, *Energy Environ. Sci.*, 2008, **1**(1), 167–174.

192 B. Reuillard, C. Costentin and V. Artero, Deciphering Reversible Homogeneous Catalysis of the Electrochemical H_2 Evolution and Oxidation: Role of Proton Relays and Local Concentration Effects, *Angew. Chem., Int. Ed.*, 2023, **62**(36), e202302779.

193 Y. Sun, J. Sun, J. R. Long, P. Yang and C. J. Chang, Photocatalytic generation of hydrogen from water using a cobalt pentapyridine complex in combination with molecular and semiconductor nanowire photosensitizers, *Chem. Sci.*, 2013, **4**, 118–124.

194 P.-A. Jacques, V. Artero, J. Pécaut and M. Fontecave, Cobalt and nickel diimine-dioxime complexes as molecular electrocatalysts for hydrogen evolution with low overvoltages, *Proc. Natl. Acad. Sci. U. S. A.*, 2009, **106**(49), 20627–20632.

195 N. Kaeffer, J. Massin, C. Lebrun, O. Renault, M. Chavarot-Kerlidou and V. Artero, Covalent Design for Dye-Sensitized H2-Evolving Photocathodes Based on a Cobalt Diimine-Dioxime Catalyst, *J. Am. Chem. Soc.*, 2016, **138**(38), 12308–12311.

196 M. Chettri, S. Saha, N. Diyali, R. Debnath, H. Bagdwal, M. Singh and B. Biswas, A pdc-pinched copper complex for sustainable hydrogen production through ligand supported-metal centric proton-coupled electron transfer, *Sustainable Energy Fuels*, 2024, **8**(23), 5553–5560.

197 D. M. Feldman, K. Pellumbi, I. Zimmermann, W. Wiesner, S. A. Sanden, S. C. B. Suhr, P. L. Holland and U.-P. Apfel, Integrating salen complexes into gas diffusion electrodes for CO2 electroreduction: considerations for employing molecular precatalysts in heterogeneous electrolyzers, *Chem. Commun.*, 2025, **61**(87), 16974–16977.

198 B. Szarłan, J. Robaszkiewicz, P. Pawluć, M. Kubicki and M. Zaranek, Salen-type nickel(ii) complexes for distinct selective hydrosilylation of alkenes under mild conditions, *Dalton Trans.*, 2025, **54**(17), 7088–7094.

199 W. L. J. Loke, C. Hu and W. Y. Fan, Tetrahedral Cu(I) complexes as electrocatalysts for the reduction of protons to dihydrogen gas, *Eur. J. Inorg. Chem.*, 2021, (25), 2499–2504.

200 M. Drosou, F. Kamatsos, G. Ioannidis, A. Zarkadoulas, C. A. Mitsopoulou, C. Papatriantafyllopoulou and D. Tzeli, Reactivity and Mechanism of Photo- and Electrocatalytic Hydrogen Evolution by a Diimine Copper(I) Complex, *Catalysts*, 2020, **10**, 1302.

201 H. B. Gray and J. R. Winkler, Electron transfer in proteins, *Annu. Rev. Biochem.*, 1996, **65**, 537–561.

202 L. F. Lindoy, K.-M. Park and S. S. Lee, Metals, macrocycles and molecular assemblies – macrocyclic complexes in metallo-supramolecular chemistry, *Chem. Soc. Rev.*, 2013, **42**(4), 1713–1727.

203 R. Ning and Q.-Q. Wang, Supramolecular catalysis with emerging, functional organic macrocycles and cages, *Chem. Soc. Rev.*, 2025, **54**(23), 11105–11140.

204 M. S. Thakur, N. Singh, A. Sharma, R. Rana, A. R. Abdul Syukor, M. Naushad, S. Kumar, M. Kumar and L. Singh, Metal coordinated macrocyclic complexes in different chemical transformations, *Coord. Chem. Rev.*, 2022, **471**, 214739.

205 H. Lei, X. Li, J. Meng, H. Zheng, W. Zhang and R. Cao, Structure Effects of Metal Corroles on Energy-Related Small Molecule Activation Reactions, *ACS Catal.*, 2019, **9**(5), 4320–4344.

206 W. Zhang, W. Lai and R. Cao, Energy-Related Small Molecule Activation Reactions: Oxygen Reduction and Hydrogen and Oxygen Evolution Reactions Catalyzed by Porphyrin- and Corrole-Based Systems, *Chem. Rev.*, 2017, **117**(4), 3717–3797.

207 X. Li, H. Lei, L. Xie, N. Wang, W. Zhang and R. Cao, Metalloporphyrins as Catalytic Models for Studying Hydrogen and Oxygen Evolution and Oxygen Reduction Reactions, *Acc. Chem. Res.*, 2022, **55**(6), 878–892.

208 K. Hou, W. Huang, M. Qi, T. H. Tugwell, T. M. Alturaifi, Y. Chen, X. Zhang, L. Lu, S. I. Mann, P. Liu, Y. Yang and W. F. DeGrado, De novo design of porphyrin-containing proteins as efficient and stereoselective catalysts, *Science*, 2025, **388**(6747), 665–670.

209 R. Buller, S. Lutz, R. J. Kazlauskas, R. Snajdrova, J. C. Moore and U. T. Bornscheuer, From nature to industry: Harnessing enzymes for biocatalysis, *Science*, 2023, **382**(6673), eadh8615.

210 O. I. Koifman and T. A. Ageeva, Main Strategies for the Synthesis of meso-Arylporphyrins, *Russ. J. Org. Chem.*, 2022, **58**(4), 443–479.

211 J. S. Lindsey, I. C. Schreiman, H. C. Hsu, P. C. Kearney and A. M. Marguerettaz, Rothemund and Adler-Longo reactions revisited: synthesis of tetraphenylporphyrins under equilibrium conditions, *J. Org. Chem.*, 1987, **52**(5), 827–836.

212 S. Mondal, T. Pain, K. Sahu and S. Kar, Large-Scale Green Synthesis of Porphyrins, *ACS Omega*, 2021, **6**(35), 22922–22936.

213 C. Costentin and J.-M. Savéant, Homogeneous Molecular Catalysis of Electrochemical Reactions: Catalyst Benchmarking and Optimization Strategies, *J. Am. Chem. Soc.*, 2017, **139**(24), 8245–8250.

214 A. M. Abudayyeh, *Catalysts for the hydrogen evolution reaction*, University of Otago, Dunedin-New Zealand, 2021.

215 R. Sanyal, S. A. Cameron and S. Brooker, Synthesis and complexes of an N_4 Schiff-base macrocycle derived from 2,2'-iminobisbenzaldehyde, *Dalton Trans.*, 2011, **40**, 12277–12287.

216 A. Fihri, V. Artero, M. Razavet, C. Baffert, W. Leibl and M. Fontecave, Cobaloxime-Based Photocatalytic Devices for Hydrogen Production, *Angew. Chem., Int. Ed.*, 2008, **47**(3), 564–567.

217 X.-W. Song, Y. Meng, C.-L. Zhang, C.-B. Ma and C.-N. Chen, A cobalt complex of a pentadentate aminopyridine ligand as an efficient catalyst for photocatalytic hydrogen generation, *Inorg. Chem. Commun.*, 2017, **76**, 52–54.

218 S. Varma, C. E. Castillo, T. Stoll, J. Fortage, A. G. Blackman, F. Molton, A. Deronzier and M.-N. Collomb, Efficient photocatalytic hydrogen production in water using a cobalt(iii) tetraaza-macrocyclic catalyst: electrochemical generation of the low-valent Co(i) species and its reactivity toward proton reduction, *Phys. Chem. Chem. Phys.*, 2013, **15**(40), 17544–17552.

219 W. Zhou, Q.-W. Deng, H.-J. He, L. Yang, T.-Y. Liu, X. Wang, D.-Y. Zheng, Z.-B. Dai, L. Sun, C. Liu, H. Wu, Z. Li and W.-Q. Deng, Heterogenization of Salen Metal Molecular Catalysts in Covalent Organic Frameworks for Photocatalytic Hydrogen Evolution, *Angew. Chem., Int. Ed.*, 2023, **62**(3), e202214143.

220 S. Roy, A. Bhunia, N. Schuth, M. Haumann and S. Ott, Light-driven hydrogen evolution catalyzed by a cobaloxime catalyst incorporated in a MIL-101(Cr) metal–organic framework, *Sustain. Energy Fuels*, 2018, **2**(6), 1148–1152.

221 N. Queyriaux, E. Giannoudis, C. D. Windle, S. Roy, J. Pécaut, A. G. Coutsolelos, V. Artero and M. Chavarot-Kerlidou, A noble metal-free photocatalytic system based on a novel cobalt tetrapyridyl catalyst for hydrogen production in fully aqueous medium, *Sustain. Energy Fuels*, 2018, **2**(3), 553–557.

222 M. Natali, E. Badetti, E. Deponti, M. Gamberoni, F. A. Scaramuzzo, A. Sartorel and C. Zonta, Photoinduced hydrogen evolution with new tetradentate cobalt(ii) complexes based on the TPMA ligand, *Dalton Trans.*, 2016, **45**(37), 14764–14773.

223 R. W. Hogue, O. Schott, G. S. Hanan and S. Brooker, A smorgasboard of 17 cobalt complexes active for photocatalytic hydrogen evolution, *Chem. Eur. J.*, 2018, **24**, 9820–9832.

224 H. Yuan, M. Ming, S. Yang, K. Guo, B. Chen, L. Jiang and Z. Han, Molecular Copper–Anthraquinone Photocatalysts for Robust Hydrogen Production, *J. Am. Chem. Soc.*, 2024, **146**(46), 31901–31910.

225 M. Papadakis, L. Delmotte, J. Mehrez, R. Hardré and M. Orio, A recent history of ligand modification for hydrogen evolution catalysts, *Coord. Chem. Rev.*, 2026, **559**, 217841.

226 S. W. Anferov, M. E. Czaikowski and J. S. Anderson, Metal-ligand cooperative transfer of protons and electrons, *Trends Chem*, 2021, **3**(12), 993–996.

227 A. Chapovetsky, M. Welborn, J. M. Luna, R. Haiges, T. F. Miller III and S. C. Marinescu, Pendant Hydrogen-Bond Donors in Cobalt Catalysts Independently Enhance CO_2 Reduction, *ACS Cent. Sci.*, 2018, **4**(3), 397–404.

228 G.-G. Luo, H.-L. Zhang, Y.-W. Tao, Q.-Y. Wu, D. Tian and Q. Zhang, Recent progress in ligand-centered homogeneous electrocatalysts for hydrogen evolution reaction, *Inorg. Chem. Front.*, 2019, **6**(2), 343–354.

229 L. Trowbridge and P. E. Sues, The Hydrogen Evolution Reaction: Using Molecular Design in Transition Metal Complexes to Control Catalytic Microenvironments on Electrode Surfaces, *ChemCatChem*, 2024, **16**(19), e202400637.

230 M. B. Brands and J. N. H. Reek, Mechanistic Insights into Electrocatalytic Hydrogen Evolution by an Exceptionally Stable Cobalt Complex, *Inorg. Chem.*, 2024, **63**(18), 8484–8492.

231 S. Zhou, L.-J. Zhang, L. Zhu, C.-H. Tung and L.-Z. Wu, Amphiphilic Cobalt Phthalocyanine Boosts Carbon Dioxide Reduction, *Adv. Mater.*, 2023, **35**(41), 2300923.

232 Z. Xing, L. Hu, D. S. Ripatti, X. Hu and X. Feng, Enhancing carbon dioxide gas-diffusion electrolysis by creating a hydrophobic catalyst microenvironment, *Nat. Commun*, 2021, **12**(1), 136.

233 M. McKee, M. Kutter, Y. Wu, H. Williams, M.-A. Vaudreuil, M. Carta, A. K. Yadav, H. Singh, J.-F. Masson, D. Lentz, M. F. Kühnel and N. Kornienko, Hydrophobic assembly of molecular catalysts at the gas–liquid–solid interface drives highly selective CO_2 electromethanation, *Nat. Chem.*, 2025, **17**(1), 92–100.

234 H.-Q. Liang, S. Zhao, X.-M. Hu, M. Ceccato, T. Skrydstrup and K. Daasbjerg, Hydrophobic Copper Interfaces Boost Electroreduction of Carbon Dioxide to Ethylene in Water, *ACS Catal.*, 2021, **11**(2), 958–966.

235 A. M. Abudayyeh, S. De Kreijger, S. Grau, E. Eryılmaz, K. Robeyns, M. Z. Ertem, A. Llobet, B. Elias and L. Troian-Gautier, Enhanced Electrocatalytic and Selective CO_2-to-CO Reduction by a Rhenium(I) Complex Bearing 6,6′-Substituted 2,2′-Bipyridines, *ACS Catal.*, 2026, **16**(1), 542–554.

236 L. Sévery, J. Szczerbiński, M. Taskin, I. Tuncay, F. Brandalise Nunes, C. Cignarella, G. Tocci, O. Blacque, J. Osterwalder, R. Zenobi, M. Iannuzzi and S. D. Tilley, Immobilization of molecular catalysts on electrode surfaces using host–guest interactions, *Nat. Chem.*, 2021, **13**(6), 523–529.

237 J. Wang, S. Dou and X. Wang, Structural tuning of heterogeneous molecular catalysts for electrochemical energy conversion, *Sci. Adv.*, 2021, **7**(13), eabf3989.

238 S. Rodríguez-Jiménez, M. S. Bennington, A. Akbarinejad, E. J. Tay, E. W. C. Chan, Z. Wan, A. M. Abudayyeh, P. Baek, H. L. C. Feltham, D. Barker, K. C. Gordon, J. Travas-Sejdic and S. Brooker, Electroactive Metal Complexes Covalently Attached to Conductive PEDOT Films: A Spectroelectrochemical Study, *ACS Appl. Mater. Interfaces*, 2021, **13**(1), 1301–1313.

239 J. Deng, X. Xu, B. Su, M. Liu, X. Lin, W. Xing, X. F. Lu, Z. Lan, G. Zhang and S. Wang, Structural amine-induced interfacial electrical double layers for efficient photocatalytic H_2 evolution, *Mater. Horiz.*, 2025, **12**(15), 5702–5709.

240 S. Pullen, H. Fei, A. Orthaber, S. M. Cohen and S. Ott, Enhanced Photochemical Hydrogen Production by a Molecular Diiron Catalyst Incorporated into a Metal–Organic Framework, *J. Am. Chem. Soc.*, 2013, **135**(45), 16997–17003.

241 C.-D. Wu and M. Zhao, Incorporation of Molecular Catalysts in Metal–Organic Frameworks for Highly Efficient Heterogeneous Catalysis, *Adv. Mater.*, 2017, **29**(14), 1605446.

242 S. Roy, Z. Huang, A. Bhunia, A. Castner, A. K. Gupta, X. Zou and S. Ott, Electrocatalytic Hydrogen Evolution from a Cobaloxime-Based Metal–Organic Framework Thin Film, *J. Am. Chem. Soc.*, 2019, **141**(40), 15942–15950.

243 J. Liu, T. A. Goetjen, Q. Wang, J. G. Knapp, M. C. Wasson, Y. Yang, Z. H. Syed, M. Delferro, J. M. Notestein, O. K. Farha and J. T. Hupp, MOF-enabled confinement and related effects for chemical catalyst presentation and utilization, *Chem. Soc. Rev.*, 2022, **51**(3), 1045–1097.

244 T. Banerjee, F. Haase, G. Savasci, K. Gottschling, C. Ochsenfeld and B. V. Lotsch, Single-Site Photocatalytic H2 Evolution from Covalent Organic Frameworks with Molecular Cobaloxime Co-Catalysts, *J. Am. Chem. Soc.*, 2017, **139**(45), 16228–16234.

245 D. Aand, S. Sk, K. Kumar, U. Pal and A. K. Singh, Boosting photocatalytic hydrogen generation by the combination of tunable cobaloxime and covalent organic framework, *Int. J. Hydrogen Energy.*, 2022, **47**(11), 7180–7188.

246 J. E. Kupferberg, Z. Syrgiannis, L. Đorđević, E. P. Bruckner, T. J. Jaynes, H. H. Ha, E. Qi, K. S. Wek, A. J. Dannenhoffer, N. A. Sather, H. C. Fry, L. C. Palmer and S. I. Stupp, Biopolymer-supramolecular polymer hybrids for photocatalytic hydrogen production, *Soft Matter*, 2024, **20**(31), 6275–6288.

247 C. Alex, S. A. Bhat, N. S. John and C. V. Yelamaggad, Highly Efficient and Sustained Electrochemical Hydrogen Evolution by Embedded Pd-Nanoparticles on a Coordination Polymer—Reduced Graphene Oxide Composite, *ACS Appl. Energy Mater.*, 2019, **2**(11), 8098–8106.

248 X. Sun, S. Wang, Y. Hou, X. F. Lu, J. Zhang and X. Wang, Self-supporting metal–organic framework-based hydrogen and oxygen electrocatalysts, *J. Mater. Chem. A*, 2023, **11**(25), 13089–13106.

249 A. J. Bagnall, M. Haake, S. Grau, T. Straistari, M. Koepf, N. Jameei Moghaddam, C. Gimbert-Suriñach, J. Benet-Buchholz, A. Llobet, M. Chavarot-Kerlidou, B. Reuillard and V. Artero, Molecular Engineering of Electrocatalytic Nanomaterials for Hydrogen Evolution: The Impact of Structural and Electronic Modifications of Anchoring Linkers on Electrocatalysis, *ACS Catal.*, 2024, **14**(8), 5630–5638.

250 A. B. Soliman, R. R. Haikal, A. A. Abugable and M. H. Alkordi, Microporous cobaloxime–graphene composite: a reloadable non-noble metal catalyst platform for the proton reduction reaction, *J. Mater. Chem. A*, 2017, **5**(5), 1957–1961.

251 S. Sowmya and V. Vijaikanth, g-C_3N_4/Chlorocobaloxime Nanocomposites as Multifunctional Electrocatalysts for Water Splitting and Energy Storage, *ACS Omega*, 2023, **8**(36), 32940–32954.

252 J. Mei, Y. Deng, X. Cheng, X. Wang and Q. Wu, Recent advances in iron-based sulfides electrocatalysts for oxygen and hydrogen evolution reaction, *Chin. Chem. Lett.*, 2024, **35**(1), 108900.

253 W. Li, X. Cheng, X. Xiong and Q. Wu, FeCo-LDH@Ni3S2 heterostructure with engineered d-band center for efficient oxygen evolution in alkaline electrolysis of freshwater and seawater, *Nano Res.*, 2026, **19**(7), 94908636.

254 M. Zou and K. M. Waldie, Redox-active ligand promoted multielectron reactivity at earth-abundant transition metal complexes, *Inorg. Chem. Front.*, 2024, **11**(18), 5795–5809.

255 C. Costentin, M. Robert and J.-M. Savéant, Catalysis of the electrochemical reduction of carbon dioxide, *Chem. Soc. Rev.*, 2013, **42**(6), 2423–2436.

256 Z. Wang, J. Zhou, Y. Shi, L. Luo, H. Li, Q. Zhou, C. Wang, Z. Xing, Z. Yang and Y. Yu, Multi-site electrocatalysts for hydrogen production under neutral conditions, *Chem. Soc. Rev.*, 2026, **55**(1), 254–298.

257 G. K. Gebremariam, A. Z. Jovanović and I. A. Pašti, The Effect of Electrolytes on the Kinetics of the Hydrogen Evolution Reaction, *Hydrogen*, 2023, **4**(4), 776–806.

258 J. M. Gisbert-González, C. G. Rodellar, J. Druce, E. Ortega, B. R. Cuenya and S. Z. Oener, Bias Dependence of the Transition State of the Hydrogen Evolution Reaction, *J. Am. Chem. Soc.*, 2025, **147**(6), 5472–5485.

259 K. E. Clary, M. Karayilan, K. C. McCleary-Petersen, H. A. Petersen, R. S. Glass, J. Pyun and D. L. Lichtenberger, Increasing the rate of the hydrogen evolution reaction in neutral water with protic buffer electrolytes, *Proc. Natl. Acad. Sci. U. S. A.*, 2020, **117**(52), 32947–32953.

260 J. P. Bigi, T. E. Hanna, W. H. Harman, A. Chang and C. J. Chang, Electrocatalytic reduction of protons to hydrogen by a water-compatible cobalt polypyridyl platform, *Chem. Commun.*, 2010, **46**, 958–960.

261 P. Wang, G. Liang, N. Smith, K. Hill, B. Donnadieu, C. E. Webster and X. Zhao, Enhanced Hydrogen Evolution in Neutral Water Catalyzed by a Cobalt Complex with a Softer Polypyridyl Ligand, *Angew. Chem., Int. Ed.*, 2020, **59**(31), 12694–12697.

262 J. L. Alvarez-Hernandez, J. W. Han, A. E. Sopchak, Y. Guo and K. L. Bren, Linear Free Energy Relationships in Hydrogen Evolution Catalysis by a Cobalt Tripeptide in Water, *ACS Energy Lett.*, 2021, **6**(6), 2256–2261.

263 L. L. Efros, H. H. Thorp, G. W. Brudvig and R. H. Crabtree, Towards a functional model of hydrogenase: electrocatalytic reduction of protons to dihydrogen by a nickel macrocyclic complex, *Inorg. Chem.*, 1992, **31**(9), 1722–1724.

264 C. Tsay and J. Y. Yang, Electrocatalytic Hydrogen Evolution under Acidic Aqueous Conditions and Mechanistic Studies of a Highly Stable Molecular Catalyst, *J. Am. Chem. Soc.*, 2016, **138**(43), 14174–14177.

265 A. Das, Z. Han, W. W. Brennessel, P. L. Holland and R. Eisenberg, Nickel Complexes for Robust Light-Driven and Electrocatalytic Hydrogen Production from Water, *ACS Catal.*, 2015, **5**(3), 1397–1406.

266 H. I. Karunadasa, C. J. Chang and J. R. Long, A molecular molybdenum-oxo catalyst for generating hydrogen from water, *Nature*, 2010, **464**, 1329.

267 H. I. Karunadasa, E. Montalvo, Y. Sun, M. Majda, J. R. Long and C. J. Chang, A Molecular MoS_2 Edge Site Mimic for Catalytic Hydrogen Generation, *Science*, 2012, **335**, 698–702.

268 D. M. Ekanayake, K. M. Kulesa, J. Singh, K. K. Kpogo, S. Mazumder, H. Bernhard Schlegel and C. N. Verani, A pentadentate nitrogen-rich copper electrocatalyst for water reduction with pH-dependent molecular mechanisms, *Dalton Trans.*, 2017, **46**(48), 16812–16820.

269 B. Roldán Cuenya and M. A. Bañares, Introduction: Operando and *In Situ* Studies in Catalysis and Electrocatalysis, *Chem. Rev.*, 2024, **124**(13), 8011–8013.
270 A. Prajapati, C. Hahn, I. M. Weidinger, Y. Shi, Y. Lee, A. N. Alexandrova, D. Thompson, S. R. Bare, S. Chen, S. Yan and N. Kornienko, Best practices for in-situ and operando techniques within electrocatalytic systems, *Nat. Commun.*, 2025, **16**(1), 2593.
271 E. Groppo, S. Rojas-Buzo and S. Bordiga, The Role of *In Situ*/Operando IR Spectroscopy in Unraveling Adsorbate-Induced Structural Changes in Heterogeneous Catalysis, *Chem. Rev.*, 2023, **123**(21), 12135–12169.
272 X. Yu, Y. Cheng, Y. Li, F. Polo-Garzon, J. Liu, E. Mamontov, M. Li, D. Lennon, S. F. Parker, A. J. Ramirez-Cuesta and Z. Wu, Neutron Scattering Studies of Heterogeneous Catalysis, *Chem. Rev.*, 2023, **123**(13), 8638–8700.
273 S. W. Chee, T. Lunkenbein, R. Schlögl and B. Roldán Cuenya, Operando Electron Microscopy of Catalysts: The Missing Cornerstone in Heterogeneous Catalysis Research?, *Chem. Rev.*, 2023, **123**(23), 13374–13418.
274 C. Santana Santos, B. N. Jaato, I. Sanjuán, W. Schuhmann and C. Andronescu, Operando Scanning Electrochemical Probe Microscopy during Electrocatalysis, *Chem. Rev.*, 2023, **123**(8), 4972–5019.
275 O. M. Magnussen, J. Drnec, C. Qiu, I. Martens, J. J. Huang, R. Chattot and A. Singer, *In Situ* and Operando X-ray Scattering Methods in Electrochemistry and Electrocatalysis, *Chem. Rev.*, 2024, **124**(3), 629–721.
276 J. T. Lang, D. Kulkarni, C. W. Foster, Y. Huang, M. A. Sepe, S. Shimpalee, D. Y. Parkinson and I. V. Zenyuk, X-ray Tomography Applied to Electrochemical Devices and Electrocatalysis, *Chem. Rev.*, 2023, **123**(16), 9880–9914.
277 X. Sun, B. Ge, S. Xue, J. Zhang, J. Chen, W. Cheng, S. Wang, Z. Yu and X. F. Lu, Lattice-matched Cu3Pd@α-MoC1-x heterointerfaces boost alkaline hydrogen evolution by accelerating water dissociation and optimizing hydrogen adsorption energy, *Appl. Catal., B*, 2026, **386**, 126418.
278 R. A. Wong, Y. Yokota and Y. Kim, Bridging Electrochemistry and Ultrahigh Vacuum: "Unburying" the Electrode–Electrolyte Interface, *Acc. Chem. Res.*, 2023, **56**(14), 2015–2025.
279 C. Costentin and J.-M. Savéant, Multielectron, Multistep Molecular Catalysis of Electrochemical Reactions: Benchmarking of Homogeneous Catalysts, *ChemElectroChem*, 2014, **1**(7), 1226–1236.
280 C. C. L. McCrory, S. Jung, I. M. Ferrer, S. M. Chatman, J. C. Peters and T. F. Jaramillo, Benchmarking Hydrogen Evolving Reaction and Oxygen Evolving Reaction Electrocatalysts for Solar Water Splitting Devices, *J. Am. Chem. Soc.*, 2015, **137**(13), 4347–4357.
281 R. Said, M. K. Abosaoda, N. Abas Ibrahim, M. M. Rekha, S. Ray, K. Chennakesavulu, R. Sharma, A. Pramanik and G. Ramaiah, Navigating the complexities of electrocatalytic water splitting: a critical examination of pitfalls and considerations in performance evaluation, *Electrochem. commun.*, 2026, **182**, 108094.
282 T. Bligaard, R. M. Bullock, C. T. Campbell, J. G. Chen, B. C. Gates, R. J. Gorte, C. W. Jones, W. D. Jones, J. R. Kitchin and S. L. Scott, Toward Benchmarking in Catalysis Science: Best Practices, Challenges, and Opportunities, *ACS Catal.*, 2016, **6**(4), 2590–2602.
283 P. Semnani, M. Bogojeski, F. Bley, Z. Zhang, Q. Wu, T. Kneib, J. Herrmann, C. Weisser, F. Patcas and K.-R. Müller, A Machine Learning and Explainable AI Framework Tailored for Unbalanced Experimental Catalyst Discovery, *J. Mater. Chem. C*, 2024, **128**(50), 21349–21367.
284 S. N. Steinmann, Q. Wang and Z. W. Seh, How machine learning can accelerate electrocatalysis discovery and optimization, *Mater. Horiz.*, 2023, **10**(2), 393–406.
285 Z. Yao, Y. Lum, A. Johnston, L. M. Mejia-Mendoza, X. Zhou, Y. Wen, A. Aspuru-Guzik, E. H. Sargent and Z. W. Seh, Machine learning for a sustainable energy future, *Nat. Rev. Mater.*, 2023, **8**(3), 202–215.
286 K. Tran and Z. W. Ulissi, Active learning across intermetallics to guide discovery of electrocatalysts for CO_2 reduction and H_2 evolution, *Nature Catalysis*, 2018, **1**(9), 696–703.
287 Z. Tan, Q. Yang and S. Luo, AI molecular catalysis: where are we now?, *Org.Chem. Front.*, 2025, **12**(8), 2759–2776.
288 R. Montoya-Gonzalez, R. d G. González-Huerta, M. L. Hernández-Pichardo and S. R. Das, Cross-laboratory validation of machine learning models for copper nanocluster synthesis using cloud-based automated platforms, *Digit. Discov.*, 2025, **4**(12), 3683–3692.
289 S. Jabeen, R. Hussain, K. Mahmood, M. Yar, A. Hussain, K. Ayub and M. Imran, In silico catalysis of hydrogen evolution reaction using transition metal loaded oxathiaporphyrin framework as electrocatalyst, *Int. J. Hydrogen Energy.*, 2025, **165**, 150917.
290 M. Foscato and V. R. Jensen, Automated in Silico Design of Homogeneous Catalysts, *ACS Catal.*, 2020, **10**(3), 2354–2377.